

Technische Universität Wien

DISSERTATION

**Constructions of  
Bidirectional Reflection Distribution Functions**

ausgeführt zum Zwecke der Erlangung des akademischen Grades  
eines Doktors der technischen Wissenschaften unter der Leitung  
VON

Univ.-Prof. Dr. Werner Purgathofer

E 186

Institut für Computergraphik und Algorithmen

eingereicht an der Technischen Universität Wien  
Fakultät für Technische Naturwissenschaften und Informatik

von

Dipl.-Math. Attila Neumann

Matr. Nr. 9727237

Batthyány u 67. H-1015 Budapest

geboren am 23. März 1957 in Budapest

Wien, im Mai 2001

# Contents

<b>1</b>	<b>Introduction</b>	<b>6</b>
1.1	Definitions, basic properties . . . . .	6
1.1.1	Radiance, irradiance, BRDF . . . . .	6
1.1.2	Physically plausible BRDFs . . . . .	8
1.1.3	An alternative definition of BRDF by reflected radiance . . . . .	9
1.1.4	Properties of BRDFs . . . . .	10
1.1.5	Further BRDF properties . . . . .	12
1.2	Survey of BRDFs . . . . .	13
1.2.1	Application's fields, types of BRDF . . . . .	13
1.2.2	Important notations, quantities . . . . .	14
1.2.3	Classical BRDFs . . . . .	15
1.2.4	First computer graphical BRDFs . . . . .	16
1.2.5	Metal models . . . . .	16
1.2.6	Empirical, semi-empirical models . . . . .	21
1.2.7	Mutiple-Layer Models . . . . .	22
1.2.8	Physically Plausible Constructions . . . . .	24
1.3	Subject of this thesis . . . . .	26
1.3.1	Required properties of material models . . . . .	26
1.3.2	Results of next chapters . . . . .	27
<b>2</b>	<b>Reflectance Models by Pumping up the Albedo Function</b>	<b>28</b>
2.1	Introduction . . . . .	28
2.1.1	Perceptual based fitting . . . . .	29
2.1.2	Physically plausible, but not physically based models . . . . .	29
2.2	Analysis of the energy reflectivity of classical BRDF models . . . . .	30
2.2.1	Divergence of the Cook–Torrance and Ward models . . . . .	30
2.3	Albedo pumping-up . . . . .	32
2.3.1	Definition of the correction term . . . . .	32
2.3.2	Controlled albedo pumping-up . . . . .	33
2.4	Simulation results . . . . .	34
2.5	Conclusions . . . . .	34
<b>3</b>	<b>New Simple Reflectance Models for Specular Materials</b>	<b>39</b>
3.1	Introduction . . . . .	39
3.2	Metals and Phong-type models . . . . .	40
3.2.1	Properties of metals and mirrors . . . . .	40
3.2.2	The new model for metals . . . . .	40
3.2.3	Transition from the Phong model to the new model: $p$ -model . . . . .	42
3.2.4	The properties of the new metal model . . . . .	42
3.3	Generalizations of the new model . . . . .	44
3.3.1	Retro-reflective materials . . . . .	44
3.3.2	Anisotropic materials . . . . .	44
3.4	Importance sampling . . . . .	45
3.4.1	Importance sampling for the Phong model . . . . .	45
3.4.2	Importance sampling for the new model . . . . .	46
3.4.3	Albedo at grazing angles . . . . .	46
3.5	Visualization of real materials . . . . .	47

3.5.1	Metals . . . . .	47
3.5.2	Plastics and ceramics . . . . .	47
3.6	Material editor . . . . .	47
3.7	Reflectance models of $(\mathbf{N} \cdot \mathbf{H})$ type . . . . .	48
3.7.1	Blinn model . . . . .	48
3.7.2	Ward model . . . . .	50
3.7.3	Cook-Torrance and He-Torrance models . . . . .	50
3.7.4	Mean albedo . . . . .	50
3.8	Simulation results . . . . .	51
3.9	Conclusions . . . . .	51
<b>4</b>	<b>Reflectance Models with Fast Importance Sampling</b>	<b>56</b>
4.1	Introduction . . . . .	56
4.2	Basic BRDF . . . . .	57
4.2.1	Reciprocity . . . . .	59
4.2.2	Energy conservation . . . . .	59
4.2.3	Importance sampling . . . . .	62
4.2.4	Importance sampling for the basic BRDF . . . . .	62
4.3	Mixture of basic BRDFs . . . . .	64
4.3.1	General description . . . . .	64
4.3.2	Albedo for a given $p(R)$ function . . . . .	66
4.4	Modified importance sampling for a given $p(R)$ . . . . .	66
4.4.1	Reducing the general case to basic BRDFs . . . . .	66
4.5	Generalization of the basic BRDF . . . . .	67
4.5.1	Generalization of the $\mathbf{L} \rightarrow \mathbf{L}'$ mirroring transformation . . . . .	67
4.5.2	The retro-reflective model . . . . .	67
4.5.3	Generalization of the metric . . . . .	67
4.5.4	Anisotropic models . . . . .	68
4.6	BRDF definition with a given scalar function . . . . .	70
4.6.1	Analytically integrable cases . . . . .	71
4.7	Real materials . . . . .	73
4.7.1	Metals and the new model . . . . .	73
4.7.2	Coated metals, metallic paints . . . . .	74
4.7.3	Plastics and polishing . . . . .	75
4.7.4	Generalized Lambertian models . . . . .	75
4.8	Conclusions and future work . . . . .	77
<b>5</b>	<b>Central Concepts and Future Directions</b>	<b>78</b>
5.1	Repairing Energy Balance . . . . .	78
5.2	Generating new physically plausible BRDFs . . . . .	79
5.2.1	Linear mixing of BRDFs . . . . .	79
5.2.2	Patch-based BRDF lasses . . . . .	79
5.2.3	Components of patch-based BRDF constructions . . . . .	80
5.2.4	Examples of patch-based BRDF-classes . . . . .	82
5.2.5	Sampling on patch-based BRDFs . . . . .	82
5.3	Distance of BRDFs . . . . .	83
5.3.1	Scalar product and normal of BRDFs . . . . .	83
5.3.2	Dimension reductive norms by special lighting . . . . .	84
5.3.3	Norm of general lighting . . . . .	84
5.3.4	Inherence between scalar product and composition's norm . . . . .	84
	<b>Bibliography</b>	<b>89</b>

# Kurzfassung

Ursprünglich beinhaltete die Untersuchung von Material-Modellen lediglich die Suche nach Formeln die das reale Material beschreiben (Lambert, Minneart). Im Bereich der Computergrafik erwies sich aber die Anwendung von virtuellen Formeln als nützlich (Phong, Blinn, ...). Diese Vorgehensweise ist jedoch nur dann akzeptabel wenn das Konzept der physikalischen Plausibilität korrekt definiert ist. Abgesehen davon ob "Realitäts"-Anforderungen erfüllt werden, müssen einige Faktoren berücksichtigt werden die speziell im Bereich der Computergrafik signifikant sind, z.B. die Kosten der Anwendung einer Formel. Die Berechnung der unmittelbaren Relation von Paaren von Einfall- und Ausfallrichtungen ist solch ein Faktor, oder die Effekte der Lichtverteilung in verschiedene Ausfallrichtungen, oder das Sampling von Radiance-Richtungen des einfallenden Lichtstrahls anhand von Monte Carlo-Methoden.

Das Albedo-Konzept das für diffuse Material-Modelle definiert ist kann in die Definition der physikalischen Plausibilität inkludiert werden. Das neue Albedo-Konzept kann für mehrere Anwendungen verwendet werden. Die erweiterte Definition von Albedo kann für die detaillierte Charakterisierung des Verhaltens eines Material-Modells verwendet werden. Es kann direkt als Effekt von gleichmäßig verteiltem Tageslicht angesehen werden. Die Tauglichkeit des Albedos kann ein signifikanter Faktor für die Tauglichkeit der BRDFs sein. Ebenso spielt es eine wichtige Rolle in der Technik des Importance Samplings. Für die korrekte Behandlung des Konzepts der Distanz für Material-Modelle kann das Konzept der Zusammensetzung als Analogon zur "Korrelation" definiert werden, welches ein interessantes neues Werkzeug für die Untersuchung der BRDF ist.

Eine Anzahl an Formeln wurden für die Beschreibung von Metallen hergeleitet. Die metallische Erscheinung von Materialien wird vor allem durch die Albedo-Funktion, Spitzen in und neben der Spiegelungsrichtung und dem Verhalten bei flachen Winkeln charakterisiert. In dieser Studie wird die physikalische Plausibilität mehrerer bekannter Material-Modelle kritisch begutachtet indem ihr Albedo-Verhalten untersucht wird. Wir beschreiben zwei einfache, allgemein anwendbare und effektive Methoden zur Eliminierung der Mängel bekannter Metall-Modelle oder, allgemein, damit Rendering-Material-Modelle realistischer erscheinen. Eine Methode eliminiert einige im allgemeinen auftretende Defekte der Albedo-Funktion praktisch ohne Berechnungskosten: sie beseitigt den Schaden an der Energie-Bilanz und gleichzeitig korrigiert sie die künstliche Verdunkelung der reflektierten Radiance. Die zweite, sogar noch einfachere Methode beinhaltet eine inverse Cosinus-Funktion, wodurch das Phong- und Blinn-Modell mittels einer einzelnen Multiplikation wesentlich verbessert wird.

Die grundlegende Aufgabe der präsentierten Arbeit war eine BRDF-Formel zu entwickeln, die die Anforderung an die physikalische Plausibilität erfüllt und für Importance Sampling verwendet werden kann, indem neue Konstruktionen verwendet werden oder indem existierende Formeln modifiziert werden. Die Patch-basierte BRDF-Konstruktion ist eine solche Formel, die Material-Modell-Funktionen produziert indem einfache BRDF-Formeln mit Parametern die den Zustand der physikalischen Plausibilität erfüllen kontinuierlich und/oder diskret gemischt werden. Die ersten Parameterwerte der einfachen BRDF-Formeln liefern ideal diffuse Reflexion und ideale Spiegelung, daher sollte diese Konstruktion als eine gemeinsame Verallgemeinerung der beiden betrachtet werden. Hierbei ist die Dichtefunktion ein freier Parameter der resultierenden BRDF Klasse. Die grundlegende Idee der präsentierten Methode ist das zulässige Mischen von zulässigen Basisfunktionen. Dies ist die erste Konstruktion die speziell auf die Verbesserung der Geschwindigkeit des Importance Samplings zielt um die Effektivität von Monte Carlo-Methoden zu erhöhen. Von einer Reihe von Verallgemeinerungen und Verfeinerungen ist das anisotropische und das retro-reflektierende Modell am interessantesten.

# Abstract

Historically the examination of material models involved searching merely for formulae that described real materials (Lambert, Minneart), but computer graphics rendered the application of virtual formulae useful (Phong, Blinn, etc). However, the latter approach is acceptable only if the concept of physical plausibility is correctly defined. Fulfillment of "reality" requirements apart, especially for computer graphics some significant factors may have to be taken into account, such as the cost of applying a formula. The computation of the immediate relationship between incoming and outgoing direction pairs is such a factor, or the effects of uniformly distributed lighting in various outgoing directions, or the sampling of radiance directions of the incoming light ray according to Monte Carlo method.

An extension of the albedo concept defined for diffuse material models is included in the definition of physical plausibility. The new albedo concept may have multiple applications. The extended definition of albedo may be used for detailed characterization of the behavior of the material model. It can be directly seen as effect of uniformly distributed daylight. Fitting of albedo can be a significant factor of a BRDFs' fitting. Similarly it plays an important role in the technique of importance sampling. For the proper treatment of the concept of distance for material models, the concept of composition may be defined as the analogue of "correlation", which is an interesting new tool for the examination of BRDF.

A number of formulae were derived for the description of metals. The metallic appearance of materials is characterized first of all by the albedo function, specular and off-specular peaks and behavior at grazing angles. In this paper the physical plausibility of several known material models will be critically examined by investigating their albedo behavior. We shall describe two simple, generally applicable and effective methods for the elimination of the deficiencies of known metal models or, in general, rendering material models to appear more realistic. One method eliminates some generally recurring defects of the albedo function practically without computational costs: it cancels the damage to the energy balance and at the same time it corrects the artificial darkening of reflected radiance. The second, even simpler method involves an inverse-cosine function, which by a single multiplication significantly improves the Phong and Blinn model, while it conserves their assets.

The basic task of this thesis the development of BRDF formulae, which fulfill the physical plausibility requirement and can be used for importance sampling, by applying new constructions or modifying existing formulae. The patch-based BRDF construction is one such formula, which produces material model functions by continuous and/or discrete mixing of basic BRDF formulae with parameters to fulfil the condition of physical plausibility. The extreme parameters of these basic BRDF formulae yield the ideal diffuse and ideal mirror options, and therefore this construction should be regarded as a mutual generalization of the two. Here a free parameter of the resultant BRDF class is a probability density function. The basic idea of the present method is to allow mixing of allowable base functions. This is the first construction aimed especially at enhancing the speed of importance sampling to improve the effectiveness of (Quasi) Monte Carlo methods. Of a number of generalizations and refinements, the anisotropic and retro-reflective models are of greatest interest.

# Acknowledgements

First of all I would like to express my special thanks to Werner Purgathofer, who has not stopped to press and to encourage me to start and to complete this dissertation. I acknowledge here, that he has been right. I thank him also for his technical help in the final round which is of similar importance. And last but not least those cooperations and consultations within or outside the topic of this study which was so fruitfull all along our connection.

Similarly I would like to express my special thanks to my brother and colleague László Neumann, whithout whom this thesis, and most of my results would have never been generated, and , may be even more important, perhaps I would not have started to deal with computergraphics at all.

I would also like to thank László Szirmay-Kalos whose consultations, have yielded a lot of professional results, and helped me to write this thesis as well.

I would also like thank Balázs Csébfalvi, Jan Prikřyl, Robert F. Tobler, Alexander Wilkie and other colleagues at the Institute of Computer Graphics who they helped me always in my technical problems. This help was really valuable for me.

And last but not at all least I would like to thank my family, my wife and my children their patience and encouragement which has helped me over usual and unusual obstacles.

# Chapter 1

## Introduction

### 1.1 Definitions, basic properties

#### 1.1.1 Radiance, irradiance, BRDF

The reflectance of surfaces is characterized by their reflectance models. Next, two basic radiometric units are reviewed.

##### Radiance

First the definition of radiance: The spectral radiance  $L_\lambda$  for a given wavelength  $\lambda$  in a given direction at a given point on surface  $A$  from a light source or receiver by Wyszecky and Stiles ([78]: Fig.1, pp.3) is as follows:

$$L_{e,\lambda} = \frac{d^2P}{dA \cdot \cos \Theta \cdot d\omega} \quad [ W m^{-2} sr^{-1} ] \quad (1.1)$$

where  $P$  is the power output from surface  $A$  at an angle of  $\Theta$  to the surface normal in  $d\omega$  solid angle. The term  $A \cdot \cos \Theta$  defines the area of surface  $A$  "from the appropriate angle", that is the projection area of surface  $A$  cast onto a "reference cross-section" at right angle to the light beam. The formula for distances between the reference cross-sections of two small surface elements and apparent solid angles from between each other leads to an interesting and important relationship. The  $\omega_1$  is the solid angle of surface  $A_2$  from a given point on surface  $A_1$ ,  $\omega_2$  is the solid angle of surface  $A_1$  from a given point on surface  $A_2$ .

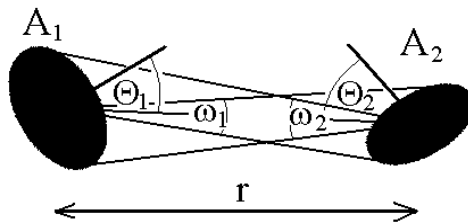


Figure 1.1: Geometrical relation between two small surface element

The angles  $\Theta_1$  and  $\Theta_2$  are the incident angles, that is the angles between the line of direction connecting the two surface elements and those of the surface normals. As the tangent of small angles approach their numerical values, they become

$$\omega_1 = r^2 \cdot A_2 \cdot \cos \Theta_2 \quad \text{and} \quad \omega_2 = r^2 \cdot A_1 \cdot \cos \Theta_1 \quad (1.2)$$

This leads to the following relationship:

$$\omega_1 \cdot A_1 \cdot \cos \Theta_1 = \omega_2 \cdot A_2 \cdot \cos \Theta_2 \quad (1.3)$$

If the incoming and outgoing light power between two surface elements are similar (that is, medium absorption is negligible), the limit values of radiance for outgoing light from the first surface and for incoming light to the second surface are also similar, assuming continuous radiance distribution:

$$L_1 = \frac{d^2 P_1}{\omega_1 \cdot A_1 \cdot \cos \Theta_1} = \frac{d^2 P_2}{\omega_2 \cdot A_2 \cdot \cos \Theta_2} = L_2 \quad (1.4)$$

Allowing boundary transition at a given point and direction, this shows that the radiance of an elemental light ray is constant at any distance, and its value is the same as that of the outgoing ray, independently of the orientation of emitting surface, that is its angle with the light ray. The position on the incoming side is the same. This principle of "preservation of radiance" in visual science is equivalent to the principle of preservation of energy in physics, and therefore radiance plays a central role in computer graphics.

### Irradiance

Irradiance is another significant concept, which may be derived from the ratio of light power falling on a surface element and its area, allowing for boundary transition:

$$E_e = \frac{dP}{dA} \quad \left[ \frac{W}{m^2} \right] \quad (1.5)$$

where P is the power [ $W = \frac{Joule}{sec}$ ] and A is the area [ $m^2$ ] of surface element. This definition does not cover the spatial distribution of incoming light or its direction in case of a point lightsource. No such information is included in irradiance. Based on this concept, radiance is in fact a light power from a visible surface element per unit solid angle, whereas irradiance is light power from the same element per unit surface area.

Therefore, "irradiance" plays the same role in the study of local behavior as "energy" does in general. Thus the relationship between irradiance values fixed at 1 wavelengths and radiance is as follows:

$$L_{e,\lambda} = \frac{dE_{e,\lambda}}{\cos \Theta \, d\omega} \quad \text{and} \quad E_{e,\lambda} = \int_{\mathbf{L} \in \Omega} L_{e,\lambda}(\mathbf{L}) \cdot \cos \Theta_{\mathbf{L}} \, d\omega_{\mathbf{L}} \quad (1.6)$$

where  $\Omega$  denotes the entire hemisphere of directions, that is the half of unit sphere pointing by the normal vector of the surface in question. Extending  $\Omega$  to whole sphere, transmittance can be treated the same way.

Clearly no fixed irradiance value can be obtained when incoming radiance distribution is limited to a **differentially small solid angle**, with zero radiance outside it. In this case we obtain  $L_{e,\lambda}(\omega) = \frac{dE_{e,\lambda}}{\cos \Theta \, d\omega}$  in the equation 1.1 yielding the sought after value along direction  $\mathbf{L}_0$  according to  $\Theta$  within the small solid angle  $\omega$ . Assuming boundary transition, this requires of a point source yielding a given irradiance by a radiance distribution, which is infinite along direction  $\mathbf{L}$ , has a zero value outside it and its integral is as follows:

$$\frac{E_{e,\lambda}}{\cos \Theta_{\mathbf{L}_0}} = \int_{\mathbf{L} \in \Omega} L_{e,\lambda}(\mathbf{L}) \, d\omega_{\mathbf{L}} \quad (1.7)$$

This can be interpreted by the concept of "distribution" as an extension of traditional functions that can be formalized in the present case by the application of the *Dirac* –  $\Delta$  function focusing on the  $\mathbf{L}_0$  point ( $\Delta_{\mathbf{L}_0}$ ):

$$L_{e,\lambda}(\omega) = \frac{E_{e,\lambda}}{\cos \Theta_{\mathbf{L}}} \cdot \Delta_{\mathbf{L}_0} \quad (1.8)$$

Consider a surface with a normal unit vector  $\mathbf{N}$  and place a point light source of output  $P$  at a unit distance in any direction of unit vector  $\mathbf{L}$  ( $\epsilon \Omega$ ). Place an observer along the observation direction of unit vector  $\mathbf{V}$  ( $\epsilon \Omega$ ). The observer perceives light reflected from the surface, which is a secondary emitter of light, and observes its radiance. The  $A_2$  corresponds to the receiver, and  $\cos \Theta_2 = \mathbf{N} \cdot \mathbf{V}$  scalar product to an observer with a pupil size of  $A_2$  area.

Taking the case of boundary transition, the observer may be assumed to be a point like object. As seen earlier the radiance value the observer measures does not depend on the observer's distance, which affects only the amount of energy (power) the observer receives. That is, the angle of observation of observed surface may be slanting and its distance may be greater, nevertheless, we see the observed surface just as bright, because radiance remains the same.



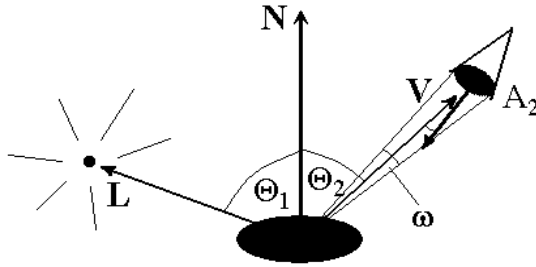


Figure 1.2: Response of a point light source toward observer's pupil

### Bidirectional Reflection Distribution Function

Reflectance may be defined by irradiance and radiance and its properties at a given point are described by the **Bi-directional Reflection Distribution Function (BRDF)**, which is the central topic of this study. The BRDF, that is  $f_r(\mathbf{L}, \mathbf{V})$  function (notated in literature also by  $\rho(\mathbf{L}, \mathbf{V})$ ) may be defined as:

$$f_r(\mathbf{L}, \mathbf{V}) = \frac{L_{e,\lambda}}{E_{e,\lambda}} \quad [sr^{-1}] \quad (1.9)$$

The BRDF is the ratio of output radiance and input irradiance caused by light from a point source from direction  $\mathbf{L}$  on a surface – this thesis does not deal with cross-effects between different wavelengths.

This definition, unlike others in some shallow literature, does not involve the assumption of boundary transition or differential ratio. These assumptions have already been made in defining irradiance and radiance! Nor does it involve the power of a point source, as this is cancelled out when the two definitions are combined. Even the intrivial fact, that irradiance at decreasing angles (for point sources of similar outputs) declines by a factor  $\cos \Theta_{\mathbf{L}} = \mathbf{L} \cdot \mathbf{V}$ , is of no serious consequence. Even though output radiance decreases, the BRDF remains in an adequate range. The direction  $\mathbf{L}$  is included in the definition only indirectly. The fact that the cause of irradiance occurs in direction  $\mathbf{L}$  is taken into account. We also know the observer's direction, which is included in the definition of radiance. The BRDF is not a dimensionless quantity, but is the reciprocal of the solid angle (steradian). From the point of view of terminology, the use of  $\mathbf{L}_{e,\lambda}$  or  $\mathbf{L}_\lambda$  for radiance or  $\mathbf{L}$  for direction is disturbing but not ambiguous.

#### 1.1.2 Physically plausible BRDFs

Thus BRDF's are  $\Omega \times \Omega \rightarrow \mathbf{R}$  functions. Can any  $\Omega \times \Omega \rightarrow \mathbf{R}$  function yield an optical material model? If not, which properties characterize them? If we can only accept a function modeling real materials, the answer to these questions is obviously ambiguous. However, the question remains unanswered even if we accept physical constructions that can be in principle modeled from real materials.

To resolve these problems, we shall list several properties, which are valid for all physically possible material models. The  $\Omega \times \Omega \rightarrow \mathbf{R}$  function fulfilling this requirement is called a **physically plausible function**. We expect of all BRDF functions investigated here to be physically plausible.

1. The BRDF,  $f_r(\mathbf{L}, \mathbf{V})$  [ $sr^{-1}$ ], is a non-negative scalar quantity at every wavelength.
2. The BRDF has the essential symmetry characteristics of:

$$f_r(\mathbf{L}, \mathbf{V}) = f_r(\mathbf{V}, \mathbf{L}) \quad (1.10)$$

for all  $\mathbf{L}, \mathbf{V} \in \Omega$  ranges. (This is the formulation of *Helmholtz's reciprocity principle* (see at Chandrasekhar [13], Wyszecky and Stiles [78]). The principle is also true in a wide range of cases that are not studied in this thesis, such as polarized light.)

3. A third essential property derives from energy-balance: total reflected energy cannot be greater than total incoming energy.

In this respect, consider the effect of a point source arriving from direction  $\mathbf{L}$ . The irradiance  $E_e(\mathbf{L})$  occurring on a surface due to a point source from direction  $\mathbf{L}$  in small solid angle  $\omega_{\mathbf{V}}$  around  $\mathbf{V}$  causes  $E_e(\mathbf{L}) = f_r(\mathbf{L}, \mathbf{V}) \cdot E_e(\mathbf{L})$  radiance. Using the definitions of radiance (equation 1.1 and irradiance (equation 1.5 involving elemental surface or solid angle respectively:

$$\begin{aligned} P^{out}(\omega_{\mathbf{V}}) &= L_e(\mathbf{V}) \cdot A \cdot \cos \Theta_{\mathbf{V}} \cdot \omega_{\mathbf{V}} = f_r(\mathbf{L}, \mathbf{V}) \cdot E_e(\mathbf{L}) \cdot A \cdot \cos \Theta_{\mathbf{V}} \cdot \omega_{\mathbf{V}} = \\ &= f_r(\mathbf{L}, \mathbf{V}) \cdot \frac{P^{in}(\mathbf{L})}{A} \cdot A \cdot \cos \Theta_{\mathbf{V}} \cdot \omega_{\mathbf{V}} = P^{in}(\mathbf{L}) \cdot f_r(\mathbf{L}, \mathbf{V}) \cdot \cos \Theta_{\mathbf{V}} \cdot \omega_{\mathbf{V}} \end{aligned} \quad (1.11)$$

Total outgoing energy is an integral of this over  $\omega_{\mathbf{V}}$ :

$$\begin{aligned} P^{out} &= \int_{\mathbf{V} \in \Omega} P^{out}(\omega_{\mathbf{V}}) d\omega_{\mathbf{V}} = \int_{\mathbf{V} \in \Omega} P^{in}(\mathbf{L}) \cdot f_r(\mathbf{L}, \mathbf{V}) \cdot \cos \Theta_{\mathbf{V}} \cdot d\omega_{\mathbf{V}} = \\ &= P^{in}(\mathbf{L}) \cdot \int_{\mathbf{V} \in \Omega} f_r(\mathbf{L}, \mathbf{V}) \cdot \cos \Theta_{\mathbf{V}} d\omega_{\mathbf{V}} \end{aligned} \quad (1.12)$$

Condition  $P^{out} \leq P^{in}(\mathbf{L})$  is equivalent with the condition for their ratio:

$$\mathbf{a}_f(\mathbf{L}) = \int_{\mathbf{V} \in \Omega} f_r(\mathbf{L}, \mathbf{V}) \cdot \cos \Theta_{\mathbf{V}} d\omega_{\mathbf{V}} \leq 1 \quad (1.13)$$

The  $\mathbf{a}_f(\mathbf{L})$  quantity, called directional-hemispherical reflectivity or shortly **albedo** of  $f_r$ , is used occasionally without index  $r$ . The name *albedo* is an extension of traditional terminology for diffuse models and general material models.

### 1.1.3 An alternative definition of BRDF by reflected radiance

The light power in solid angle  $\omega_{\mathbf{V}}$  in the case of incoming power concentrated in  $\omega_{\mathbf{L}}$  is  $P^{in}(\omega_{\mathbf{L}}) \cdot f_r(\mathbf{L}, \mathbf{V}) \cdot \cos \Theta_{\mathbf{V}} \cdot \omega_{\mathbf{V}}$ , therefore, the effect of power distributed over the entire half space in  $\omega_{\mathbf{V}}$ :

$$\begin{aligned} P^{out}(\omega_{\mathbf{L}}) &= \int_{\mathbf{L} \in \Omega} P^{in}(\mathbf{L}) \cdot f_r(\mathbf{L}, \mathbf{V}) \cdot \cos \Theta_{\mathbf{V}} \cdot \omega_{\mathbf{L}} \cdot \cos \Theta_{\mathbf{L}} d\omega_{\mathbf{L}} = \\ &= \cos \Theta_{\mathbf{V}} \cdot \omega_{\mathbf{V}} \cdot \int_{\mathbf{L} \in \Omega} P^{in}(\mathbf{L}) \cdot f_r(\mathbf{L}, \mathbf{V}) \cdot \cos \Theta_{\mathbf{L}} d\omega_{\mathbf{L}} \end{aligned} \quad (1.14)$$

From the definitions of radiance (equation 1.1) and irradiance (equation 1.5) it follows:

$$L_{\lambda}^{out}(\mathbf{V}) = \int_{\mathbf{L} \in \Omega} L^{in}(\mathbf{L}) \cdot f_r(\mathbf{L}, \mathbf{V}) \cdot \cos \Theta_{\mathbf{L}} d\omega_{\mathbf{L}} \quad (1.15)$$

As a matter of fact, in addition to the three requirements of physical plausibility, we could have also used this formula to define BRDF, thus circumventing the definition of irradiance and the necessity of assuming a boundary transition when giving the point source. This approach, which can easily give rise to theoretical inaccuracies, was necessary to improve the definition of concepts and to make the legitimacy of definitions credible. These definitions lead to the present formula. Starting from this formula and the *Dirac* –  $\Delta$  function, the cases of irradiance and point light source can be similarly derived. But we can obtain a coherent system without non-traditional tools that agrees well with earlier conditions in actual cases. Thus this formula could be the basis of further work. Its justification is supported by the central role of radiance; relating merely initial and reflected radiance values. Furthermore, the formula facilitates the comprehension of the BRDF [  $sr^{-1}$  ] unit independently of the unit of radiance or even without any knowledge on it! Since the integrand is a product of radiance, BRDF, scalar value and solid angle, the result of its integration is radiance, therefore the dimensions of BRDF are unambiguously [  $sr^{-1}$  ].

According to the definition of irradiance, the concentrated unit energy (more precisely power per area, that is irradiance) arriving from direction  $\mathbf{L}$  is equivalent to the incoming radiance distribution of  $L_{\lambda}^{in}(\mathbf{L}) = \frac{1}{\cos \Theta_{\mathbf{L}}} \cdot \Delta_{\mathbf{L}}$ . According to the – alternative – definition of BRDF, the result of this in direction  $\mathbf{V}$  is:

$$\begin{aligned} L_{\lambda}^{out}(\mathbf{V}) &= \int_{\mathbf{L} \in \Omega} L_{\lambda}^{in}(\mathbf{L}) \cdot f_r(\mathbf{L}, \mathbf{V}) \cdot \cos \Theta_{\mathbf{L}} d\omega_{\mathbf{L}} = \\ &= \int_{\mathbf{L} \in \Omega} \frac{1}{\cos \Theta_{\mathbf{L}}} \cdot \Delta_{\mathbf{L}} \cdot f_r(\mathbf{L}, \mathbf{V}) \cdot \cos \Theta_{\mathbf{L}} d\omega_{\mathbf{L}} = \int_{\mathbf{L} \in \Omega} \Delta_{\mathbf{L}} \cdot f_r(\mathbf{L}, \mathbf{V}) d\omega_{\mathbf{L}} = f_r(\mathbf{L}, \mathbf{V}) \end{aligned} \quad (1.16)$$

This agrees with the original definition (9). Similarly we can derive the estimation of albedo (equation 1.13) from the alternative definition (equation 1.15) by the description of  $P^{out} \leq P^{in}$  energy balance:

$$\begin{aligned}
P^{out} &= \int_{\mathbf{V} \in \Omega} L_{\lambda}^{out}(\mathbf{V}) \cdot A \cdot \cos \Theta_{\mathbf{V}} \, d\omega_{\mathbf{V}} = \\
&= \int_{\mathbf{V} \in \Omega} \left( \int_{\mathbf{L} \in \Omega} L_{\lambda}^{in}(\mathbf{L}) \cdot f_r(\mathbf{L}, \mathbf{V}) \cdot \cos \Theta_{\mathbf{L}} \, d\omega_{\mathbf{L}} \right) \cdot A \cdot \cos \Theta_{\mathbf{V}} \, d\omega_{\mathbf{V}} = \\
&= \int_{\mathbf{L} \in \Omega} L_{\lambda}^{in}(\mathbf{L}) \cdot A \cdot \cos \Theta_{\mathbf{L}} \cdot \left( \int_{\mathbf{V} \in \Omega} f_r(\mathbf{L}, \mathbf{V}) \cdot \cos \Theta_{\mathbf{V}} \, d\omega_{\mathbf{V}} \right) \, d\omega_{\mathbf{L}} = \\
&= \int_{\mathbf{L} \in \Omega} L_{\lambda}^{in}(\mathbf{L}) \cdot A \cdot \cos \Theta_{\mathbf{L}} \cdot \mathbf{a}_f(\mathbf{L}) \, d\omega_{\mathbf{L}} \leq \int_{\mathbf{V} \in \Omega} L_{\lambda}^{in}(\mathbf{L}) \cdot A \cdot \cos \Theta_{\mathbf{L}} \, d\omega_{\mathbf{L}} = P^{in}
\end{aligned} \tag{1.17}$$

is given for all  $L_{\lambda}^{in}$  incoming radiance distribution. Therefore, based on the indirect assumption of  $\mathbf{a}_f(\mathbf{L}) > 1$ , an  $L_{\lambda}^{in}$  sufficiently concentrated in direction  $\mathbf{L}$  led to a contradiction because of the continuity of  $\mathbf{a}_f$ .

### 1.1.4 Properties of BRDFs

#### Albedo

The previously introduced concept of albedo resembles in some way to that of the expected value in probability calculus.

$$\mathbf{a}_f(\mathbf{L}) = \int_{\mathbf{V} \in \Omega} f_r(\mathbf{L}, \mathbf{V}) \cdot \cos \Theta_{\mathbf{V}} \, d\omega_{\mathbf{V}} \tag{1.18}$$

The homogeneous, constant unit of radiance arriving from an entire half space is described by  $L_{\lambda}^{in}(\mathbf{L}) = 1$ . Therefore

$$L_{\lambda}^{out}(\mathbf{V}) = \int_{\mathbf{L} \in \Omega} 1 \cdot f_r(\mathbf{L}, \mathbf{V}) \cdot \cos \Theta_{\mathbf{L}} \, d\omega_{\mathbf{L}} = \int_{\mathbf{L} \in \Omega} f_r(\mathbf{V}, \mathbf{L}) \cdot \cos \Theta_{\mathbf{L}} \, d\omega_{\mathbf{L}} = \mathbf{a}_f(\mathbf{V}) \tag{1.19}$$

In this derivation we exploited the definition of reciprocity and albedo function. Clearly albedo indicates both the radiance response of distributed light of constant radiance (daylight) in a given direction and the "conserved" ratio of energy arriving from a given direction and reflected to the entire half space. Due to the effects of constant distributed light (diffuse daylight), the observer "directly perceives" the value of the albedo function. In this way the albedo function of numerous applications gains a direct graphic content, a visible quantity. This phenomenon may be used, for example, for visualizations with the aid of non-diffuse ambient terms by using pre-tabulated albedo functions (by Neumann et al. [49]). The albedo of a diffuse material  $f_r(\mathbf{L}, \mathbf{V}) = c$  constant BRDF is  $a(\mathbf{L}) = c \cdot \pi$ , a constant value independent of  $\mathbf{L}$ . It follows from this that the maximum permissible value of  $c$  is  $\frac{1}{\pi}$ .

#### Mean albedo

Mean albedo values relating to BRDF ( $\cos \Theta_{\mathbf{L}}$ -weighted according to energy considerations) can be interpreted even if the albedo function is not constant (defined by Neumann et al. [51]), describing the energy reflecting characteristics of a surface by a single number:

$$\mathbf{A}_f = \frac{\int_{\mathbf{L} \in \Omega} \mathbf{a}_f(\mathbf{V}) \cdot \cos \Theta_{\mathbf{L}} \, d\omega_{\mathbf{L}}}{\int_{\mathbf{L} \in \Omega} \cos \Theta_{\mathbf{L}} \, d\omega_{\mathbf{L}}} = \frac{1}{\pi} \cdot \int_{\mathbf{L} \in \Omega} \mathbf{a}_f(\mathbf{V}) \cdot \cos \Theta_{\mathbf{L}} \, d\omega_{\mathbf{L}} \tag{1.20}$$

Accordingly hemispherical-hemispherical reflectivity, or shortly **mean albedo** defines the ratio of the entire homogeneous daylight energy reflected by the surface. Of course, in different cases different weighting can be applied.

### Composition

The concept of **composition** (introduced by the author) may be used for the description of the relationship between two BRDF functions.

Definition of composition, or directional-hemispherical-directional reflectivity is:

$$C_{f_1, f_2}(\mathbf{L}, \mathbf{V}) = \int_{\mathbf{X} \in \Omega} f_1(\mathbf{L}, \mathbf{X}) \cdot f_2(\mathbf{X}, \mathbf{V}) \cdot \cos \Theta_{\mathbf{X}} \, d\omega_{\mathbf{X}} \quad (1.21)$$

The construction yields the coordination of composition  $\leftrightarrow$  correlation in parallel with the similar albedo  $\leftrightarrow$  expected value – more precisely a rebuild form of composition can accord to correlation. The  $C$  may also be visualized by physical content:  $f_r(\mathbf{L}, \mathbf{V})$  as well as  $C_f(\mathbf{L}, \mathbf{V})$  agree with the radiance response in direction  $\mathbf{V}$  produced by a system upon unit irradiance arriving from direction  $\mathbf{L}$ . But while in the case of  $f_r(\mathbf{L}, \mathbf{V})$  this system characterizes only a small part of material model  $f$ , the construction in the case of  $C_f(\mathbf{L}, \mathbf{V})$  is as follows (see figure 1.3). Light arrives on surface described by  $f_1$  from direction  $\mathbf{L}$ , from there it is reflected into the entire half space, but then it returns from the outgoing direction in unaltered intensity (having been reflected by a nearly spherical mirror) and arrives on surface described by  $f_2$  from the entire hemisphere, and finally the radiance leaving from there in direction  $\mathbf{V}$  yields the value of composition. In both cases this physical construction is a visual aid for listing, understanding and deriving properties.

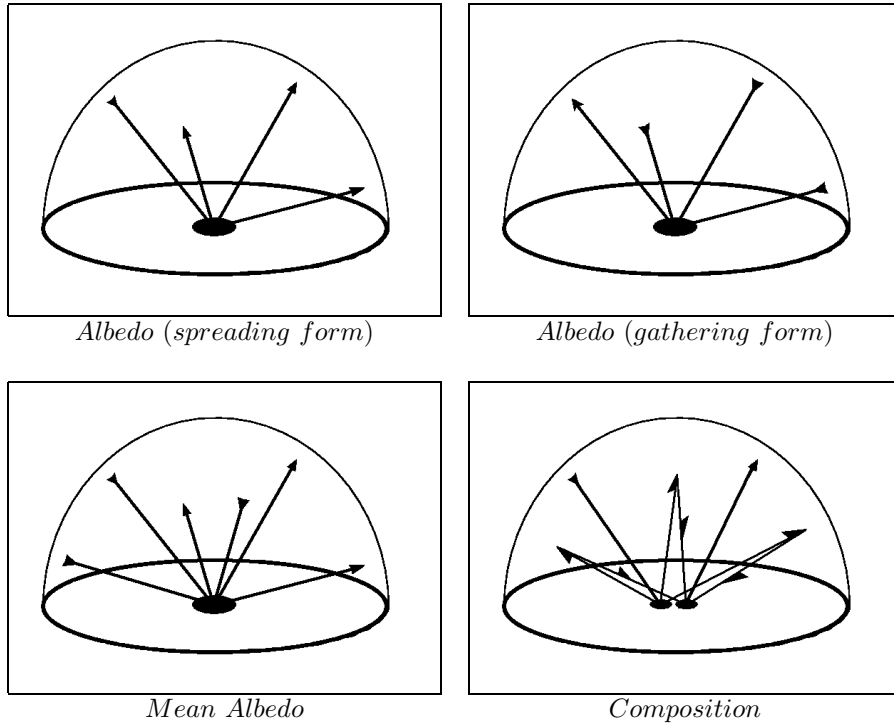


Figure 1.3: Schemes of BRDF's integral-formulae

### The relationship between composition and albedo

Of the three conditions of physical plausibility, non-negativity is an obvious characteristic of the *composition* function. However, in place of symmetry only the  $C_{f_1, f_2}(\mathbf{L}, \mathbf{V}) = C_{f_2, f_1}(\mathbf{V}, \mathbf{L})$  semi-symmetry is obtained. Thus in general  $C$  is not a BRDF and the concept of albedo for  $C$  has to be defined separately according to two variables:

$$\mathbf{a}_C^{in}(\mathbf{L}) = \int_{\mathbf{V} \in \Omega} C(\mathbf{L}, \mathbf{V}) \cdot \cos \Theta_{\mathbf{V}} \, d\omega_{\mathbf{V}} \quad \text{and} \quad \mathbf{a}_C^{out}(\mathbf{V}) = \int_{\mathbf{L} \in \Omega} C(\mathbf{L}, \mathbf{V}) \cdot \cos \Theta_{\mathbf{L}} \, d\omega_{\mathbf{L}} \quad (1.22)$$

The condition of energy balance is however fulfilled for both variables (proven by visual construction):

$$\begin{aligned} \mathbf{a}_{f_1}(\mathbf{L}) \cdot \min_{\mathbf{V} \in \Omega}(\mathbf{a}_{f_2}(\mathbf{V})) &\leq \mathbf{a}_{C_{f_1, f_2}}^{in}(\mathbf{L}) \leq \mathbf{a}_{f_1}(\mathbf{L}) \cdot \max_{\mathbf{V} \in \Omega}(\mathbf{a}_{f_2}(\mathbf{V})) \quad \text{and} \\ \min_{\mathbf{L} \in \Omega}(\mathbf{a}_{f_1}(\mathbf{L})) \cdot \mathbf{a}_{f_2}(\mathbf{V}) &\leq \mathbf{a}_{C_{f_1, f_2}}^{out}(\mathbf{V}) \leq \max_{\mathbf{L} \in \Omega}(\mathbf{a}_{f_1}(\mathbf{L})) \cdot \mathbf{a}_{f_2}(\mathbf{V}) \end{aligned} \quad (1.23)$$

It follows from the semi-symmetry of composition, that the in-out albedo values swap, that is  $\mathbf{a}_{C_{f_1, f_2}}^{in}(\mathbf{L}) = \mathbf{a}_{C_{f_2, f_1}}^{out}(\mathbf{L})$ . However, the mean albedo concerning composition is:

$$\mathbf{A}_{C_{f_1, f_2}} = \frac{1}{\pi} \cdot \int_{\mathbf{L} \in \Omega} \mathbf{a}_{C_{f_1, f_2}}^{in}(\mathbf{L}) \cdot \cos \Theta_{\mathbf{L}} \, d\omega_{\mathbf{L}} = \frac{1}{\pi} \cdot \int_{\mathbf{V} \in \Omega} \mathbf{a}_{C_{f_1, f_2}}^{out}(\mathbf{V}) \cdot \cos \Theta_{\mathbf{V}} \, d\omega_{\mathbf{V}} \quad (1.24)$$

Estimation of  $\mathbf{A}_C$  referring to  $\mathbf{a}_C^{in}$  and  $\mathbf{a}_C^{out}$  can be approximated from  $\mathbf{A}_{f_1} \cdot \mathbf{A}_{f_2}$ :

$$\begin{aligned} \max \left( \mathbf{A}_{f_1} \cdot \min_{\mathbf{V} \in \Omega} \mathbf{a}_{f_2}(\mathbf{V}), \mathbf{A}_{f_2} \cdot \min_{\mathbf{L} \in \Omega} \mathbf{a}_{f_1}(\mathbf{L}) \right) &\leq \mathbf{A}_{C_{f_1, f_2}} \quad \text{and} \\ \mathbf{A}_{C_{f_1, f_2}} &\leq \min \left( \mathbf{A}_{f_1} \cdot \max_{\mathbf{V} \in \Omega} \mathbf{a}_{f_2}(\mathbf{V}), \mathbf{A}_{f_2} \cdot \max_{\mathbf{L} \in \Omega} \mathbf{a}_{f_1}(\mathbf{L}) \right) \end{aligned} \quad (1.25)$$

Notice the cases of (serialized) composition with some special BRDF values at given f BRDF as well as cases of constant ( $diffuse = \frac{1}{\pi}$ ) reflectance (to be detailed later) and retro-reflective ideal mirror ( $RRIM(\mathbf{L}, \mathbf{V}) = \frac{\Delta_{V \cdot \mathbf{e}_L}}{\cos \Theta_{\mathbf{L}}}$ ):

$$\begin{aligned} C_{f, diffuse}(\mathbf{V}, \mathbf{L}) &= C_{diffuse, f}(\mathbf{L}, \mathbf{V}) = \mathbf{a}_f(\mathbf{L}) \quad \text{and} \\ C_{f, RRIM}(\mathbf{V}, \mathbf{L}) &= C_{RRIM, f}(\mathbf{L}, \mathbf{V}) = f(\mathbf{L}, \mathbf{V}) \end{aligned} \quad (1.26)$$

To fulfil the remaining conditions of physical plausibility, that is to achieve symmetry, function of composition has to be a BRDF. The  $f$  composed with itself (named **self-composition**) is such an example, that is  $C_{f, f}$  is a BRDF (and illustrating physical constructions can readily be produced)! The operation of self-composition is really an injection of BRDF space into itself. The composition is linear on both indices (maintaining linear composition), therefore self-composition may be regarded as a kind of quadratic derivation. An interesting research topic: which BRDF functions can be produced in this way?

A reversal of the question is; for a given  $f$  which BRDF composed with  $f$  produces a given BRDF? Such compositions are  $f$  itself and the mirror (universally) and it's easy to see that their linear compositions are appropriate as well. Mirrors and self combinations apart, which BRDF displays these properties universally? Can initial functions be recovered from such a composition by further compositions? Composition with a diffuse constant leads to loss of information, because it produces a single variable result, the identity- and coordinate-swapping transformation is obtained by the retro-reflective and reflective mirror respectively. From which compositions can the original BRDF be recovered? Does the concept of "information loss" have to be defined (with help of composition) for this?

### 1.1.5 Further BRDF properties

#### Isotropic and anisotropic BRDFs

If the pair  $(\mathbf{L}, \mathbf{V})$  is spun around axis  $\mathbf{N}$  and its value remains unaltered, we refer to them as an isotropic model; if the reverse is true, the model is said to be anisotropic. There are numerous materials with anisotropic surfaces produced at the time of their formation, and therefore they are characterized by anisotropic BRDFs, as for example at Kajiyama [34], Ward [75], Schlick [61] and Neumann et al. [51].

#### Retro-reflectivity

The reflectance model of the full moon has been investigated, because it has been found to possess a constant radiance, rather than the radiance of Lambertian materials varying along a cosine curve. Clearly reflectance backward (towards the incoming direction) exceeds the value of reflectance forward. Such backward reflectivity or retro-reflectivity was first incorporated into a model by Minneart [44]. Of models describing retro-reflectivity, the empirical Hapke–Lommel–Seeliger [27], Beard–Maxwell [5], Oren–Nayar [56] models are best known. The Neumann [51] and Lafortune [41] models also allow retro-reflectivity. However, some models (Minneart, Hapke–Lommel–Seeliger, Beard–Maxwell models) violate the principle of energy conservation.

### Transmittance, self-emission

Some surfaces are luminescent, expending energy (light source, CRT, phosphorescing materials). These are not to be confused with fluorescent materials, which fulfill the principle of energy conservation for the entire spectrum, although energy received at one wavelength may be re-emitted at another. Finally transmittance involves at least partial transmission of light as well as reflection. This is an optical property of a number of materials. Fluorescence apart these phenomena will also be covered elsewhere in this dissertation.

### Compactness, fitting, importance sampling

There are a number of important practical points to consider when applying BRDFs in computer graphics. First the computations of BRDFs should involve few operations and/or the BRDFs should be compact. Compactness means simple, closed formulae, obviously involving rapid computations. Minimum operations can also be achieved, however, by using pre-calculated data bases. Another cardinal problem is how well can a BRDF family approximate measured data even if their free parameters are appropriately adjusted? The quality of an approximation (the difference between measured and fitted value) may be assessed from the distance definitions mentioned earlier. The most important of these are the definitions based on function differences between pairs of points or between albedo differences directly measurable by the integrator sphere. The investigation of albedo may also help in controlling the fulfillment of physical plausibility conditions. Another essential property is applicability for importance sampling. This can be achieved if the direction  $\mathbf{V}$  along which the outgoing energy is distributed from  $\mathbf{L}$  is generated simply. This is an important, fundamental technique in the distributed ray tracing, random walk and Monte Carlo methods.

## 1.2 Survey of BRDFs

### 1.2.1 Application's fields, types of BRDF

The field of BRDF application is very wide, stretching far beyond computer graphics, involving remote sensing, material analysis, image processing, optics, radioactive heat transfer, astronomy, rendering, color measurement, etc. BRDFs may be used in studying speculative or theoretical, semi-empirical, empirical (decoding series or tables fitted to measured data) or physically based models. Full physical models are not known, because the exact surface geometry cannot be known. A single parameter theoretical model is used for estimating the rough surface geometry and geometric attenuation of even high precision metal models or the complex He-Torrance model. Theoretical and empirical models however can be physically plausible models if constructed with care, whereas the principle of energy conservation is usually violated in physically based models, especially at grazing angles.

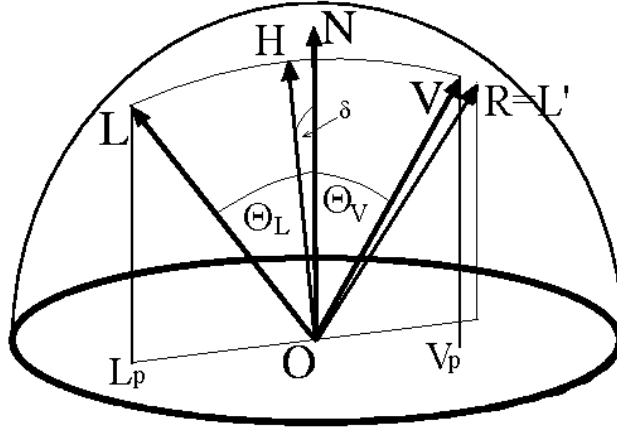


Figure 1.4: Most important notations in BRDF literature

### 1.2.2 Important notations, quantities

$\mathbf{L} = (\Theta_L, \varphi_L) = (\Theta_i, \varphi_i)$	unit vector directed to light (i=incoming)
$\mathbf{V} = (\Theta_V, \varphi_V) = (\Theta_r, \varphi_R)$	unit vector directed to viewer (r=reflected)
$\mathbf{N} = (0, \varphi)$	normal unit vector of surface ( $\varphi$ arbitrary)
$\cos \Theta_L = \mathbf{NL}$	
$\cos \Theta_V = \mathbf{NV}$	
$\mathbf{L}_p = \mathbf{L} - (\mathbf{NL}) \cdot \mathbf{N}$	vector (with length of $\sin \Theta_L$ ) points from origin to projection of $\mathbf{L}$ onto base plan
$\mathbf{V}_p = \mathbf{V} - (\mathbf{NV}) \cdot \mathbf{N}$	vector (with length of $\sin \Theta_V$ ) points from origin to projection of $\mathbf{V}$ onto base plan
$\mathbf{R} = \mathbf{L}' = 2 \cdot (\mathbf{NL}) \cdot \mathbf{N} - \mathbf{L}$	unit vector toward main mirror direction of $\mathbf{L}$
$\mathbf{RV} = \mathbf{L}'\mathbf{V} = 2 \cdot \mathbf{NL} \cdot \mathbf{NV} - \mathbf{LV}$	
$\mathbf{R}_p = \mathbf{L}'_p = -\mathbf{L}_p$	vector (with length of $\sin \Theta_L$ ) points from origin to projection of $\mathbf{R}$ onto base plan
$\mathbf{h} = \mathbf{L} + \mathbf{V}$	<i>non</i> -normalized vector having length in $[0, 2]$ interval
$\mathbf{H} = \frac{\mathbf{h}}{ \mathbf{h} } = \frac{\mathbf{L} + \mathbf{V}}{ \mathbf{L} + \mathbf{V} }$	half-way unit vector between $\mathbf{L}$ and $\mathbf{V}$
$\cos \angle(\mathbf{N}, \mathbf{H}) = \mathbf{NH} = \frac{\mathbf{NL} + \mathbf{NV}}{ \mathbf{N} + \mathbf{V} }$	
$ \mathbf{L}'_p - \mathbf{V}_p  =  \mathbf{h} - (\mathbf{N}\mathbf{h}) \cdot \mathbf{N} $	distance of projected unit vectors at viewing direction and at main mirror direction
$(\mathbf{RV})^+ = \max(0, \mathbf{RV})$	usual notation for positive part
$(\mathbf{LV})^+ = \max(0, \mathbf{LV})$	usual notation for positive part
$\alpha = \max(\Theta_L, \Theta_V)$	
$\cos \alpha = \min(\mathbf{NL}, \mathbf{NV})$	
$\beta = \min(\Theta_L, \Theta_V)$	
$\cos \beta = \max(\mathbf{NL}, \mathbf{NV})$	
$\gamma = \arccos \mathbf{LV}$	
$\delta = \arccos \mathbf{NH}$	
$(\tan \delta)^2 = \frac{\mathbf{NH}^2}{1 - \mathbf{NH}^2}$	
$s = m$	standard deviation of slope-area distribution of rough surface = root-mean-square slope of the microfacets
$\mathbf{u}, \mathbf{v}$	2 ortonormal vectors on given surface perpendicular also to $\mathbf{N}$ , that are used in anisotropic models

Other notation will be introduced contextually.

### 1.2.3 Classical BRDFs

#### Lambertian model

The ideal, diffuse material, constant BRDF of the first BRDF model, the Lambertian model:

$$f_r(\mathbf{L}, \mathbf{V}) = \text{const} \quad \text{where} \quad 0 \leq \text{const} \leq \frac{1}{\pi} \quad (1.27)$$

The albedo of this model is independent of direction. In literature on radiosity it is referred to as reflectivity. The constant value according to the definition is:

$$\mathbf{a}_{\mathbf{L}} \equiv \mathbf{a} \equiv f_r = \pi \cdot \text{const} \quad (0 \leq a \leq 1) \quad (1.28)$$

#### Ideal mirror

The ideal mirror constitutes a degenerate BRDF that cannot be interpreted in traditional functions. The  $\mathbf{V} = \mathbf{R}$  in main mirror direction yields an outgoing radiance the same as the incoming radiance in direction  $\mathbf{L}$ , with zero radiance in other direction and an albedo of unity. The mirror component is treated as a separate member in most BRDF models. In some case partial mirroring occurs, i.e. from polished surfaces. The mirror may be defined by the *Dirac* –  $\Delta$  function. The definition below may involve a somewhat unusual terminology, but the BRDF is defined by an exact, symmetric function:

$$f_r(\mathbf{L}, \mathbf{V}) = \frac{\Delta_{\mathbf{h}}(\mathbf{V})}{\cos \Theta_{\mathbf{h}}} \cdot F(\mathbf{h}) \quad (1.29)$$

where  $\mathbf{h} = \mathbf{h}(\mathbf{L}', \mathbf{V})$  is a symmetric function, for which  $\mathbf{h} = \mathbf{R}$  exclusively in the case of  $\mathbf{R} = \mathbf{L}' = \mathbf{V}$ , furthermore  $\int_{\mathbf{V} \in \Omega} \frac{\Delta_{\mathbf{h}}(\mathbf{V})}{\cos \Theta_{\mathbf{h}}} \cdot \cos \Theta_{\mathbf{V}} d\omega_{\mathbf{V}} = 1$  and  $\Delta_{\mathbf{h}}(\mathbf{V}) = 0$  if  $\mathbf{X} \neq \mathbf{R}$ . In general function  $F(\mathbf{h}) = F(\Theta_{\mathbf{h}})$  is the Fresnel function. The advantage of this definition is that in place of  $\Delta_{\mathbf{h}}$  relating to the ideal mirror it can be described by certain (e.g. only  $\mathbf{h}$  and constant dependent) traditional functions approximating  $\Delta_{\mathbf{h}}$  that represent also physically plausible BRDF functions. That is, by rewriting the definition the ideal mirror may be approximated by a real mirror. The albedo value of the mirror:

$$\mathbf{a}(\mathbf{L}) = \int_{\mathbf{V} \in \Omega} f_r(\mathbf{L}, \mathbf{V}) \cdot \cos \Theta_{\mathbf{V}} d\omega_{\mathbf{V}} = \int_{\mathbf{V} \in \Omega} \frac{\Delta_{\mathbf{R}}}{\cos \Theta_{\mathbf{R}}} \cdot F(\mathbf{R}) \cdot \cos \Theta_{\mathbf{V}} d\omega_{\mathbf{V}} = F(\mathbf{R}) \quad (1.30)$$

In the isotropic case  $\mathbf{a}(\mathbf{L}) = F(\mathbf{R}) = F(\Theta_R) = F(\Theta_L) = F(\mathbf{L})$  is obtained, that is  $\mathbf{a} = F$ .

#### Minneart model

The Minneart model is one of the oldest retro-reflective models. The author searched for the BRDF that describes the nearly constant radiance reflected by the full moon, which differs from the diffuse model.

$$f_r(\mathbf{L}, \mathbf{V}) = ((\mathbf{NL}) \cdot (\mathbf{NV}))^k \quad (1.31)$$

In Minneart's original work [44],  $-0.4 < k < -0.2$  was found to fit lunar data best, depending on the part of moon being studied. For  $k = 0$  it is a Lambertian BRDF.  $k > 1$  produces a specular peak, like the lacquer model of Neumann [48]. Minneart's model is a so called separable model. If  $k = -\frac{1}{2}$  in position  $\mathbf{L} = \mathbf{V}$ , reflected radiance would be constant: a sphere is seen as a homogeneous disc. Unfortunately this model violates the principle of energy conservation at grazing angles especially in the case of  $k < 0$  with any normalizing constant, that is characteristic of retro-reflection. The case of power  $k = 1$  is an interesting case resembling electron micrographs. In the case of  $k \geq 0$  the model can be made to obey the energy conservation principle and take a physically plausible form:

$$f_r(\mathbf{L}, \mathbf{V}) = \frac{k+2}{2\pi} \cdot ((\mathbf{NL}) \cdot (\mathbf{NV}))^k \quad \text{if } k \geq 0 \quad (1.32)$$

Therefore a maximum product constant of  $\frac{1}{\pi}$  arises in the case  $k = 0$  and  $\frac{3}{2\pi}$  in the case of  $k = 1$ . In general the listed BRDF product constants represent maximum values.



### 1.2.4 First computer graphical BRDFs

#### Phong model

After the Lambert model, first physically non-plausible models were introduced for the purpose of simple rendering, such as Phong's classical shadowing model [57], which fulfills neither the condition of reciprocity nor that of energy balance, but it visualizes well the direct effect of point sources. A version of the Phong model fulfilling the reciprocity condition is possibly the simplest model for depicting light peaks and dim mirroring. Because of its simplicity the model is still widely used even in its original form. The physically plausible version without diffuse components is:

$$f_r(\mathbf{L}, \mathbf{V}) = \frac{k+2}{2\pi} \cdot ((\mathbf{RV})^+)^n \quad (1.33)$$

#### Blinn model

The Blinn or Phong–Blinn model is another similarly simple model, which employs the half-vector and assumes a cosine distribution of microfacets [8]. A physically plausible version of this without diffuse terms is:

$$f_r(\mathbf{L}, \mathbf{V}) = C(n) \cdot ((\mathbf{NH})^+)^n \quad (1.34)$$

where the permitted maximum  $C(n)$  may be expressed in a closed but complex form. Values of  $n$  are given in some cases below:

$n = 1$	$C = 0.350$	$n = 32$	$C = 1.52$
$n = 2$	$C = 0.382$	$n = 64$	$C = 2.79$
$n = 4$	$C = 0.449$	$n = 128$	$C = 5.34$
$n = 8$	$C = 0.592$	$n = 256$	$C = 10.4$
$n = 16$	$C = 0.895$	$n = 512$	$C = 20.6$

Table 1.1: Constant factor of Blinn model at different exponents

### 1.2.5 Metal models

#### Cook–Torrance model

This is a computer graphic adaptation [14] of the Torrance–Sparrow microfacets model [71]. Even though recent investigations revealed by the author [53] this model to be imprecise at grazing angles because it violates the energy conservation principle, it is still one of the most useful, and perhaps the best known model for visualizing metals.

$$f_r(\mathbf{L}, \mathbf{V}) = \frac{D \cdot G \cdot F_\lambda}{(\mathbf{NL}) \cdot (\mathbf{NV})} \quad (1.35)$$

where  $D$  is the *microfacet distribution function*, recommended in this model by the Beckmann microfacet-model [7]:

$$D = \frac{1}{\frac{4}{\pi} \cdot \sigma^2 \cdot \cos^4 \delta} \cdot e^{-\left(\frac{\tan \delta}{\sigma}\right)^2} = \frac{1}{\frac{4}{\pi} \cdot \sigma^2 \cdot (\mathbf{NH})^4} \cdot e^{-\frac{\mathbf{NH}^2}{(1-\mathbf{NH}^2) \cdot \sigma^2}} \quad (1.36)$$

Other microfacet distributions may also be applicable, since the distributions and dimensions of these are the subject of very rough assumptions in many models. In general they are characterized by a single free parameter. Therefore the  $D$  and the more recent  $G$  functions include a number of arbitrary assumptions. All physically based models are really semi-speculative in nature, because microfacets cannot be described exactly owing to their microscopic geometry. Their behavior at grazing angles becomes confusing and consequently many turn out to be non-physical, violating the principle of energy balance.

The application of many simple distributions is recommended for  $D$  (the facet slope distribution function).

- Torrance's [73] distribution function:  $D = \text{const} \cdot e^{-(s \cdot \delta)^2}$
- Trowbridge's [74] distribution function:  $D = \left( \frac{q^2}{1+(q^2-1) \cdot \cos^2 \delta} \right)^2$

- Blinn's [8] proposal:  $D = \text{const} \cdot \cos^t \delta$

Where  $s$ ,  $t$  and  $q$  values empirically determine the width of spectral lobe. As Blinn [8] observes, if we define  $g$  to be the value of  $d$  at which a distribution drops to half its peak value, we have

- $s = -\frac{\log 2}{\log \cos \gamma}$
- $q = \sqrt{\frac{\cos^2 \gamma - 1}{\cos^2 \gamma - \sqrt{2}}}$
- $t = \sqrt{\frac{\log 2}{\gamma}}$

Finally in the case of Beckmann distribution  $\sigma$  (frequently denoted as  $m$ ):

- $s = \frac{\tan \gamma}{\sqrt{\log 2 - 4 \cdot \log \cos \gamma}}$

Therefore using the above relationships, the shape of light peaks can be adjusted to be similar. Function  $G$  is the *geometrical attenuation factor*:

$$G = \min \left( 1, 2 \cdot \frac{\mathbf{NH}}{\mathbf{VH}} \cdot \mathbf{NL}, 2 \cdot \frac{\mathbf{NH}}{\mathbf{VH}} \cdot \mathbf{NV} \right) \quad (1.37)$$

This is the best known geometrical attenuation factor, which describes the effect of microfacets masking and shadowing each other. The value of  $G$  lies in the  $[0, 1]$  interval. Such a  $G$  construction cannot be continuously derived. Many other shadowing/masking factors have appeared in the literature. Of these, the one due to Smith [64] is continuous in all derivatives and has been found to agree with statistical numerical simulations of a *Gaussian* rough surface. The function has appropriate smoothness and symmetry.

The He–Torrance model uses this  $G$  function too:

$$G(\mathbf{N}, \mathbf{L}) = G^*(\mathbf{NL}) \cdot G^*(\mathbf{NV}) \quad (1.38)$$

where  $G^*(x) = \frac{g}{g+1}$ ,  $g = \sqrt{\pi \cdot h} \cdot (2 - \text{erfc}(\sqrt{h}))$  and  $h = \frac{x^2}{2 \cdot m^2 \cdot (1 - x^2)}$

Finally the  $F_\lambda$  factor of the Cook–Torrance model is the wavelength dependent *Fresnel function*. For this, first take the complex index of refraction at given  $\lambda$  wavelength:

$$\mathbf{n} = n - i n \kappa = n - ik \quad (1.39)$$

where  $n = \frac{\lambda_0}{\lambda}$  is the ratio of wavelengths in vacuum and study medium,  $\kappa$  is the absorption index of the metal, and  $k$  is the extinction coefficient. If  $\mathbf{H}$  is the normal of an actual microfacet selected with  $D$  distribution function,  $\Theta_{\mathbf{HL}}$  is the incident angle relative to  $\mathbf{H}$  and  $\Theta_{\mathbf{HT}}$  is the angle of refraction, for dielectrics in cases of real refraction index:  $\sin \Theta_{\mathbf{HT}} = n \cdot \sin \Theta_{\mathbf{HL}}$  (according to the *Snellius–Descartes law* of refraction). The measurement of  $n$  and  $k$  is difficult, because the surface structure of metals may differ in an undeterminable manner and extent from the ideal surface of a pure metal due to polishing, cleaning, oxidation, etc. Data for several metals at certain wavelengths are listed below for the purpose of demonstration:

Metal	$\lambda$ [nm]	$n$	$k$	$a_0 = \rho$
Aluminium	578	0.93	6.33	91.5
Gold	550	0.331	2.324	81.5
Silver	589	0.18	3.64	95.1
Mercury	600	1.39	4.32	77.2
Chromium	579	2.97	4.58	69.8
Nickel	589	1.79	3.33	62.1
Platinum	589	2.06	4.26	70.1

Table 1.2: Parameters of different metals

Here  $\mathbf{a}_0$  ( $= \rho$ ) is the fraction of reflected energy at perpendicular incidence, that is in the position of *albedo* = 0:

$$\mathbf{a}_0 = \rho = \frac{(n-1)^2 + k^2}{(n+1)^2 + k^2} \quad (1.40)$$

The *Fresnel equation* expressing the ratio of the energy of the reflected beam and the energy of the incident beam for directions parallel and perpendicular to the electric field:

$$F_{\perp} = \left( \frac{\cos \Theta_{\mathbf{HL}} - (n - ik) \cdot \cos \Theta_{\mathbf{HT}}}{\cos \Theta_{\mathbf{HL}} + (n - ik) \cdot \cos \Theta_{\mathbf{HT}}} \right)^2 = \left( \frac{\mathbf{HL} - n \cdot \mathbf{HT}}{\mathbf{HL} + n \cdot \mathbf{HT}} \right)^2 \quad (1.41)$$

$$F_{\parallel} = \left( \frac{\cos \Theta_{\mathbf{HT}} - (n - ik) \cdot \cos \Theta_{\mathbf{HL}}}{\cos \Theta_{\mathbf{HT}} + (n - ik) \cdot \cos \Theta_{\mathbf{HL}}} \right)^2 = \left( \frac{\mathbf{HT} - n \cdot \mathbf{HL}}{\mathbf{HT} + n \cdot \mathbf{HL}} \right)^2 \quad (1.42)$$

These equations can be derived from *Maxwell's* fundamental formulae describing the basic laws of electromagnetic waves. If light is unpolarized, that is, the parallel and perpendicular electric field have the same amplitude, the total reflectivity is:

$$F = F(\lambda, \Theta_{\mathbf{HT}}) = \frac{F_{\parallel} + F_{\perp}}{2} \quad (1.43)$$

The Fresnel function is known for numerous materials and wavelengths. Cook–Torrance proposed formulae of approximation in cases when no other information is available than perpendicular illumination and the value of reflection at observer's location,  $F_{0,\lambda}$ . For non-metals  $k = 0$ . When lacking data metals are described by a model with real refraction index:  $k = 0$  as with non-metals.

In general models are derived from perpendicular and horizontal incidental positions, i.e. from the  $F(\lambda, 0)$  and  $F(\lambda, \frac{\pi}{2})$  representations. The values of  $F_{0,\lambda} = F(\lambda, 0) = \mathbf{a}_0 = \rho$  are measurable (these values were listed in the table 1.2); the original, complex refractivity  $\mathbf{n}$  is replaced by  $\mathbf{n}^*$  :

$$\mathbf{n}^* = \frac{1 + \sqrt{F_{0,\lambda}}}{1 - \sqrt{F_{0,\lambda}}} = \frac{1 + \sqrt{r}}{1 - \sqrt{r}} \quad (1.44)$$

$$\left( \frac{1 - (n - ik)}{1 + (n - ik)} \right)^2 = \frac{(n - 1)^2 + k^2}{(n + 1)^2 + k^2} = \left( \frac{\mathbf{n}^* - 1}{\mathbf{n}^* + 1} \right)^2 \quad (1.45)$$

On the other hand in a horizontal case obviously  $F(\lambda, \frac{\pi}{2}) = 1$ . Between these two cut-off points the Fresnel equation for dielectrics can be applied or various simple estimations are used. The simplest way is linear approximation, which can be applied up to three color channels, according to the model's designers. The Schlick approximation is also known [60].

### Ward model

The Ward model is a simplified version of the Cook–Torrance model, preserving its metallic properties [75]. The non-diffuse, metallic highlight component:

$$f_r(\mathbf{L}, \mathbf{V}) = \frac{D}{\sqrt{\mathbf{NL} \cdot \mathbf{NV}}} , \quad \text{where} \quad (1.46)$$

$$D = \frac{1}{4 \cdot \pi \cdot \sigma^2} \cdot e^{-\left(\frac{\tan \delta}{\sigma}\right)^2} = \frac{1}{4 \cdot \pi \cdot \sigma^2} \cdot e^{-\left(\frac{\mathbf{NH}^2}{(1 - \mathbf{NH}^2) \cdot \sigma^2}\right)^2}$$

This is the Cook–Torrance model (equation 1.35) without terms for

1. division by the  $\mathbf{NH}^4$  factor of microfacet distribution function  $D$  in equation 1.36
2. the complex  $G$  geometric attenuation factor, and
3. the Fresnel function, which is needed in some form or another for the visualization of non-ferrous metals even if it is grossly simplified.

Note that this model violates the principle of energy conservation at grazing angles as the author has recognised it [53]. Despite simplifications this is, nevertheless, a highly usable model. Ward has also introduced its anisotropic version:

$$D = \frac{1}{4 \cdot \pi \cdot \sigma_x \sigma_y} \cdot e^{-\tan^2 \delta \cdot \left( \frac{\cos^2 \varphi}{\sigma_x^2} + \frac{\sin^2 \varphi}{\sigma_y^2} \right)} \quad (1.47)$$

where the  $\sigma_x$  and  $\sigma_y$  are the standard deviations of surface slope in  $x$  and  $y$  directions, the  $\varphi$  is the azimuth angle of the half vector projected into the surface plane.

A computationally convenient approximation for BRDF using diffuse component:

$$f_r(\mathbf{L}, \mathbf{V}) = \frac{\mathbf{a}_D}{\pi} + \frac{\mathbf{a}_S}{\sqrt{\mathbf{NL} \cdot \mathbf{NV}} \cdot (4 \cdot \pi \cdot \sigma_x \sigma_y)} \cdot e^{-2 \cdot \frac{\left(\frac{\mathbf{Hu}}{\sigma_x}\right)^2 + \left(\frac{\mathbf{Hv}}{\sigma_y}\right)^2}{1 + \mathbf{NH}}} \quad (1.48)$$

where the  $\mathbf{a}_D + \mathbf{a}_S \leq 1$  condition must be satisfied. In this way in the case of  $\sigma < 0.2$ , as recommended by Ward (ignoring energy violations at grazing angles, that limit the permitted level of illumination), the condition of energy balance is closely fulfilled.

### He–Torrance model

This is the most important and complex physically based model, which has been developed for the description of metals. It has been constructed from diffuse, "directional-diffuse" and mirror components. Its albedo properties especially at grazing angles have not been studied. Because of their complexity its constituent formulae will not be listed in this dissertation (in all 86 numbered formulae are described in the original publication [29]). Its running time is 75 times that of the Ward model. A simplified version of the He–Torrance model is found in an earlier publication of Schlick [61].

The He–Torrance model has been characterized as follows, by Rusinkiewicz [59]:

Over the past twenty years, a variety of physically-based BRDF models of increasing sophistication have been proposed. We will look closely at one of the more recent, and more complex models in this series, namely that proposed by He and Torrance [29]. This model contains most of the features common to these models, starting with specific assumptions about surface microgeometry, and considering factors such as self-shadowing, Fresnel reflection, the effects of the wave nature of light, and subsurface scattering. The result is a model with a small number of parameters that can, at least in theory, be monitored from an actual surface. Most of the currently popular theoretical models start with the assumption that the large-scale BRDF is the result of fine-scale roughness of the surface. This roughness is described by a collection of microfacets with random sizes and orientations. The statistical distribution of sizes has traditionally been taken to be Gaussian, because this distribution is easy to work with and has many mathematically desirable properties. Each facet is taken to be a perfect reflector, obeying the physical laws of reflection for dielectrics. It is assumed that light can interreflect off of several facets before leaving the surface, and that the facets, due to their orientations, can occlude each other. In addition, He's model assumes that the facets might be of size comparable to the wavelength of light. This means that the wave nature of light, and hence phenomena such as interference, must be taken into account. The final model for the BRDF is extremely complex, but agrees well with actually measured BRDFs. This model does a good job of accounting for the many physical phenomena seen as a result of a rough-surface modeling, and predicts actually observed phenomena better than older, simpler models. It cannot, however, make any predictions for surfaces that cannot be modeled as having randomly oriented microfacets. In particular, it cannot model any non-isotropic surfaces. These are surfaces, such as woven cloth or brushed aluminum, for which the BRDF is not independent of azimuth. Therefore, He's model, despite its complexity, is clearly inadequate for predicting all BRDFs that could potentially be of interest in computer graphics.

### Schlick models

Schlick simplified the Cook–Torrance model by incorporating easily computable functions but also developed his own empirical/speculative model ([60], [61]). His models can be made physically plausible. According to the non-diffuse component of the version that includes anisotropy [60]:

$$f_r(\mathbf{L}, \mathbf{V}) = \frac{Z(\mathbf{NH}) \cdot A(w) \cdot G(\mathbf{NL}) \cdot G(\mathbf{NV})}{4 \cdot \pi \cdot (\mathbf{NL}) \cdot (\mathbf{NV})} \quad (1.49)$$

$$\text{with } Z(\mathbf{NH}) = \frac{r}{(1 - (1 - r) \cdot (\mathbf{NH})^2)^2}$$

The  $A(w) = \sqrt{\frac{p}{p^2 + (1 - p^2) \cdot w^2}}$  serves to describe anisotropy with the  $w(\varphi_L, \varphi_V)$  direction parameter. The  $p = 1$  indicates perfect isotropy,  $p = 0$  indicates perfect anisotropy, the *Dirac* –  $\Delta$  function. The geometrical attenuation factor  $G$  is a component of symmetric product function, a practical and simple

approximation of the function introduced by Smith [64]:  $G(x) = \frac{x}{r+(1-r)x}$  (where  $x = \mathbf{NL}$  or  $x = \mathbf{NV}$  and  $r$  is a parameter of model).

Next, the part of BRDF is simplified that lies outside its  $Z \cdot A$  factor:

$$\frac{G(\mathbf{NL}) \cdot G(\mathbf{NV})}{4 \cdot \pi \cdot (\mathbf{NL}) \cdot (\mathbf{NV})} = \frac{1}{4 \cdot \pi \cdot (r + (1-r) \cdot \mathbf{NL}) \cdot (r + (1-r) \cdot \mathbf{NV})} \quad (1.50)$$

The behavior of light peaks may be investigated by studying them in isotropic models. If parameter  $r$  characterizing surface smoothness decreases, light peaks increase to unrealistic levels. As free parameter  $r$  approaches zero, the ratio of reflected/incoming radiance (in case of directions approaching the horizontal) approaches infinity, instead of around 1 characterizing metals. Here is a demonstration of the phenomenon of grazing angles.

The *albedo* may freely exceed the value of 1 according to the description of the model above. Therefore the model in its original form is not physically plausible. In a corrected form the albedo is greatly reduced in cases of highly polished metals receiving illumination from normal direction. All this causes no great problems, if the model is not used for computing multiple reflections in an exacting manner and it is an anisotropic metal model, which can be treated simply. This is analogous to the practical usefulness of the Ward model.

### Stam model

Stam bases his model on the *Kirchhoff-integral* takes also wavelength into consideration formalizing Huygens' principle, and treats an arbitrary height-function-defined structure of surface [67]. This is the first physically based general BRDF-definition, which takes wavelength into account as well. In addition, it can be taken as a common generalization of earlier approximative models (Ward, Cook-Torrance, He-Torrance, Schlick), and handles "arbitrary structure" of surface in a natural manner, involving anisotropy as well. The formula is:

$$f_r(\mathbf{L}, \mathbf{V}) = F^2 \cdot \frac{G}{w^2} \cdot \left( \frac{k^2}{4 \cdot \pi^2} \cdot S_p(k \cdot u, k \cdot v) + |\langle p \rangle|^2 \cdot \delta(u, v) \right) \quad (1.51)$$

- $F$  is the *Fresnel factor*,
- $G = \frac{(1-\mathbf{LV})^2}{(\mathbf{NL}) \cdot (\mathbf{NV})}$  is the geometrical factor,
- $(u, v, w) = \mathbf{L} - \mathbf{V}$  in local coordinate-system of surface - i.e. with  $(0, 0, 1)$  surface-normal vector,
- $k = \frac{2 \cdot \pi}{\lambda}$  is the *wavenumber*,
- $\delta$  notation signs here the *Dirac -  $\Delta$*  function,
- $\langle . \rangle$  signs average (over considered local area) and
- $|\cdot|$  signs absolute value of a (complex) number.

$p$  and  $S_p$  describe the structure of surface, being the central concepts of Stam's derivation, since

- $p(x, y) = e^{ikwh(x,y)}$  with  $h(x, y)$  surface-function, while surface's points are  $(x, y, h(x, y))$
- $C_p(x', y') = \langle p^*(x, y) \cdot p(x + x', y + y') \rangle - |\langle p \rangle|^2$  is the *correlation-function* of  $p$ , and
- $S_p(u, v)$  is the *spectral density*, it is the Fourier transformed of  $C_p$ .

In this general form  $p$  can be defined e.g. by a correlation-function following any (anisotropic) probability density, and derivation can be completed on it. This way, the surface of a compact disc has been implemented.

The attenuation factor involving effects of occlusions can also be added, and interreflections have to be treated in further research as well. A more serious defect occurs in the derivation (pp.103. Eq.4 in [67]) where the effect of incoming or outgoing direction lying on the invisible back-side of half-space pointed out by the normal-vector of an actual point on the curved surface is counted into the integral with nonzero value whereas their opposite directions are ignored at the same time. This fact makes the final closed form of general description theoretically incorrect. The correct derivation is certainly more complicated, but an additional occlusion factor can correct this miscalculation in practice.

## 1.2.6 Empirical, semi-empirical models

### Hapke–Lommel–Seeliger model

The Hapke–Lommel–Seeliger BRDF [27] was also developed to model the Lunar surface. It deviates from Lambert's law at large angles and has provisions for retro-reflection (the opposition effect) and strong forward or backward scattering. The BRDF is given (at  $\gamma = \arccos(\mathbf{LV})$ ) by

$$f_r(\mathbf{L}, \mathbf{V}) = \frac{\rho}{\pi} \cdot \frac{R_f(g, g) \cdot S(g)}{(\mathbf{N}, \mathbf{L}) \cdot (\mathbf{N}, \mathbf{V})} \quad (1.52)$$

$$\text{where } R_f(g, g) = \begin{cases} 2 - \frac{\tan g}{2 \cdot g} \cdot (1 - e^{-\frac{g}{\tan g}}) \cdot (3 - e^{-\frac{g}{\sin g}}) & \text{if } g > \frac{p}{2} \\ 1 & \text{otherwise} \end{cases}$$

$g$  is the ratio of separation between scatter and  $e^{-1}$  the attenuation length.  $S$  is the scattering function whose form depends on the predominant type of scattering. For forward scattering:

$$S(g) = \frac{4}{9} \cdot (1 - \frac{1}{2} \cdot \cos g) \quad (1.53)$$

for isotropic scattering the function is unity, and for back scattering

$$S(g) = \frac{\sin g - (p - g) \cdot \cos g}{p} \quad (1.54)$$

### Beard–Maxwell model

The Beard–Maxwell model [5] is an empirically based model developed to characterize the BRDF of paint coatings. It is a six parameter model assuming that the primary surface scattering can be modeled by Fresnel reflection from randomly oriented facets and the diffuse scattering can be modeled by the sum of Lambertian an *isotropic Hapke–Lommel–Seeliger* BRDF.

$$f_r(\mathbf{L}, \mathbf{V}) = \frac{\rho_D}{\pi} + f_{FIRST}(\mathbf{L}, \mathbf{V}) \cdot \frac{F(\delta) \cdot (\mathbf{N}, \mathbf{H})^2}{F(0) \cdot (\mathbf{NL}) \cdot (\mathbf{NV})} \cdot \frac{1 + \delta}{1 + \frac{\delta}{\Omega} \cdot e^{-\frac{\tau}{\Omega}}} + 2 \cdot \frac{\rho_V}{(\mathbf{NL}) + (\mathbf{NV})} \quad (1.55)$$

Where parameters :

- $n - ik$  is the complex refractive index of the coating binder,
- $\rho_D = a_D$  is the albedo or reflectivity of diffuse component of the BRDF,
- $\rho_V$  is the volumetric component of the BRDF,
- $f_{FIRST}(\mathbf{L}, \mathbf{V})$  is the first surface BRDF,
- $\Omega$  and  $\tau$  are two shadowing and obscuration function parameter,
- $g = \arccos \mathbf{LV}$  ,
- $\delta = \arccos \mathbf{NH}$  .

The Fresnel reflectance  $F(\cdot)$  introduces polarization effects into the model. The refractive index parameters used to compute Fresnel reflectance can be determined by either measuring the Brewster angle or by fitting polarized measurements to Fresnel relations. The first surface BRDF is obtained from near-zero bistatic ( $\Omega_L = \Omega_V$ ) polarimetric measurements. It is assured that the reflected energy is not depolarized if it reflects from the top surface but is completely depolarized if it reflects from the subsurface. Thus the energy reflected by the top surface is taken to be the difference between the co-polarized and obscuration function. The parameters are estimated by fitting this function to the ratio of the measured data and the BRDF model without the shadowing and obscuration function. The first and third terms in this model are Lambertian and volumetric scattering components. They are determined by fitting them to near-zero bistatic cross-polarized data.

### Oren–Nayar model

In Oren–Nayar model [56] the surface is modeled as a collection of Lambertian facets. The model accounts for complex geometric and radiometric phenomena such as masking, shadowing, and interreflections between samples of rough diffuse surfaces, such as, plaster, sand, clay, and cloth. All these surfaces demonstrate significant deviation from Lambertian behavior. The reflectance measurements obtained are in strong agreement with the reflectance predicted by the model. In a practical, simplified version of the model, small value elements of interreflections between diffuse microfacets are neglected, as is another small component:

$$\begin{aligned} f_r(\mathbf{L}, \mathbf{V}) &= \frac{\rho}{\pi} \cdot (A + B \cdot (\cos(\varphi_{\mathbf{V}} - \varphi_{\mathbf{L}}))^+ \cdot \sin \alpha \cdot \tan \beta) = \\ &= \frac{\rho}{\pi} \cdot \left( A + B \cdot \frac{(\mathbf{LV} + (\mathbf{NL}) \cdot (\mathbf{NV}))^+}{\max(\mathbf{NL}, \mathbf{NV})} \right) \end{aligned} \quad (1.56)$$

where  $A = 1 - \frac{\frac{1}{2} \cdot \sigma^2}{\frac{1}{2} + \sigma^2}$ ,  $B = \frac{0.45 \cdot \sigma^2}{0.09 + \sigma^2}$

The content of  $\sigma$  measured in radians: standard deviation of slope area distribution of rough surface, a collection of Lambertian facets. In case of  $A$ , the condition that the albedo of the Lambertian part does not exceed 1 (or a value of  $\rho$ ) is fulfilled; in case of  $\sigma = 0$ , smooth white surface, albedo approaches 1, the value for diffuse white material. The above simplifications can only be made for illumination at grazing angles, therefore it is not a satisfactory model. This is because in the case of  $\cos(\varphi_{\mathbf{V}} - \varphi_{\mathbf{L}})$  negativity there is no retro-reflective tag. At near perpendicular illumination this could lead to a rather disturbing degradation, as the non-retro-reflective half space contains only the Lambert component.

A less simplified form of this BRDF consists of two part:

$$f_r(\mathbf{L}, \mathbf{V}) = f_r^I(\mathbf{L}, \mathbf{V}) + f_r^{II}(\mathbf{L}, \mathbf{V}) \quad (1.57)$$

The first component describes the surface without interreflections between surface facets:

$$\begin{aligned} f_r^I(\mathbf{L}, \mathbf{V}) &= \frac{\rho}{\pi} \cdot \left( A + B \cdot \frac{\mathbf{LV} + (\mathbf{NL}) \cdot (\mathbf{NV})}{\max(\mathbf{NL}, \mathbf{NV})} + B \cdot Q(\mathbf{L}, \mathbf{V}) + \right. \\ &\quad \left. + \frac{5}{18} \cdot B \cdot (1 - |\cos(\varphi_{\mathbf{V}} - \varphi_{\mathbf{L}})|) \cdot \left( \frac{4 \cdot \alpha \beta}{\pi^2} \right)^2 \cdot \tan \frac{\alpha + \beta}{2} \right) \end{aligned} \quad (1.58)$$

$$\text{where } Q(\mathbf{NV}) = \begin{cases} -\cos(\varphi_{\mathbf{V}} - \varphi_{\mathbf{L}}) \cdot \left( \frac{2 \cdot \beta}{\pi} \right)^3 \cdot \tan \beta & \text{if } (\mathbf{LV} + (\mathbf{NL}) \cdot (\mathbf{NV}))^+ = 0 \\ 0 & \text{otherwise} \end{cases}$$

In condition  $(\mathbf{LV} + (\mathbf{NL}) \cdot (\mathbf{NV}))^+ = 0$  is equivalent to  $\cos(\varphi_{\mathbf{V}} - \varphi_{\mathbf{L}}) < 0$ . In  $f_r^I(\mathbf{L}, \mathbf{V})$  the formation of positive part in its first member was omitted!

The second component describes effects of interreflections:

$$\begin{aligned} f_r^{II}(\mathbf{L}, \mathbf{V}) &= C \cdot \frac{\rho}{\pi} \cdot \left( \cos(\varphi_{\mathbf{V}} - \varphi_{\mathbf{L}}) \cdot \left( \frac{2 \cdot \beta}{\pi} \right)^2 \right) \\ \text{where } C &= 0.17 \cdot \frac{\sigma^2}{0.13 + \sigma^2} \end{aligned} \quad (1.59)$$

## 1.2.7 Mutiple-Layer Models

### Phong model

Certain models with surface layer(s) constitute an important class of BRDFs that, in addition to light absorption, also account for the phenomenon of scattering light due to particles in the layer. Of the classical models the Kubelka–Munk (see at Wyszecky and Stiles [78]), Hanrahan–Krueger [26] models do not yield simple, practical, closed format BRDFs. The Hapke–Lommel–Seeliger [27] and the Beard–Maxwell models [5] described previously yield the effect of scattering very empirically by the control of a single free parameter. Actually the solution of this problem in a simple, relatively generalized, closed form does not seem possible. Therefore the two simple models of closed form discussed next will not include scattering.

### Lacquer model

The class of *separable material models* defined by Neumann et al. [48] compares in complexity (quantity of information) with that of diffuse models, is the most general such BRDF class and the lacquer model is given as a concrete example, composed of a white diffuse surface covered by a layer of lacquer:

$$f_r(\mathbf{L}, \mathbf{V}) = \frac{1}{\pi} \cdot e^{-s \cdot (\frac{1}{\mathbf{NL}} + \frac{1}{\mathbf{NV}})} \quad (s \leq 0 \text{ const}) \quad (1.60)$$

Absorption in lacquer layer at perpendicular illumination ( $\mathbf{L} = \mathbf{N}$ ) and viewing direction ( $\mathbf{V} = \mathbf{N}$ ), yields  $f_r(\mathbf{N}, \mathbf{N}) = e^{-2 \cdot s}$ . Light bouncing to and fro in the lacquer layer is attenuated by this multiplication factor. The case of  $s = 0$  is the model of white diffuse base layer without lacquer.

In practice the boundary layer of lacquer reflects light. By neglecting the interreflection of light at a given wavelength between the base BRDF and boundary surface the following model is obtained:

$$f_r(\mathbf{L}, \mathbf{V}) = F(\Theta_{\mathbf{H}}) \cdot \frac{\Delta(\Theta_{\mathbf{H}})}{\cos \Theta_{\mathbf{H}}} + (1 - F(\Theta_{\mathbf{H}})) \cdot e^{-s \cdot (\frac{1}{\mathbf{NL}} + \frac{1}{\mathbf{NV}})} \cdot f_r^{BASE}(\mathbf{L}, \mathbf{V}) \quad (1.61)$$

where  $f_r^{BASE}(\mathbf{L}, \mathbf{V})$  is an optional BRDF which the lacquer layer covers. Details of mirror components are covered in this thesis in the section headed "Mirror".

If the changes in Fresnel component are considerable, interesting effects can be obtained. For example, if a material is coated with a thin layer of color glass, the Fresnel component converges to 0.04 at perpendicular incidence and to 1 when approaching the angle of perpendicular incidence. Therefore the mirror effect dominates at grazing angles if background lighting is evenly distributed. This is because the lacquer layer attenuates reflected light from the base layer due to absorption, which increases steeply with  $\Omega_{\mathbf{L}}$  or  $\Omega_{\mathbf{V}}$ . With a multi-spectral approach very interesting color transitions can be obtain in this model. The fact that lacquer activity declines the least at the peak of spectral curve can be exploited, although the point of maximum may be far from the characteristic wavelength of lacquer at perpendicular incidence. For example, the latter occurs at yellowish color, whereas the maximum at turquoise. The color of reflection due to the refraction index can be strongly wavelength dependent, as is the base layer. The model yields an elegant effect in case of a base surface of dark unsaturated color and a lacquer of low absorption, when mirroring becomes a dominant but nevertheless not an exclusive phenomenon.

### Sandwich models

Models can be prepared from numerous layers of lacquer. In such a case underneath each other lie layers of lacquer and a semi-transparent layers. The latter can be illustrated by an infinitely thin and wholly transparent flat sheet that is composed of patches that are characterized by a given BRDF  $f_r^{BASE}$  and distributed arbitrarily fine. Assume that the back of each fleck is ideally black, causing no interreflection between layers. For a layer-pair a given  $\varepsilon$  part of the surface reflects light according to  $f_r^{BASE}$  and the  $1 - \varepsilon$  part of the light energy passes through the lacquer layer, then absorbed at a rate characteristic of each wavelength. In case of more layer-pairs each layer reflects and absorbs some light energy as well. Thus light rays arising from deep layers are quickly attenuated. A version of the model constituting an infinite number of layers may be constructed. For this model the  $k$  ( $> 0$ ) parameter may be given instead of  $\varepsilon$  and  $s$ , because both the value of  $\varepsilon$ , and  $s$  may be approximated by zero in a boundary value case. The  $k$  parameter indicates the ratio of reflected light energy by a given layer and light absorption by the layer underneath, in case of perpendicular illumination. The "limit sandwich" model may is derived by Neumann et al. [47] as:

$$f_r(\mathbf{L}, \mathbf{V}) = \frac{f_r^{BASE}(\mathbf{L}, \mathbf{V})}{2 + k \cdot (\frac{1}{\mathbf{NL}} + \frac{1}{\mathbf{NV}})} \quad (1.62)$$

The  $k = k(\lambda)$  is wavelength dependent. As the angle of incidence increases, the absorption effect of lacquer layers will occur at any small  $k$  value, even if not at an exponential rate as in the case of a single layer model. Of course, the above theoretical model may also be constructed recursively, that is the flecks can also be composed of higher order multi-sandwich models. The version of  $n$ -th order:

$$f_r^{(n)}(\mathbf{L}, \mathbf{V}) = \frac{f_r^{BASE}(\mathbf{L}, \mathbf{V})}{(2 + k \cdot (\frac{1}{\mathbf{NL}} + \frac{1}{\mathbf{NV}}))^n} \quad (1.63)$$

Even if  $n = 1$  the new model is going to be at least twice as dark as the base model. The situation gets rapidly worse for models of higher order. Therefore, breaking with physically demonstrative constructions, these models should be enhanced by a multiplication constant till the albedo reaches 1 at  $\mathbf{L} = \mathbf{N}$ .



### 1.2.8 Physically Plausible Constructions

#### Lafortune Model

The specular form of the classical symmetric Phong model has been generalized by Lafortune et al. [41]:

$$f_r(\mathbf{L}, \mathbf{V}) = C \cdot (\mathbf{R}\mathbf{V})^n = C \cdot (\mathbf{L} \cdot (2 \cdot \mathbf{N}^0 \mathbf{N}\mathbf{T} - \mathbf{I}) \cdot \mathbf{V})^n \quad (1.64)$$

The cosine can be expressed as a dot product, and as mentioned by Arvo [3], mirroring around the normal  $\mathbf{N}$  can be written using a Hausholder matrix: (binary product, mirroring matrix). The zero value has to be taken in stead of negative cosine. Lafortune's observation is, that this equation can be generalized by replacing the Hausholder transform together with the normalization factor by a general  $3 \times 3$  matrix  $\mathbf{M}$ :

$$f_r^*(\mathbf{L}, \mathbf{V}) = \mathbf{L}^T \cdot \mathbf{M} \cdot \mathbf{V} \quad (1.65)$$

where we assume that the direction vectors are defined with respect to a fixed local coordinate system at the surface. In order for this reflectance function to be reciprocal, the matrix has to be symmetrical:  $\mathbf{M} = \mathbf{M}^T$ . We can apply a singular value decomposition of  $\mathbf{M}$  into  $\mathbf{Q}^T \cdot \mathbf{D} \cdot \mathbf{Q}$ . This yields the transformation  $\mathbf{Q}$  for going into a new local coordinate system, in which the matrix simplifies to a diagonal matrix  $\mathbf{D}$ . Except for unusual types of anisotropy the axes are aligned to the normal and to the principal directions of anisotropy. The diagonal matrix can be seen as weighting the terms of the dot product  $\mathbf{L}\mathbf{V}$ :

$$f_r(\mathbf{L}, \mathbf{V}) = (C_x \cdot L_x \cdot V_x + C_y \cdot L_y \cdot V_y + C_z \cdot L_z \cdot V_z)^n \quad (1.66)$$

This formulation of the model is convenient to use in the case of isotropic reflection,  $C_x = C_y$ . The original cosine lobe model was obtained by choosing  $C_x = C_y = -C_z = -C^{\frac{1}{n}}$ . The generalized function has a very practical property: for each given incident direction  $\mathbf{L}$  the function can be rewritten as a scaled version of an ordinary cosine lobe. The direction  $\mathbf{L}^* = \frac{\mathbf{L}^T \cdot \mathbf{M}}{\|\mathbf{L}^T \cdot \mathbf{M}\|}$  is a transformed and normalized version of incident direction  $\mathbf{L}$ . The scaling factor  $C(\mathbf{L}) = \|\mathbf{L}^T \cdot \mathbf{M}\|^n$  is a power function of the normalization factor and therefore varies with incident direction. For the specific direction

$$\mathbf{L}^* = \frac{(C_x \cdot L_x, C_y \cdot L_y, C_z \cdot L_z)}{\sqrt{C_x^2 \cdot L_x^2 + C_y^2 \cdot L_y^2 + C_z^2 \cdot L_z^2}} \quad (1.67)$$

and the scaling factor

$$C(\mathbf{L}) = \sqrt{C_x^2 \cdot L_x^2 + C_y^2 \cdot L_y^2 + C_z^2 \cdot L_z^2} \quad (1.68)$$

This observation shows how the original cosine lobe function is now generalized in its orientation and scaling.

The representation of complex real-life reflectance function can be written as a sum of several primitive modified cosine lobe functions. Polishing appropriate to the missing albedo part is used in the model. Despite all this the model can produce a highly specular material only by many cosine sums, and it cannot be applied to approximate off-specular peaks either. The value of BRDF without a mirror term is always finite.

It is worth further consideration how far the Lafortune model can be generalized with a continuous mixing function. To do this the entire diagonal matrix has to have parameters and a mixing function (thickness function) of two or even three dimensions to be applicable. The closed form of the model or its use for exclusive importance sampling is, however, questionable.

#### Patch-based BRDFs

The basic idea of the patch-based BRDF is defined by Neumann et al. [51], a physically plausible BRDF is done by a continuous mixture of its elements the so called base BRDFs. According to the latter article, the base BRDF is a discontinuous, wholly mathematical construction deriving from  $\{0, 1\}$ -function, but the mixture is a model applicable also for the description of real materials. The domain of constant, non-zero values of base BRDF projected onto a reference plane yields a disc, whose radius serves as the parameter of base BRDF. As an infinite cluster of parameters, the mixing function simultaneously ensures flexible construction and fitting as well as easy handling. The recommended mixing functions are exponential or polynomial functions. This is the first BRDF construction, which deliberately incorporated executable sampling.

Extreme cases of base BRDF, and therefore also special cases of the model are the ideal diffuse model, or an unusual mirror, which reflects back the entire energy toward the mirror direction, but the return

radiance does not follow the  $\frac{1}{\cos \Theta_L}$  characteristics of metals and mirror. This family of models is able to reproduce the visual properties of coated metals, plastics, and ceramics. Its modified cases yield retro-reflective and anisotropic materials. The model is described in the article in greater detail.

### A Phong Generalization

Apart from the definition on the plane (see at Neumann et al. [51]), the definition on the hemisphere is also relevant. The  $\rho_\alpha(\mathbf{L}, \mathbf{V})$  basic BRDF is the *common part* (intersection) of a circular cone of a half apex angle  $\alpha$  and axis  $\mathbf{L}'$  and the hemisphere. Inside this conic part the  $\rho_\alpha(\mathbf{L}, \mathbf{V})$  is constant, outside of it is zero. Obviously,  $0 < \alpha \leq \pi$ . The lower limit defines a mirror, which absorbs energy at grazing angles, the upper limit is the ideal diffuse model. In the latter case, the cone of  $\pi$  half apex angle becomes a sphere at the bounday situation. These elementary models can be mixed also by using a p probability distribution function, parameterized with  $\alpha$ . The model obtained in this way can be seen as a generalization of the Phong model. The  $p(a) = C_{\max} \cdot \cos^s \alpha$  probability density function, which is a generalization of the Phong model is discussed by Lafortune et al. [40] from a different theoretical approach and with closed formulae.

### Tobler Model

Another base BRDF construction has been introduced by Tobler [70]. The new base BRDF definition has been based on a new analogue for deriving form factors and a projection transformation. In stead of the reference plane used for the previous model, a half radius centrally positioned sphere touching the reference plane is placed into the hemisphere, which represents  $\mathbf{L}, \mathbf{V}$  directions. The same principle is used for the definition of transformed vectors for determining base BRDFs. Projected vectors are:

$$\begin{aligned} \mathbf{L}_S &= 2 \cdot (\mathbf{NL}) \cdot \mathbf{L} - \mathbf{N}, & \mathbf{V}_S &= 2 \cdot (\mathbf{NV}) \cdot \mathbf{V} - \mathbf{N}, & \text{and} \\ \mathbf{R}_S &= 2 \cdot (\mathbf{NR}) \cdot \mathbf{L} - \mathbf{N} = 4 \cdot (\mathbf{NL})^2 \cdot \mathbf{N} - 2 \cdot (\mathbf{NL}) \cdot \mathbf{L} - \mathbf{N} \end{aligned} \quad (1.69)$$

In this way the metrics:

$$m = m(\mathbf{L}, \mathbf{V}) = m^*(\mathbf{R}_S, \mathbf{V}_S) = 1 - (\mathbf{R}_S \mathbf{V}_S) \quad (1.70)$$

The base BRDFs are circular sections on the half radius sphere with diameter the same as that of the sections. In this construction the albedo of base BRDFs is always constant 1. The model appears to be metallic in normal position, whereas at grazing angles light peaks are dim and a little retro-reflection occurs. Although such materials do not occur in nature, there are in these interreflection pictures interesting, even beautifully emphasized contour effects appearing along adjoining lines between objects reflecting on each other. Two analytic models are recommended for this construction. The power function yields a BRDF that can be thought of as a analogue to the Phong BRDF, but defined with the vectors  $\mathbf{R}_S$  and  $\mathbf{V}_S$  instead  $\mathbf{R}$  and  $\mathbf{V}$ :

$$f_r(\mathbf{L}, \mathbf{V}) = (n + 1) \cdot ((\mathbf{R}_S \mathbf{V}_S)^+)^n \quad (1.71)$$

The exponential function:

$$f_r(\mathbf{L}, \mathbf{V}) = \frac{s}{1 - e^{-2 \cdot s}} \cdot e^{-s \cdot m} = \frac{s}{1 - e^{-2 \cdot s}} \cdot e^{-s \cdot (1 - \mathbf{R}_S \mathbf{V}_S)} \quad (s > 0) \quad (1.72)$$

The task of Neumann et al. [51] and Tobler et al. [70] was the development of simply importance sampling with which these models could be effectively used in Monte Carlo algorithms. It has been accomplished.

### Metallic Models with Stretching Operator

The behavior of material models can be roughly characterized by the responses to various point lights and to evenly diffuse (daylight) illuminations. The characteristic metallic response of point lights is the specular (or rather off-specular) peak occurring in the direction of reflection, or the conservation of the sum of energies from point lights varying roughly according to the Fresnel function. Because of symmetry the latter response is the same as that of daylight in the direction of point lights, that is the value of albedo function in the specified direction. The metallic appearance of material models may be grossly degraded by the strongly declining character of the albedo function, especially at grazing angles, dimming, weakening the metallic effect. This defect is usually a reason for the application of a mirror component. Neumann et al [53] proposed a method for increasing the albedo of any material model

(albedo pumping), that preserves the character of the original material model, imposes practically no computational overcosts and conserves physical plausibility (and even corrects the models violating the principle of energy balance). This method may be applied iteratively.

By applying  $\frac{1}{\cos \Theta_{\min}}$  multiplication factors  $\cos \Theta_{\min} = \min(\cos \Theta_{\mathbf{L}}, \cos \Theta_{\mathbf{V}})$  to the Phong and Blinn models, respectively, Neumann and the author of this thesis [52] arrived at metallic models which are physically plausible and their sampling is more effective. These are discussed in a subsequent section.

## 1.3 Subject of this thesis

In the following section we define the initial problem which this thesis set out to solve, that is we define the questions about materials models we are interested in, and on which we want to focus. Subsequent section give various answers to these problems.

### 1.3.1 Required properties of material models

Modelling materials for computergraphics has at least two essentially different aspects, reality and useability. Shortly said reality means reproduction and description of physical events, and useability means low computational cost – over the realistic effect and relatively simple and flexible formulas. Flexibility has also two meanings here, one of them ensures different appearance by varying parameters of model up to fitting it to given measured data, while the other one extends the capabilities of model to special effects such as anisotropy and retro-reflectivity. In the history of this discipline different kind of materials (diffuse, plastics, metallic characteristics, and so on) were discussed in different approaches (physically, empirically, mathematically based, and their mixtures). We should point on, that there is no pure physically based model, because there is an infinite number of defining factors of real surfaces, so every model can be seen only as a more or less adequate abstraction of the material which one wants to model. On the other hand there is no useable model which would not take into consideration some features of a class of real materials which need to be modelled. In our discussion models and model families are not expected to be correct descriptions of real materials, or only to be heuristic play of formulas. In this thesis we will realize some mathematical features stated on the discussed class of materials by formulas that are as useable as possible. So firstly classes of materials have to be characterized by some – possibly simple – properties, secondly requirements of useabilities are to draw up, and finally we should find appropriate formulas to satisfy these requirements.

Which features describe real materials or the appearance of them? A break or discontinuity of BRDF can easily be observed as an error in the model. Every model also has to incorporate the three properties of physical plausibility, that is non-negativity, property of energy-balance and reciprocity. Only non-negativity is obvious and (perhaps) unmissable of, both other properties are not met even in well-known and generally accepted models. Formally even less obvious, but visibly even more observable a further condition is the proper behaviour of the albedo-function. In fact the albedo-function describes energy-balance as well, so the shape of that function and the physical plausibility are tightly connected to each other. The behaviour of this function is critical at grazing angles, a fact which has not been seriously considered so far. Thus it has not been researched and measured in itself sufficiently, despite of its practical and theoretical importance, that is of modelling specific phenomena of surfaces, and revealing intrinsic inconsistency of some BRDF formulas. Focussing on metallic appearance, we can observe further features, which are not seen in duller materials. First, the value of the albedo-function cannot be radically less than one – i.e. response has to conserve energy well – even at smaller angles. (Of course energy-balance condition always has to be performed, that is to be less or equal to one). Secondly, not only is the reflected energy kept possibly in a small region, but the same pointlike lightsource placed at different incoming directions, results in a response radiance at the mirror-directions of input that is about the same for the different situations. Thirdly, the distribution of reflected energy in this case (i.e. of a pointlike lightsource) has a maximum-value at the exact mirroring direction of input, and has a smoothly decreasing shape around it. From later condition follows an "inverse-cosine" behaviour of BRDF at mirroring directions (which compensates anyhow effect of cosine factor changes radiance to irradiance at the incoming side), and furthermore follows the necessity of the specularly of model and the so called off-specular peak of BRDF as well. The last feature means that the maximum-point of the radiance-response on the half-sphere is further down than the maximum point of energy, which can be easily observed in real metals. Each phenomenon (except of course the last one) can be demonstrated and understood as an ideal mirror which can be taken as the limit case of all metals.

On the other hand, that is pertaining to their usability in computer graphics, two essentially different uses of BRDFs can be distinguished. One can be titled by "Virtual Reality" which summarize the

requirements of speed and storage, the other one is of the importance sampling by using Monte Carlo techniques, included forward and also backward random ray-generating methods. On the side of BRDF (as a seed of these processes) it requires possibly fast and uniformly chosen directions represent the whole outgoing energy. (The situation is the same in the reversed direction because of the reciprocity principle). In other words, the albedo as an integral – of outgoing radiance times a cosine of outgoing direction's angle – has to be represented by sampling with the possibly smallest variance. So the cost of ray-generation as the most expensive part of these algorithms will be minimized. So far this aspect has not been sufficiently highlighted in BRDF literature.

### 1.3.2 Results of next chapters

With respect to above established set of requirements this thesis focuses on BRDFs in aspect of behaviour of albedo, fast importance sampling, inverse cosine character at mirror direction and relatively simple and variable formulas, conserving of physical plausibility as well. In this thesis there we do not introduce a single model satisfying all of these requirements in parallel, our proposed models satisfy different sets of the listed properties, offering methods to generate new models or to correct existing ones. In the chapter "Reflectance Models by Pumping up the Albedo Function" we present a simple and general method that corrects the break in the principle of energy-balance of some BRDFs, and improves relatively dark models such as Phong's and Blinn's ones. In the chapter "New Simple Reflectance Models for Metals and other Specular Materials" we propose a simple and attractive inverse cosine factor that generates metallic models. "Metallized" Phong and Blinn models are defined and also offered as a corrected modification of Ward model. The chapter "Reflectance Models with Fast Importance Sampling" defines a class of new patch-based models for a quick and varianceless importance sampling. In addition to their freedom, the variability of these models is infinite, since they are defined by functions and metrics. As a continuation of this work, we refer in the last chapter highlighting further research directions and answering some open questions asked here.

## Chapter 2

# Reflectance Models by Pumping up the Albedo Function

### 2.1 Introduction

In computer graphics the optical material properties are usually modelled by Bi-directional Reflection Distribution Functions or BRDFs for short. Intuitively, the BRDF represents the radiance reflected off the material illuminated by point light-sources from a given direction.

The most famous BRDF model that can describe specular materials was proposed by Phong [57] and improved by Blinn [8]. This model does not have physical interpretation but is only a mathematical construction. Since the original forms violate physics (they are not symmetric), their corrected versions [33][43] are preferred in global illumination algorithms.

The first model that has physical base was proposed by Torrance and Sparrow [72], which was applied in rendering algorithms in [14]. Later, He, Torrance et. al. [29] introduced another model that even more accurately represented the underlying physical phenomena [6]. These models are not suitable for importance sampling since it would require the integration and inversion of the probability density functions that are expected to be proportional to the reflected power. Not only is it impossible to compute the required integral and inversion analytically, but even the calculation of BRDF values requires significant computational effort for these physically based models. In their recent paper Lafortune et. al. approximated a non-linear, metallic BRDF by the sum of modified Phong models [41]. The resulting BRDF is simple, but this approach requires a great number of elementary terms to sufficiently represent highly specular materials at grazing angles.

Radiosity and Monte-Carlo ray-tracing rendering algorithms require that the BRDFs do not violate physics. Such shading models must satisfy both reciprocity and energy balance, and are called *physically plausible* [43].

*Reciprocity* that was recognized by Helmholtz is the symmetry property of the BRDF (see in [44]) ( $f_r$ ,  $[\text{sr}^{-1}]$ ), which is defined by the following equation:

$$f_r(\mathbf{L}, \mathbf{V}) = f_r(\mathbf{V}, \mathbf{L}), \quad (2.1)$$

where  $\mathbf{L}$  is the unit vector pointing towards the incoming light and the unit vector  $\mathbf{V}$  defines the viewing direction. Several rendering algorithms, including ray-tracing, takes advantage of this symmetry property.

Suppose that the surface is illuminated by a beam from direction  $\mathbf{L}$ . *Energy balance* means that the *albedo*, that is the fraction of the total reflected power, cannot be greater than 1:

$$\mathbf{a}(\mathbf{L}) = \int_{\Omega} f_r(\mathbf{L}, \mathbf{V}) \cdot \cos \Theta_{\mathbf{V}} \, d\omega_{\mathbf{V}} \leq 1 \quad (2.2)$$

Energy balance makes the linear operator of the rendering equation or some of its powers [49] a contraction, which is usually required by iterative and random walk methods to converge to the solution. Particularly, the albedo together with occlusion conditions determine the norm of the integral operator and consequently the conditioning of the rendering equation, and thus describe the speed of convergence of the iterative methods, and can be used to specify how many light bounces are to be computed during random walks.

### 2.1.1 Perceptual based fitting

The albedo and the BRDF characterize a material in two different aspects. The BRDF expresses the *radiance reflectivity* of the material – that is the response to point light-sources –, while the albedo describes its *energy reflectivity*, that is the response to uniformly distributed (so called *daylight*) illumination. Concentrated point-like and uniformly distributed light-sources represent the two extreme cases of possible illuminations.

Formally, if a surface is illuminated by a point light-source of power  $4\pi$  at distance 1 in direction  $\mathbf{L}$ , then the observer at direction  $\mathbf{V}$  will perceive:

$$L^{\text{out}}(\mathbf{V}) = f_r(\mathbf{L}, \mathbf{V}) \cdot \cos \Theta_{\mathbf{L}} \quad (2.3)$$

On the other hand, if the illumination is constant in all directions and its radiance is 1, then the perceived radiance is:

$$L^{\text{out}}(\mathbf{V}) = \int_{\Omega} f_r(\mathbf{L}, \mathbf{V}) \cdot \cos \Theta_{\mathbf{L}} d\omega_{\mathbf{L}} = \mathbf{a}(\mathbf{V}) \quad (2.4)$$

Since perception is affected by both point light-sources (sun, electric bulbs) and daylight illumination (sky, diffuse room, large area light-sources), in order for a reflectance model to be realistic, both the BRDF weighted by the cosine factor and the albedo should accurately follow the corresponding characteristics of the real materials. So far, fitting has been made only on the the BRDF using usually least square error metric. In perceptual based fitting the albedo should also be considered, and the maximal relative errors of both the weighted BRDF and of the albedo should be minimized simultaneously. The relative error corresponds to the logarithmic characteristics of the human vision system.

### 2.1.2 Physically plausible, but not physically based models

Let us consider the specular part of the original versions of the Phong [57] and Blinn [8] models. Using the widely accepted notations where  $\mathbf{R}$  is the mirror direction of  $\mathbf{L}$ ,  $\mathbf{N}$  is the unit normal vector, and  $\mathbf{H}$  is the halfway unit vector between  $\mathbf{L}$  and the view vector  $\mathbf{V}$ , the Phong and Blinn models are defined as the  $n$ th power of the dot products  $(\mathbf{R}\mathbf{V})$  and  $(\mathbf{N}\mathbf{H})$ , respectively, divided by the cosine of the incident angle.

$$\begin{aligned} f_{r,\text{Phong}}(\mathbf{L}, \mathbf{V}) &= \frac{c_{\text{Phong}}(n)(\mathbf{R} \cdot \mathbf{V})^n}{\cos \Theta_{\mathbf{L}}} \\ f_{r,\text{Blinn}}(\mathbf{L}, \mathbf{V}) &= \frac{c_{\text{Blinn}}(n)(\mathbf{N} \cdot \mathbf{H})^n}{\cos \Theta_{\mathbf{L}}} \end{aligned} \quad (2.5)$$

These models are not symmetric because of the division by  $\cos \Theta_{\mathbf{L}}$ , and thus are not physically plausible. A simple way of making them physically plausible is the elimination of this division [43], resulting in the following versions:

$$\begin{aligned} f'_{r,\text{Phong}}(\mathbf{L}, \mathbf{V}) &= c_{\text{Phong}}(n)(\mathbf{R} \cdot \mathbf{V})^n, \\ f'_{r,\text{Blinn}}(\mathbf{L}, \mathbf{V}) &= c_{\text{Blinn}}(n)(\mathbf{N} \cdot \mathbf{H})^n. \end{aligned} \quad (2.6)$$

The Lafortune model [41] also falls into this category, but uses a special type of dot product:

$$f_{r,\text{Lafortune}}(\mathbf{L}, \mathbf{V}) = c_{\text{Lafortune}}(n, s)(\mathbf{R}_x \mathbf{V}_x + \mathbf{R}_y \mathbf{V}_y + s \mathbf{R}_z \mathbf{V}_z)^n \quad (2.7)$$

where  $c_{\text{Phong}}(n), c_{\text{Blinn}}(n), c_{\text{Lafortune}}(n, s)$  are scalar functions of material constants.

For large  $n$  values the BRDF gets highly specular. However, the Phong and Blinn models cannot provide metallic or mirror looking since for large incident angles they get darker. More precisely, as the incident angle grows towards the grazing angle, the ratio of the reflected power and the incoming power as well as the output radiance decrease. If  $n$  goes to infinity, then the reflected radiance and the albedo converge to zero for  $90^\circ$  incident angle since in this limit case the albedo follows the cosine function. Intuitively, the decrease of the radiance means that if we look at a Phong-mirror, then the image reflected in the mirror gets darker for greater reflection angles (the non-plausible versions do not exhibit this darkening). Note that Lafortune's model tries to reduce this phenomenon by using a factor  $s$  to suppress the BRDF close to perpendicular angles and thus giving an emphasis to grazing angles.

## 2.2 Analysis of the energy reflectivity of classical BRDF models

The energy balance of the reflectance models can be represented by their albedo function. Supposing that the Fresnel term is 1 (for silver this is practically true), the albedos of the Phong, He–Torrance, Cook–Torrance and the Ward [75] models are shown in figure 2.1. Note that the Cook–Torrance and the Ward models diverge at grazing angles, while the Phong, He–Torrance and Ward BRDFs badly decrease for greater incident angles. Since shiny metals tend to be good energy mirrors even for larger incident angles, the decrease of the albedo for larger incident angles makes a model not realistic for representing metallic objects.

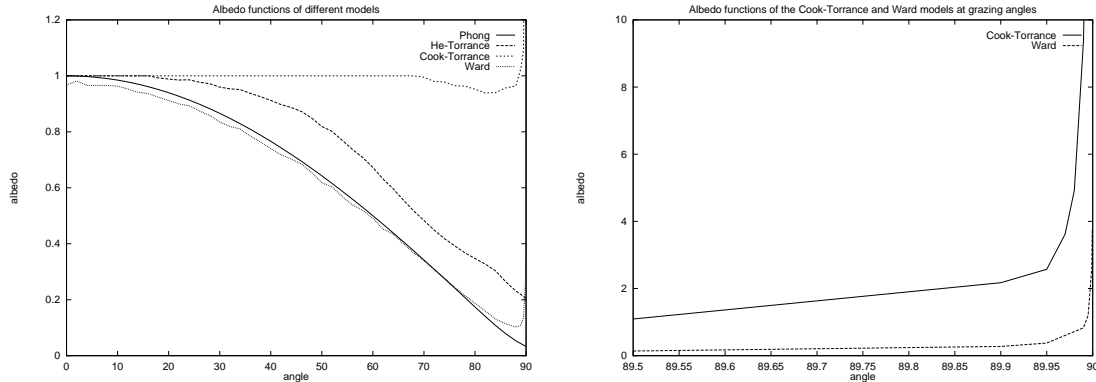


Figure 2.1: Albedo functions of the Phong ( $n = 150$ ), He–Torrance ( $\sigma_0 = 0.1, \tau = 1.7$ ), Cook–Torrance ( $m = 0.1$ ) and Ward ( $m = 0.1$ ) models

The divergent behavior of the Cook–Torrance and the Ward models was quite unexpected, since these models have been believed to be physically plausible, and this type of divergence may generate incorrect results and may cause instability when rendering special scenes. This kind of divergence is caused by the application of  $\mathbf{H}$  instead of  $\mathbf{R}$  in the reflectance model. Models of type  $\mathbf{N} \cdot \mathbf{H}$  cannot effectively separate viewing directions that are close to the mirror direction and therefore the size of the solid angle of the highlight cannot shrink depending on  $\mathbf{L}$ . For grazing angles the BRDF should converge to a Dirac- $\delta$  like shape (the value of BRDF goes to infinity, while the albedo should be limited). The following section formally examines this phenomenon.

### 2.2.1 Divergence of the Cook–Torrance and Ward models

Let us denote the angle between the normal vector and the halfway vector by  $\delta$ , and the surface roughness parameter by  $m$ . The BRDF function of the Ward model [75] is

$$f_{r,\text{Ward}}(\mathbf{L}, \mathbf{V}) = \frac{1}{4\pi m^2} \cdot e^{-\frac{\tan^2 \delta}{m^2}} \cdot \frac{1}{\sqrt{(\mathbf{N} \cdot \mathbf{L})(\mathbf{N} \cdot \mathbf{V})}} \quad (2.8)$$

Assuming that the Fresnel factor is 1, the BRDF of the Cook–Torrance model [14] is

$$f_{r,\text{Cook}}(\mathbf{L}, \mathbf{V}) = \frac{1}{4\pi m^2 \cos^4 \delta} \cdot e^{-\frac{\tan^2 \delta}{m^2}} \cdot \frac{G(\mathbf{N}, \mathbf{L}, \mathbf{V})}{(\mathbf{N} \cdot \mathbf{L})(\mathbf{N} \cdot \mathbf{V})} \quad (2.9)$$

where the *geometry factor*  $G$  [68] is

$$G(\mathbf{N}, \mathbf{L}, \mathbf{V}) = \min\left\{2 \cdot \frac{(\mathbf{N} \cdot \mathbf{H})(\mathbf{N} \cdot \mathbf{V})}{(\mathbf{V} \cdot \mathbf{H})}, 2 \cdot \frac{(\mathbf{N} \cdot \mathbf{H})(\mathbf{N} \cdot \mathbf{L})}{\mathbf{L} \cdot \mathbf{H}}, 1\right\} \quad (2.10)$$

Let us consider the situation around the highlight close to the grazing angles, that is where  $\mathbf{V} \approx \mathbf{R}$ ,  $\mathbf{H} = \frac{\mathbf{L} + \mathbf{V}}{|\mathbf{L} + \mathbf{V}|} \approx \mathbf{N}$ ,  $\mathbf{N} \cdot \mathbf{L} \approx 0$  and  $\mathbf{N} \cdot \mathbf{V} \approx 0$ . We have to show that it is possible to move  $\mathbf{L}$  towards grazing angles in a way that the albedo will diverge along this path. An appropriate path is a sufficiently small arc of the main circle of the directional hemisphere. For a given vector  $\mathbf{L}$ , the albedo integral

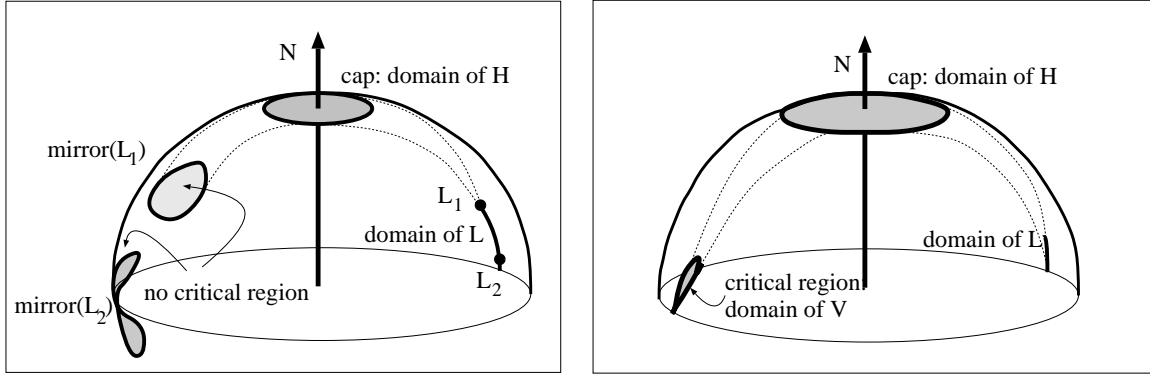


Figure 2.2: The relations between the domains of  $\mathbf{L}$ ,  $\mathbf{H}$  and  $\mathbf{V}$  vectors (left figure: domain of  $\mathbf{L}$  is too big compared to the domain of  $\mathbf{H}$ ; right figure: domain of  $\mathbf{L}$  is small compared to the domain of  $\mathbf{H}$ )

requires the consideration of all vectors  $\mathbf{V}$ . However, establishing a lower bound, only those viewing vectors are considered which, together with  $\mathbf{L}$  result in those  $\mathbf{H}$  halfway vectors that are inside a *cap* (spherical circle around  $\mathbf{N}$ ) (figure 2.2). Since  $\mathbf{H} = \frac{\mathbf{L}+\mathbf{V}}{|\mathbf{L}+\mathbf{V}|}$  should hold, the allowable domain of viewing vectors  $\mathbf{V}$  can be determined from these two regions by “spherical mirroring” of each point in the domain of  $\mathbf{L}$  onto each point in the domain of  $\mathbf{H}$ . The left figure demonstrates that if the domain of  $\mathbf{L}$  is too big compared to that of  $\mathbf{H}$ , then those  $\mathbf{V}$  vector sets which correspond to different  $\mathbf{L}$  vectors will not have a common intersection. However, if the domain of  $\mathbf{L}$  is small compared to that of  $\mathbf{H}$ , then the  $\mathbf{V}$  vector sets corresponding to different  $\mathbf{L}$  vectors will have a common intersection (right figure 2.2). This region of intersection constrained to the the upper hemisphere is called the *critical region*.

In the Ward model, factor  $\frac{1}{4\pi m^2} \cdot e^{-\frac{\tan^2 \delta}{m^2}}$  can be lower-bounded inside the *cap*, so can the  $\frac{1}{4\pi m^2 \cos^4 \delta} \cdot e^{-\frac{\tan^2 \delta}{m^2}}$  factor of the Cook–Torrance model. Thus we can find appropriate positive constants  $\mu_{\text{Ward}}$ , and  $\mu_{\text{Cook}}$  so that

$$\begin{aligned} \frac{1}{4\pi m^2} \cdot e^{-\frac{\tan^2 \delta}{m^2}} &\geq \mu_{\text{Ward}} , \\ \frac{1}{4\pi m^2 \cos^4 \delta} \cdot e^{-\frac{\tan^2 \delta}{m^2}} &\geq \mu_{\text{Cook}} . \end{aligned} \quad (2.11)$$

Considering the geometry term and the denominator of the Cook–Torrance model, we can further restrict the domain of  $\mathbf{L}$  and the *cap* for  $\mathbf{H}$  to guarantee that the constant 1 is the real minimum in the geometry term, thus here we can apply the following substitution

$$\frac{G(\mathbf{N}, \mathbf{L}, \mathbf{V})}{(\mathbf{N} \cdot \mathbf{L})(\mathbf{N} \cdot \mathbf{V})} = \frac{1}{(\mathbf{N} \cdot \mathbf{L})(\mathbf{N} \cdot \mathbf{V})} \quad (2.12)$$

Using the constant lower bounds valid inside the *cap*, we can obtain:

$$\begin{aligned} \frac{\mu_{\text{Ward}}}{\sqrt{(\mathbf{N} \cdot \mathbf{L})(\mathbf{N} \cdot \mathbf{V})}} &\leq f_{r, \text{Ward}}(\mathbf{L}, \mathbf{V}) \\ \frac{\mu_{\text{Cook}}}{(\mathbf{N} \cdot \mathbf{L})(\mathbf{N} \cdot \mathbf{V})} &\leq f_{r, \text{Cook}}(\mathbf{L}, \mathbf{V}) \end{aligned} \quad (2.13)$$

For the albedo, a lower-bound can be established by bounding the hemispherical domain  $\Omega$  to the *critical region*  $\Omega_{\text{critical}}$  and using inequality (2.13). Let us consider the Ward model:

$$a_{\text{Ward}}(\mathbf{L}) \geq \int_{\Omega_{\text{critical}}} \frac{\mu_{\text{Ward}}}{\sqrt{(\mathbf{N} \cdot \mathbf{L})(\mathbf{N} \cdot \mathbf{V})}} \cdot (\mathbf{N} \cdot \mathbf{V}) \, d\omega_{\mathbf{V}} = \frac{\mu_{\text{Ward}}}{\sqrt{(\mathbf{N} \cdot \mathbf{L})}} \int_{\Omega_{\text{critical}}} = \frac{\mu_{\text{Ward}}}{\sqrt{(\mathbf{N} \cdot \mathbf{L})}} \quad (2.14)$$

For the albedo of the Cook–Torrance model, we can obtain:

$$a_{\text{Cook}}(\mathbf{L}) \geq \int_{\Omega_{\text{critical}}} \frac{\mu_{\text{Cook}}}{(\mathbf{N} \cdot \mathbf{L})(\mathbf{N} \cdot \mathbf{V})} (\mathbf{N} \cdot \mathbf{V}) \, d\omega_{\mathbf{V}} = \frac{\mu_{\text{Cook}}}{\mathbf{N} \cdot \mathbf{L}} \cdot |\Omega_{\text{critical}}|. \quad (2.15)$$

Since at grazing angles  $(\mathbf{N}\mathbf{L})$  converges to zero, the lower-bounds in equations (2.14) and (2.15) diverge, which forces the albedo of the Ward and Cook–Torrance models to diverge as well.



## 2.3 Albedo pumping-up

Examining the albedo functions of the plausible Phong and Blinn models, we can realize that they are two small for higher incident angles, thus they cannot provide, for example, metallic appearance. If we could find an operation that is not too complicated and preserves reciprocity and energy balance of a known BRDF model, but increases its albedo, then the application area of these models could be significantly widened.

We propose the following operation, which starts with an arbitrary, but symmetric BRDF  $f_r(\mathbf{L}, \mathbf{V})$ , or with a symmetric function, and corrects this as follows to obtain a new BRDF:

$$f_r^*(\mathbf{L}, \mathbf{V}) = \frac{f_r(\mathbf{L}, \mathbf{V})}{g(\mathbf{L}, \mathbf{V})} \quad (2.16)$$

where we require function  $g$  to be a symmetric function of  $\mathbf{L}$  and  $\mathbf{V}$ , and also

$$\max(\mathbf{a}(\mathbf{L}), \mathbf{a}(\mathbf{V})) \leq g(\mathbf{L}, \mathbf{V}) \leq 1 \quad (2.17)$$

to hold.

Note that even if the original BRDF is only symmetric, but is not energy preserving, then the first pumping-up operation makes it energy preserving and thus physically plausible.

Assume that function  $g$  is not zero (except for a set of null measure). Since  $g(\mathbf{L}, \mathbf{V}) \leq 1$ , we obtain  $a^*(\mathbf{L}) \geq \mathbf{a}(\mathbf{L})$  for the albedo  $a^*$  of  $f_r^*(\mathbf{L}, \mathbf{V})$ . Furthermore, if for some of the directions  $g(\mathbf{L}, \mathbf{V}) < 1$ , then  $a^*(\mathbf{L})$  is definitely greater than  $\mathbf{a}(\mathbf{L})$ . Consequently, equation (2.16) increases the albedo, which justifies our name “*pumping-up*”.

The new BRDF is obviously symmetric, thus only the energy conservation must be proven to demonstrate that the pumped-up model is also physically plausible.

The albedo of  $f_r^*(\mathbf{L}, \mathbf{V})$  is

$$\begin{aligned} a^*(\mathbf{L}) &= \int_{\Omega} \frac{f_r(\mathbf{L}, \mathbf{V})}{g(\mathbf{L}, \mathbf{V})} \cdot \cos \Theta_{\mathbf{V}} \, d\omega_{\mathbf{V}} \leq \int_{\Omega} \frac{f_r(\mathbf{L}, \mathbf{V})}{\max(\mathbf{a}(\mathbf{L}), \mathbf{a}(\mathbf{V}))} \cdot \cos \Theta_{\mathbf{V}} \, d\omega_{\mathbf{V}} = \\ &= \frac{1}{\mathbf{a}(\mathbf{L})} \int_{\Omega} f_r(\mathbf{L}, \mathbf{V}) \cdot \cos \Theta_{\mathbf{V}} \, d\omega_{\mathbf{V}} + \int_{\Omega_{\mathbf{V}}} f_r(\mathbf{L}, \mathbf{V}) \cdot \left( \frac{1}{\mathbf{a}(\mathbf{V})} - \frac{1}{\mathbf{a}(\mathbf{L})} \right) \cos \Theta_{\mathbf{V}} \, d\omega_{\mathbf{V}} \leq 1 \end{aligned} \quad (2.18)$$

where  $\Omega_{\mathbf{V}}$  contains those directions for which  $\max(\mathbf{a}(\mathbf{L}), \mathbf{a}(\mathbf{V})) = \mathbf{a}(\mathbf{V})$ .

In order to realize that the albedo is less than 1, let us consider the sum of the last two terms. The integral of the first term is  $\mathbf{a}(\mathbf{L})$ , thus the complete first term equals to 1. Since in  $\Omega_{\mathbf{V}}$ , factor  $\frac{1}{\mathbf{a}(\mathbf{V})} - \frac{1}{\mathbf{a}(\mathbf{L})}$  is negative, the second integral is negative and thus the albedo is less than 1. Summarizing, we obtain:

$$\mathbf{a}(\mathbf{L}) \leq a^*(\mathbf{L}) \leq 1. \quad (2.19)$$

The set  $\Omega_{\mathbf{V}}$  is empty only if  $\mathbf{a}(\mathbf{L}) = 1$ , which results in  $a^*(\mathbf{L}) = 1$ . Since real materials absorb some energy, albedo pumping-up always increases the albedo.

Equation (2.16) can also be used recursively several times, which generates a monotonically increasing sequence of albedo functions. In order to make the evaluation of the pumped-up BRDF fast during rendering, the albedo should be pre-computed and stored in a one-variate table.

### 2.3.1 Definition of the correction term

We examine two alternatives for the definition of correction term  $g$  and analyze their effect on the Phong and Blinn models.

First, let the correction term be

$$g_1(\mathbf{L}, \mathbf{V}) = \max(\mathbf{a}(\mathbf{L}), \mathbf{a}(\mathbf{V})) \quad (2.20)$$

This function obviously satisfies inequality (2.17).

The effects of this type of pumping-up on the Phong and Blinn models are shown in figure 2.3 and figure 2.4, respectively. Note that the albedos resulted by recursive pumping-ups converge to the albedo of the ideal mirror (constant 1).

It is also worth examining the output radiance assuming a single point-like light-source of intensity  $4\pi$  at distance 1 in direction  $\mathbf{L}$ . In this case the irradiance is  $\cos \Theta_{\mathbf{L}}$ . The output radiances of the pumped-up

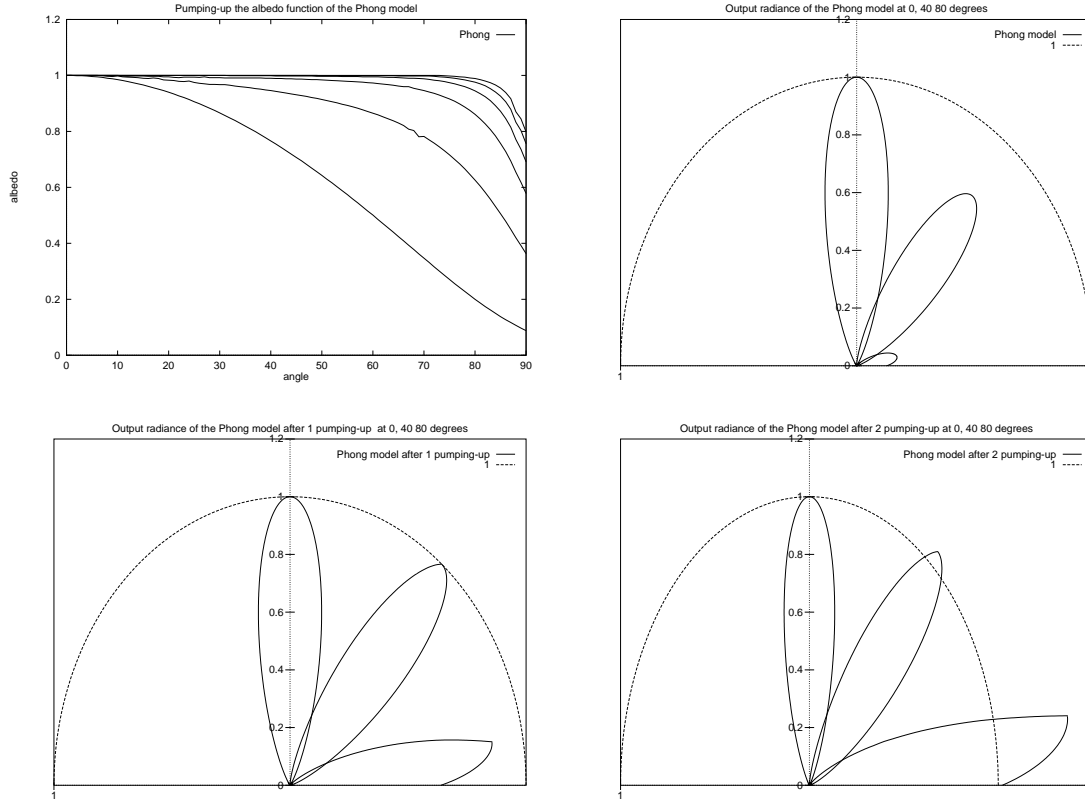


Figure 2.3: Albedo and reflected radiance of the reciprocal Phong model and its pumped-up versions ( $n=20$ )

Phong and Blinn models at different incident directions are shown in figure 2.3 and figure 2.4, respectively. These figures demonstrate that the “Phong and Blinn mirrors” get darker for greater incident angles, but the pumping-up reduces this effect. However, after several pumping-up operations the output radiance can significantly exceed the received irradiance. This means that for certain viewing directions the mirror image is brighter than the original one. This phenomenon can be observed on rough metals and is called the *off-specular peak*. However, if this effect is too strong, then the image will be unrealistic.

This artifact can be eliminated by the “*controlled albedo pumping-up*” that is discussed by the following section.

### 2.3.2 Controlled albedo pumping-up

In order to control the radiance at grazing angles, another correction term is chosen:

$$g_2(\mathbf{L}, \mathbf{V}) = \max(\mathbf{a}(\mathbf{L}), \mathbf{a}(\mathbf{V}), (\mathbf{N} \cdot \mathbf{V}), (\mathbf{N} \cdot \mathbf{L})) \quad (2.21)$$

Since the dot products are not greater than 1, function  $g_2$  also meets requirement (2.17).

The albedos and the output radiances of the Phong and the Blinn models after controlled pumping-up are shown in figure 2.5 and in figure 2.6, respectively.

Note that this type of controlling also has its price. Namely, the perfect energy mirror cannot be generated using many recursive pumping-up operations. The process will converge to an albedo that is below the constant 1. Note that for  $n = 20$ , the Phong model is worth pumping-up 2 or 3 times, but the albedo of the Blinn model does not significantly increase with the second and consecutive pumping-up operations.

The limitation of the output-radiance and the increase of the albedo are two contradicting objectives. If we optimize for one, then the other will get farther from its desired shape. Since the Phong model’s lobes are thinner, it is better in redistributing bigger power response if the albedo is pumped-up.

If we consider the repetition of the controlled pumping-ups of the Phong model, an interesting observation can be made. The final, pumped-up BRDF can also be obtained in the following, very simple

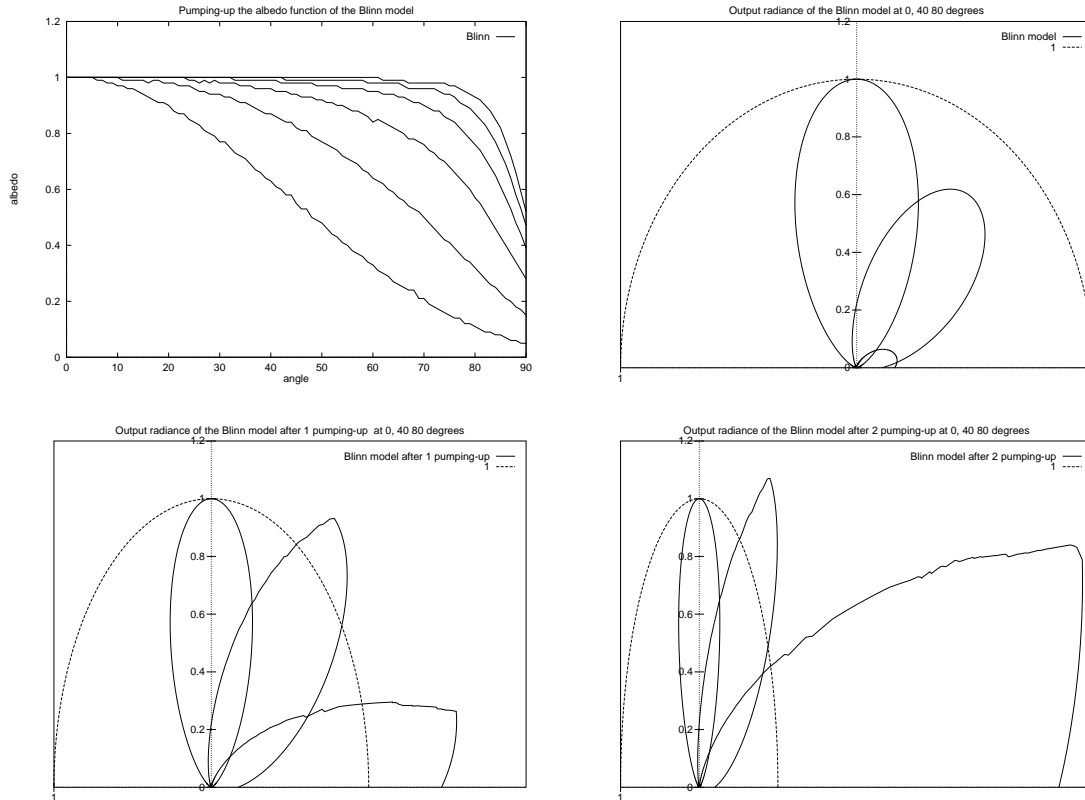


Figure 2.4: Albedo and reflected radiance of the reciprocal Blinn model and its pumped-up versions ( $n = 20$ )

form:

$$f_r(\mathbf{L}, \mathbf{V}) = c_n \cdot \frac{(\mathbf{R} \cdot \mathbf{V})^n}{\max((\mathbf{N} \cdot \mathbf{L}), (\mathbf{N} \cdot \mathbf{V}))} \quad (2.22)$$

where  $c_n \leq \frac{n+2}{2\pi}$  must hold in order for the model to preserve energy balance.

The albedo functions of different exponents  $n$  and the output radiance of this *new model* are shown in figure 2.7.

## 2.4 Simulation results

The following images have been rendered by Monte-Carlo ray-tracing method applying importance sampling. Color computation was carried out at 8 discrete wavelengths, then using the color matching functions the XYZ primaries were generated, which were finally converted to RGB. The material properties of the metals (index of refraction and extinction coefficient), color matching functions and the XYZ to RGB conversion matrix were taken from [22].

Figure 2.8 show images of metallic objects, rendered with the reciprocal Phong and its pumped-up reflection models, using  $n = 20$  and  $n = 5000$  exponent parameters. The scene is illuminated by both point light-sources and daylight. Note that pumping-up makes the image brighter and also more metallic looking. Images of  $n = 5000$  demonstrate that the original Phong model is a bad energy mirror, since the daylight illumination cannot make the surfaces bright where the angle of viewing is large. However, pumping-up eliminates this problem.

## 2.5 Conclusions

The paper presented a method to control and tune the shape of the albedo function, which is called the “albedo pumping-up”. The operation can be applied recursively. Albedo pumping-up can improve the energy response without violating the physical plausibility.

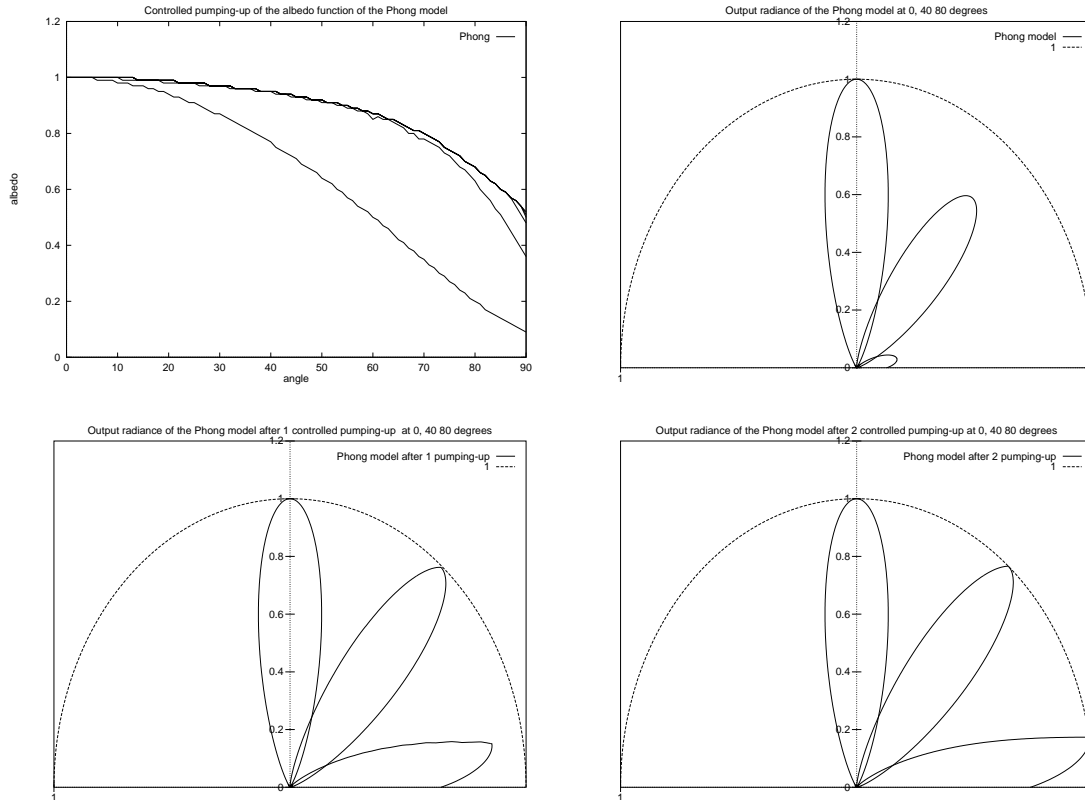


Figure 2.5: Controlled pumping-up of the reciprocal Phong model ( $n = 20$ )

The elaboration of this operation was inspired by the need to make the Phong and Blinn models appropriate for metallic objects. The original Phong and Blinn BRDFs are “dark” for greater incident angles from two different aspects. On the one hand, the output radiance converges to zero. On the other hand, the fraction of the total reflected energy also converges to zero if the exponents of these models go to infinity when approximating highly specular materials. These models are poor radiance-mirrors and energy-mirrors at grazing angles. Our intention was to improve the albedo function by the introduced pumping-up operation to get a better “energy-mirror”, and hoped that it also results in a good “radiance-mirror”. This worked well for the Phong model, but the Blinn model showed super-metal characteristics even for moderate increase of the albedo function (the output radiance of super-metals significantly exceeds the input radiance and the allowed size of the off-specular peak). In order to limit the output radiance, we introduced the *controlled albedo pumping-up*, which guarantees that the output radiance does not exceed the input radiance, but it also drastically limited the increase of the albedo for the Blinn model.

Based on these experiences, other reflectance models of the  $\mathbf{N} \cdot \mathbf{H}$  family have been analyzed to find out how they tried to compromise these two contradicting objectives. The analysis and the numerical simulations resulted in an unexpected conclusion that the Ward and the Cook–Torrance models violate energy balance and their albedos diverge to infinity at grazing angles, thus these models are not physically plausible. We believe that the  $\mathbf{N} \cdot \mathbf{H}$  family is not appropriate for the construction of metallic BRDFs. Their albedos either badly decrease (Blinn model) or diverge (Ward and Cook–Torrance models) at grazing angles.

The albedo is not an abstract feature of a material but can be seen directly. The perceived radiance reflected of an object illuminated by uniform distributed light is just proportional to the albedo function at the viewing direction if the BRDF is reciprocal. This phenomenon is also demonstrated by the color images, where the albedo pumping-up improved not only the highlights but also the parts affected only by the daylight illumination and viewed at large angles.

In order to emphasize the role of the albedo, the *perceptually based fitting* was proposed, which fits both the BRDF (response to point light-sources) and the albedo (response to daylight) simultaneously to find minimal relative error. The application of relative error metric is justified by the logarithmic

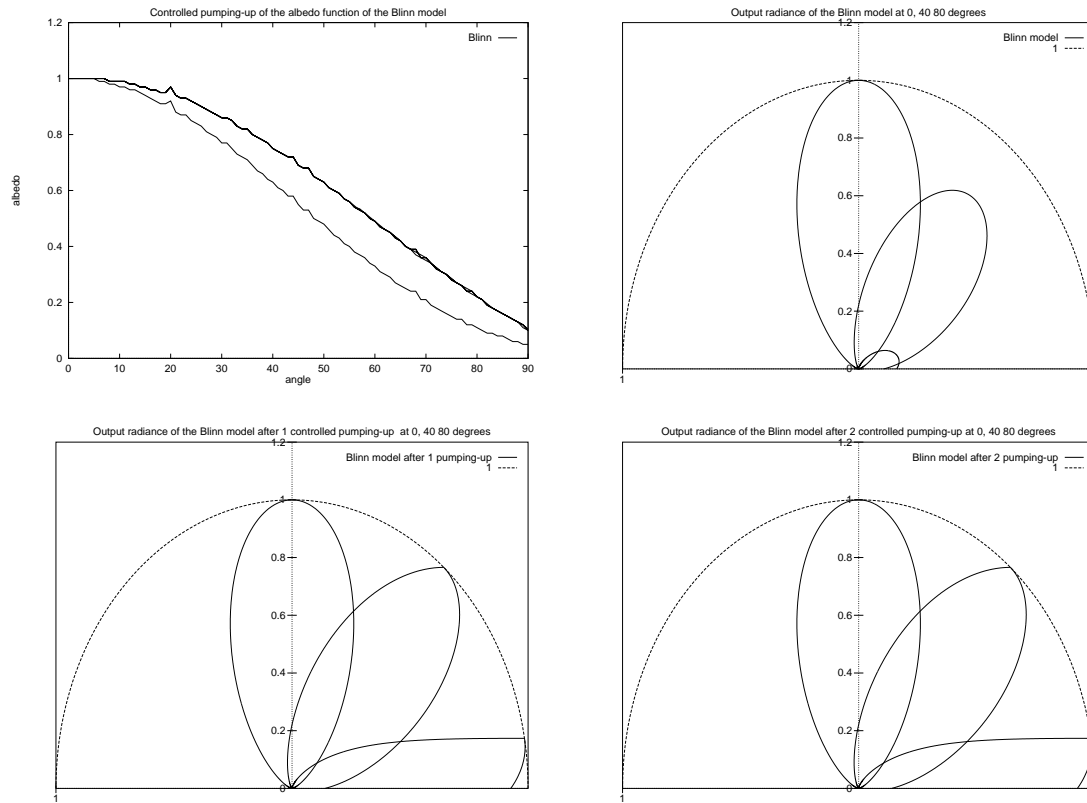


Figure 2.6: Controlled pumping-up of the reciprocal Blinn model ( $n = 20$ )

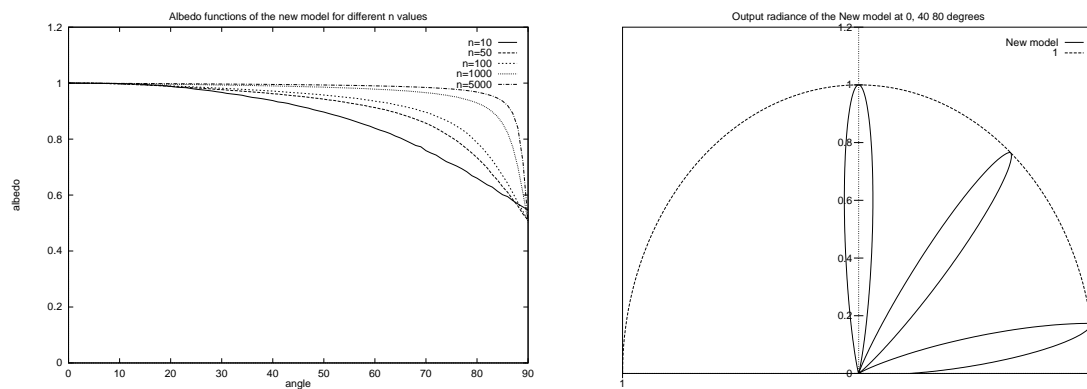


Figure 2.7: The albedo function for different  $n$  parameters and the output radiance ( $n = 100$ ) of the new model

---

characteristics of the perception. This type of fitting requires the storage of the albedo functions in addition to BRDFs in material databases. The albedo can be measured by integrating sphere or using distributed lighting.

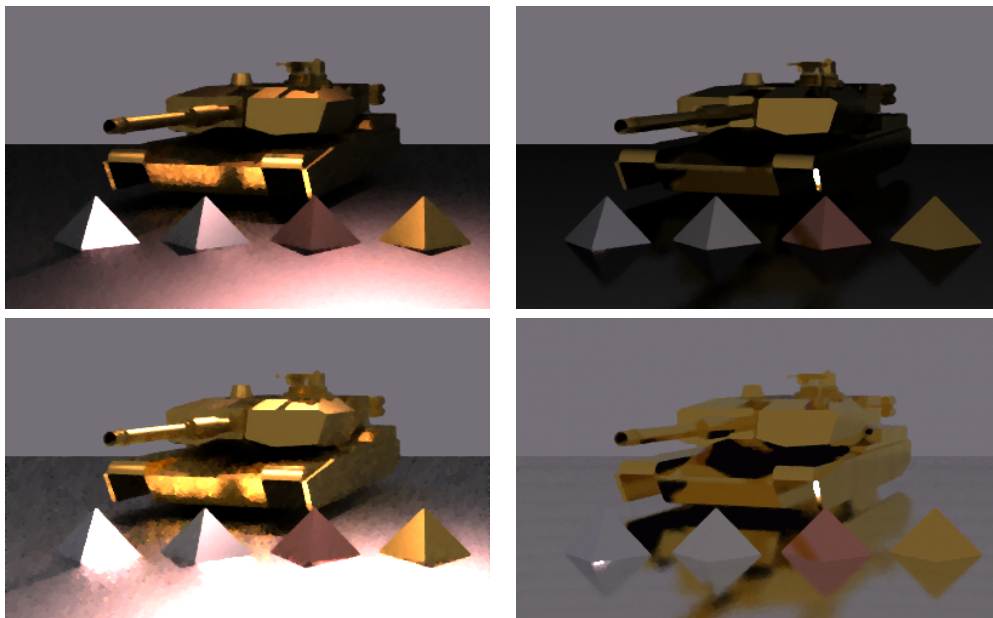


Figure 2.8: A golden tank with aluminum, silver, copper and golden pyramids rendered using the reciprocal Phong model (top) and using the Phong model pumped-up once (bottom) (left:  $n = 20$ , right:  $n = 5000$ )

## Chapter 3

# New Simple Reflectance Models for Specular Materials

### 3.1 Introduction

The most famous BRDF model that can describe specular materials was proposed by Phong [57] and improved by Blinn [8]. This model does not have physical interpretation but is only a mathematical construction. Since the original form violates physics, its corrected version [33][43] is preferred in global illumination algorithms.

The first model that has physical base was proposed by Torrance and Sparrow [72], which was applied in rendering algorithms in [14]. Later, He, Torrance et. al. [29] introduced another model that even more accurately represented the underlying physical phenomena [6]. These models are not suitable for *importance sampling* since it would require the integration and inversion of the probability density functions that are expected to be proportional to the BRDF. Not only is it impossible to compute the required integral and inversion analytically, but even the calculation of BRDF values requires significant computational effort for these physically based models.

In their recent paper Lafortune et. al. approximated a non-linear, metallic BRDF by the combination of modified Phong models [41]. The resulting BRDF is simple, but this approach requires a great number of elementary terms to sufficiently represent highly specular materials. Another drawback of this method is that the BRDF is always bounded for grazing angles.

Radiosity and Monte-Carlo ray-tracing rendering algorithms usually assume that the BRDFs do not violate physics. Such shading models must satisfy both reciprocity and energy balance, and are called *physically plausible* [43].

*Reciprocity* that was recognized by Helmholtz is the symmetry property of the BRDF ( $f_r$ , [st<sup>-1</sup>]), which is defined by the following equation [44]:

$$f_r(\mathbf{L}, \mathbf{V}) = f_r(\mathbf{V}, \mathbf{L}) \quad (3.1)$$

where  $\mathbf{L}$  is the unit vector pointing towards the incoming light and unit vector  $\mathbf{V}$  defines the viewing direction. Reciprocity is important because it allows for the backward tracing of the light as happens in ray-tracing algorithms.

Suppose that the surface is illuminated by a beam from direction  $\mathbf{L}$ . *Energy balance* means that the *albedo*, that is the fraction of the total reflected power cannot be greater than 1:

$$\mathbf{a}(\mathbf{L}) = \int_{\Omega} f_r(\mathbf{L}, \mathbf{V}) \cdot \cos \Theta_{\mathbf{V}} \, d\omega_{\mathbf{V}} \leq 1 \quad (3.2)$$

Energy balance makes the linear operator of the rendering equation a contraction, which is usually required by iterative and random walk methods to converge to the solution.

For the representation of metals, there has been no simple, physically plausible model so far that is also good for highly specular materials and can give back the mirror as the limit case. This chapter intends to fill this gap.



## 3.2 Metals and Phong-type models

### 3.2.1 Properties of metals and mirrors

Metals have several important properties:

- Their diffuse reflectance is usually negligible.
- The color reflected off the metals is determined by the Fresnel function. Due to the angle dependence of the Fresnel function, this color fades at grazing angles.
- If the surface roughness goes to zero, metals become shinier and converge to the *ideal mirror*. The reflectance function of the ideal mirror is  $\delta \cdot \frac{F(\Theta)}{\cos \Theta_{\mathbf{L}}}$ , where  $\delta$  is the Dirac-delta,  $F$  is the Fresnel function and  $\Theta_{\mathbf{L}}$  is the incident angle. If the Fresnel term of the material is 1, then an ideal mirror would reflect all energy independently of the illumination, that is the albedo is 1 and the reflected radiance is equal to the corresponding input radiance. At directions other than the reflection direction, the radiance is zero. As the material properties converge to that of the ideal mirror, both the *energy reflectivity* (albedo) and the *radiance reflectivity* (BRDF) are expected to converge to the corresponding functions of the ideal mirror.
- The BRDF function of metals has  $\frac{1}{\cos \Theta_{\mathbf{L}}}$  characteristics that can compensate for the  $\cos \Theta_{\mathbf{L}}$  factor of the irradiance.
- For great incident angles, the peak of the reflection lobe (so called off-specular peak) occurs at an angle greater than the angle of incidence.

When the new models are compared to the different versions of the Phong model, these properties are examined. We shall conclude that the new models meet all but the last requirements.

Let us consider the specular part of the physically plausible versions of the Phong and the Blinn models [43]. Using the widely accepted notations where  $\mathbf{R}$  is the mirror direction of  $\mathbf{L}$ ,  $\mathbf{N}$  is the unit normal vector, and  $\mathbf{H}$  is the halfway unit vector between  $\mathbf{L}$  and the view vector  $\mathbf{V}$ , the Phong and Blinn models are defined as the  $n$ -th power of the dot products  $(\mathbf{R} \cdot \mathbf{V})$  and  $(\mathbf{N} \cdot \mathbf{H})$ , respectively. For large  $n$  values the BRDF gets highly specular. However, these models cannot provide metallic or mirror looking since as the incident angle grows towards the grazing angle, the ratio of the reflected power as well as the output radiance decrease. If  $n$  goes to infinity, then the reflected radiance and the albedo converges to zero for  $90^\circ$  incident angle since in this limit case the albedo follows the cosine function. Intuitively, the decrease of the radiance means that if we look at a Phong-mirror, then the image reflected in the mirror gets darker for greater reflection angles.

### 3.2.2 The new model for metals

This section discusses a construction method which preserves the reciprocity and the energy balance of the BRDF, but solves the mentioned problems of Phong-type models.

Considering the limit case, we should realize that in order to eliminate the undesired behavior of the Phong model, its cosine term must be compensated by an  $\frac{1}{\cos \Theta_{\mathbf{L}}}$  factor. However, if we multiplied the specular part of the reciprocal Phong model [40] by  $\frac{1}{\cos \Theta_{\mathbf{L}}}$ , then we would get back the original, non-reciprocal Phong [57] expression. On the other hand, if we multiplied it with  $\frac{1}{\cos \Theta_{\mathbf{L}}} \cdot \cos \Theta_{\mathbf{V}}$ , then the radiance would be unacceptably high around the reflection direction at grazing angles and the energy balance could not be preserved. We can come to the same conclusion with  $\frac{1}{\sqrt{\cos \Theta_{\mathbf{L}} \cdot \cos \Theta_{\mathbf{V}}}}$  correction factor as well [75].

However, the  $\frac{1}{\max(\cos \Theta_{\mathbf{L}}, \cos \Theta_{\mathbf{V}})}$  function have been found appropriate. Let the minimum of the incident and the viewing angles be  $\Theta_{\min}$ :

$$\Theta_{\min} = \min(\Theta_{\mathbf{L}}, \Theta_{\mathbf{V}}) \quad (3.3)$$

The proposed correction term is

$$\frac{1}{\cos \Theta_{\min}} = \frac{1}{\max(\cos \Theta_{\mathbf{L}}, \cos \Theta_{\mathbf{V}})} \quad (3.4)$$

Let  $\cos \alpha = (\mathbf{R} \cdot \mathbf{V})^+$  where  $(\mathbf{R} \cdot \mathbf{V})^+ = (\mathbf{R} \cdot \mathbf{V})$  if  $(\mathbf{R} \cdot \mathbf{V}) \geq 0$  and 0 otherwise. The BRDF of the reciprocal Phong model is

$$f_{r,\text{Phong}}(\mathbf{L}, \mathbf{V}) = c_n \cdot \cos^n \alpha \quad (3.5)$$

where  $c_n$  is a scalar parameter. Lafortune [40] has shown that

$$c_n \leq \frac{n+2}{2\pi} \quad (3.6)$$

must hold in order for the model to preserve energy balance.

The new, corrected, reciprocal BRDF, which is the main result of this chapter, is

$$f_r(\mathbf{L}, \mathbf{V}) = c_n \cdot \frac{\cos^n \alpha}{\cos \Theta_{min}} \quad (3.7)$$

This model meets the mentioned requirements and really provides metallic impression as we demonstrate it later.

Since the reflection vector  $\mathbf{R}$  is

$$\mathbf{R} = 2(\mathbf{N} \cdot \mathbf{L})\mathbf{N} - \mathbf{L} \quad (3.8)$$

the formula to compute  $(\mathbf{R} \cdot \mathbf{V})$  can be expressed as

$$(\mathbf{R} \cdot \mathbf{V}) = (2(\mathbf{N} \cdot \mathbf{L})\mathbf{N} - \mathbf{L}) \cdot \mathbf{V} = 2(\mathbf{N} \cdot \mathbf{L})(\mathbf{N} \cdot \mathbf{V}) - (\mathbf{L} \cdot \mathbf{V}) \quad (3.9)$$

Substituting this into equation 3.7, we can obtain the following formula for the new BRDF:

$$f_r(\mathbf{L}, \mathbf{V}) = c_n \cdot \frac{[(2(\mathbf{N} \cdot \mathbf{L})(\mathbf{N} \cdot \mathbf{V}) - (\mathbf{L} \cdot \mathbf{V}))^+]^n}{\max((\mathbf{N} \cdot \mathbf{L}), (\mathbf{N} \cdot \mathbf{V}))} \quad (3.10)$$

The albedo function of the new model can be computed from the Phong BRDF as the sum of the following two integrals:

$$\begin{aligned} \mathbf{a}(\mathbf{L}) = & \int_{\Omega((\mathbf{N} \cdot \mathbf{L}) < (\mathbf{N} \cdot \mathbf{V}))} f_{r, \text{Phong}}(\mathbf{L}, \mathbf{V}) d\omega_{\mathbf{V}} + \\ & + \int_{\Omega((\mathbf{N} \cdot \mathbf{L}) \geq (\mathbf{N} \cdot \mathbf{V}))} f_{r, \text{Phong}}(\mathbf{L}, \mathbf{V}) \cdot \frac{(\mathbf{N} \cdot \mathbf{V})}{(\mathbf{N} \cdot \mathbf{L})} d\omega_{\mathbf{V}} \end{aligned} \quad (3.11)$$

Analyzing the albedo functions we can come to the conclusion that the  $c_n$  constant of inequality 3.6 is also good for the new model. More precisely, the albedo of the BRDF of equation 3.7 has only a negligible overshooting where it exceeds value 1 if  $n \geq 1$ . The overshooting occurs at small incident angles where  $\mathbf{L}$  is close to  $\mathbf{N}$ .

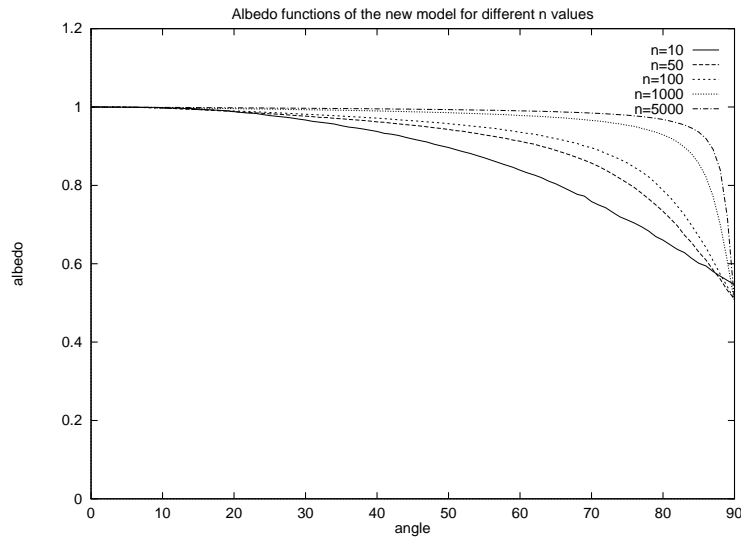


Figure 3.1: Albedo functions of the new model for different  $n$  values

Below the arbitrarily selected  $n = 1$  minimum, the  $c_n$  value should be decreased in order to preserve energy balance, which would shift the maximum of the albedo function and the BRDF from the perpendicular incident direction. For example, if  $n = 1$  or 0.5, then the maximum  $c_n$  constant would result in 0.0003, and 0.01 maximum overshooting at 13 and 30 degrees, respectively.

Figure 3.1 shows the albedo functions for different  $n$  values. We can see that in the limit case the albedo converges to constant 1, which is the albedo of the ideal mirror.

### 3.2.3 Transition from the Phong model to the new model: $p$ -model

Using a  $p \in [0, 1]$  parameter, a continuous transition can be developed between the reciprocal Phong model defined by equation 3.5 and the new metal model, as follows:

$$f_r(\mathbf{L}, \mathbf{V}) = c_n \cdot \frac{\cos^n \alpha}{\cos^p \Theta_{\min}}, \quad 0 \leq p \leq 1 \quad (3.12)$$

Let us call this formula the  $p$ -model. If  $n \geq 1$ , then the maximum of the multiplicative factor  $c_n$  is as shown in equation 3.6 for any  $p \in [0, 1]$ .

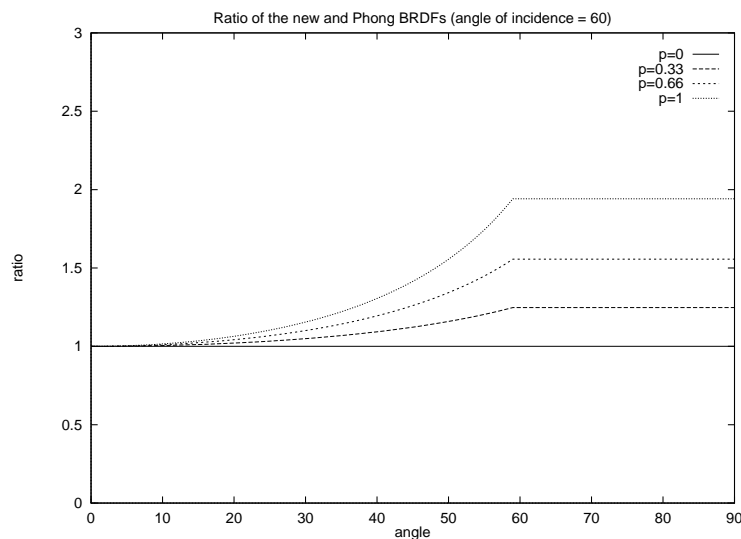


Figure 3.2: Ratio of the  $p$ -model and the Phong BRDFs for different viewing angles

Figure 3.2 shows the ratio of the BRDFs of the  $p$ -model and the Phong model for different viewing angles  $\Theta_{\mathbf{V}}$  and for different transition parameters  $p$ . The case of  $p = 0$  represents the reciprocal Phong model, while the case of  $p = 1$  means the new metal model.

### 3.2.4 The properties of the new metal model

This section examines the properties of the new model. Figure 3.3 compares the specular lobes of the Phong, new, Cook–Torrance and He–Torrance models at  $42^\circ$  incident angle. The models have been calibrated to provide similar response for perpendicular illumination.

Supposing that the Fresnel term is 1 (for silver this is practically true), the albedos of the Phong, He–Torrance, Cook–Torrance, Ward and the new models are shown in figure 3.4. Note that the Cook–Torrance and the Ward models diverge at grazing angles, while the Phong, He–Torrance and Ward BRDFs badly decrease for greater incident angles. The new model converges to a value that is not lower than 0.5 for grazing angles.

The maximum of the new BRDF is always at the mirror direction  $\mathbf{R}$  and its value is  $\frac{c_n}{\cos \Theta_{\mathbf{L}}}$  for any  $n$ , while the maximum of the Phong model is always  $c_n$ .

Figure 3.5 compares the normalized BRDF functions of the Phong and the new models for 0, 40 and 80 degree incident angles (normalization scales the BRDF to be 1 at 0 incident angle).

It is also worth examining the output radiance assuming a single point-like light-source of intensity  $4\pi$  at distance 1 in direction  $\mathbf{L}$ . In this case the irradiance is  $\cos \Theta_{\mathbf{L}}$ . The output radiances of the Phong and the new models at different incident directions are shown in figure 3.6. This figure demonstrates

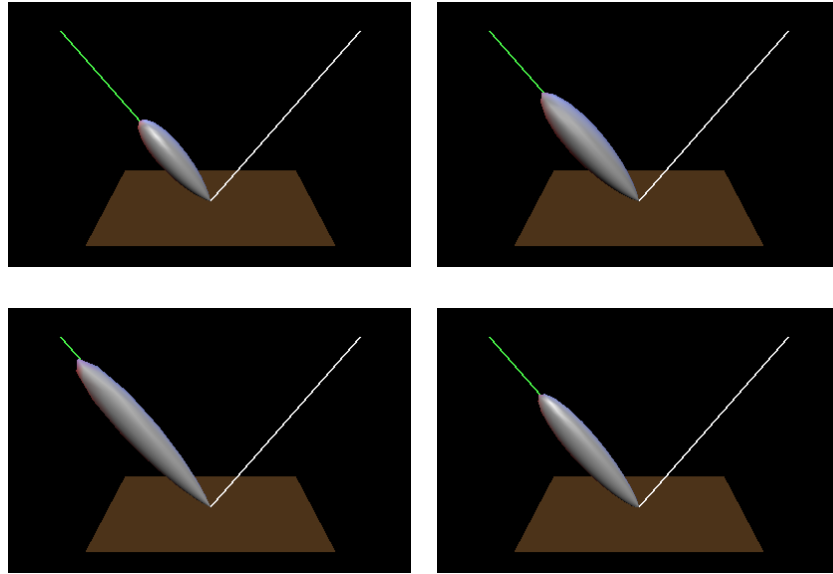


Figure 3.3: Specular lobes of the Phong ( $n = 20$ ), new ( $n = 20$ ), Cook-Torrance ( $m = 0.1$ ,  $n = 5$ ) and He-Torrance ( $\sigma_0 = 0.1$ ,  $\tau = 1.4$ ,  $n_i = 6$ ,  $n_r = 0.8$ ) models

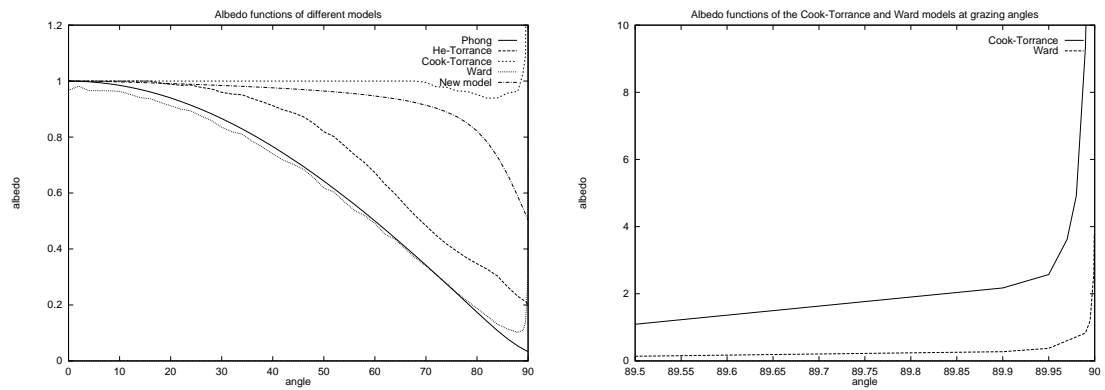


Figure 3.4: Albedo functions of the Phong ( $n = 150$ ), new ( $n = 150$ ), Cook-Torrance ( $m = 0.1$ ), Ward ( $m = 0.1$ ) and He-Torrance ( $\sigma_0 = 0.1$ ,  $\tau = 1.7$ ) models

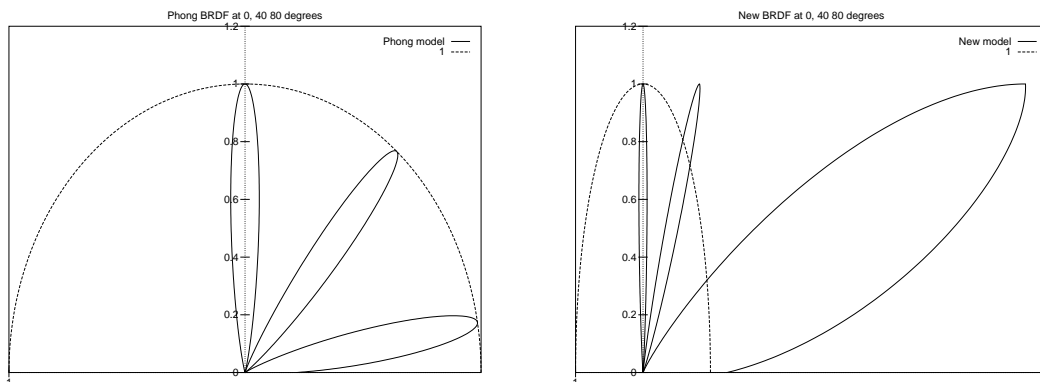


Figure 3.5: Comparison of the BRDFs of the Phong and the new models ( $n = 100$ )

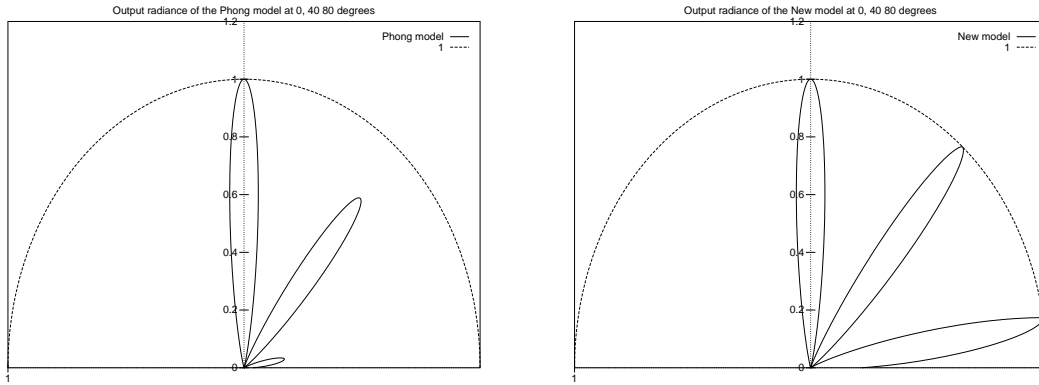


Figure 3.6: Comparison of the output radiances of the Phong and the new models ( $n = 100$ )

the earlier statement that the “Phong-mirror” gets darker for greater incident angles, but the new model eliminates this artifact.

### Behavior at grazing angles

The new model slightly differs from real metals at grazing angles. Unfortunately no reliable data are available about the reflection of metals around  $90^\circ$  incident angle. However, when the He–Torrance model was fitted, the following observation was made [41]: The normalized BRDF has about 1 value at the mirror direction while the maximum which is of order  $\frac{1}{\cos \Theta_L}$  is significantly below the mirror direction (off-specular peak). Although this feature is not included in the new model, according to our experience this error is not visually observable.

### Ideal mirror

The new model gives back the normalized BRDF of the ideal mirror for  $n \rightarrow \infty$ , which is  $\frac{1}{\cos \Theta_L}$ . The output radiance is  $L^{\text{out}}(\mathbf{V}) = L^{\text{in}}(\mathbf{L})$  if  $\mathbf{V} = \mathbf{L}$  and 0 otherwise.

Note that the new model can arbitrarily approximate the ideal mirror. Selecting  $n$  in an appropriate way (e.g.  $n = 10^4 \dots 10^8$ ), realistic, glossy mirrors can easily be generated. Using, for example, distributed ray-tracing, the mirrors do not require a special case.

## 3.3 Generalizations of the new model

### 3.3.1 Retro-reflective materials

The proposed model can easily be generalized to provide a *retro-reflective* BRDF which has the maximum at the direction of the incident illumination. Practical examples of retro-reflective objects are a projection screen, a traffic sign, etc. For retro-reflective materials, mirror direction vector  $\mathbf{R}$  should be replaced by the illumination direction  $\mathbf{L}$ . The BRDF formula can be simplified to the following form:

$$f_r(\mathbf{L}, \mathbf{V}) = c_n \cdot \frac{[(\mathbf{L} \cdot \mathbf{V})^+]^n}{\max((\mathbf{N} \cdot \mathbf{L}), (\mathbf{N} \cdot \mathbf{V}))} \quad (3.13)$$

The maximum value of  $c_n$  is as defined in equation 3.6.

### 3.3.2 Anisotropic materials

Lafortune et. al. [41] introduced the anisotropic generalization of the Phong model as:

$$f_r(\mathbf{L}, \mathbf{V}) = C_{\max} \cdot (C_x(R_x V_x) + C_y(R_y V_y) + C_z(R_z V_z))^n = C_{\max} \cdot [(\mathbf{R} \cdot \mathbf{V})_M]^n \quad (3.14)$$

where  $(\mathbf{R} \cdot \mathbf{V})_M = \mathbf{R}^T M \mathbf{V}$  is a special dot product containing also a multiplication with diagonal matrix  $M$ . The values at the diagonal of  $M$  are  $C_x$ ,  $C_y$  and  $C_z$ , respectively.

As for the original Phong model, the anisotropic generalization can also be normalized with  $p$ -th power of the maximum of the dot products  $(\mathbf{N} \cdot \mathbf{L})$ ,  $(\mathbf{N} \cdot \mathbf{V})$ , thus we can obtain:

$$f_r(\mathbf{L}, \mathbf{V}) = C_{\max} \cdot \frac{[(\mathbf{R} \cdot \mathbf{V})_M]^n}{\max((\mathbf{N} \cdot \mathbf{L}), (\mathbf{N} \cdot \mathbf{V}))^p} \quad (3.15)$$

This model is able to approximate metals even with a single term, but several terms can also be combined together. The resulting approximation is better than Lafortune's scheme since letting  $p = 0$  this formula gives back his original expression as a special case. The general formula containing a combination of several terms is:

$$f_r(\mathbf{L}, \mathbf{V}) = \sum_i C_i \cdot \frac{[(\mathbf{R} \cdot \mathbf{V})_{M_i}]^{n_i}}{\max((\mathbf{N} \cdot \mathbf{L})(\mathbf{N} \cdot \mathbf{V}))^{p_i}} \quad (3.16)$$

### 3.4 Importance sampling

Importance sampling is an effective technique to reduce the variance of Monte-Carlo algorithms. It requires the generation of random samples according to a probability density which is proportional, or at least approximately proportional to the integrand.

In order to generate the output radiance  $L^{\text{out}}(\mathbf{V})$  from the incident illumination  $L^{\text{in}}(\mathbf{L})$  ( $\mathbf{L} \in \Omega$ ) in Monte-Carlo ray-tracing, the following integral should be evaluated:

$$L^{\text{out}}(\mathbf{V}) = \int_{\Omega} L^{\text{in}}(\mathbf{L}) \cdot f_r(\mathbf{L}, \mathbf{V}) \cdot \cos \Theta_{\mathbf{L}} \, d\omega_{\mathbf{L}}. \quad (3.17)$$

If  $p(\mathbf{L})$  is a probability density and directions  $\mathbf{L}_1, \mathbf{L}_2, \dots, \mathbf{L}_M$  are sampled following this probability distribution, then the Monte-Carlo estimate of this integral is:

$$L^{\text{out}}(\mathbf{V}) \approx \frac{1}{M} \cdot \sum_{m=1}^M L^{\text{in}}(\mathbf{L}_m) \cdot \frac{f_r(\mathbf{L}_m, \mathbf{V}) \cdot \cos \Theta_{\mathbf{L}_m}}{p(\mathbf{L}_m)} \quad (3.18)$$

According to the concept of *importance sampling*,  $p(\mathbf{L})$  should be approximately proportional to the integrand to minimize the variance of the solution. If no a-priori information is available about  $L^{\text{in}}$ , then it is assumed to be constant, thus the probability density should be proportional to  $f_r(\mathbf{L}, \mathbf{V}) \cdot \cos \Theta_{\mathbf{L}}$ .

#### 3.4.1 Importance sampling for the Phong model

For the Phong model where the integrand is  $L^{\text{in}}(\mathbf{L}) \cdot c_n \cdot (\mathbf{V} \cdot \mathbf{R})^n \cdot \cos \Theta_{\mathbf{L}} = L^{\text{in}}(\mathbf{L}) \cdot c_n \cdot \cos^n \alpha \cdot \cos \Theta_{\mathbf{L}}$ , Lafortune [40] proposed the following probability density:

$$p(\mathbf{L}) = \frac{n+1}{2\pi} \cdot [(\mathbf{V} \cdot \mathbf{R})^+]^n = \frac{n+1}{2\pi} \cdot \cos^n \alpha \quad (3.19)$$

Samples according to this probability density can be generated in the following way. Suppose that we can get  $(u_m, v_m)$  samples from a set containing uniformly distributed points in the unit square. Note that this sampling will be used in Monte-Carlo ray-tracing where rays are traced backwards. It means that for a given  $\mathbf{V}$  an appropriate  $\mathbf{L}$  vector should be found, which consists of two steps. In the first step reflection direction  $\mathbf{R}_m$  is found, then  $\mathbf{L}_m$  is generated by mirroring.

In order to find a reflection direction  $\mathbf{R}_m$ , angles  $\alpha_m$  and  $\phi_m$  in the lobe around  $\mathbf{V}$  is generated:

$$(\alpha_m, \phi_m) = (\arccos u_m^{\frac{1}{n+1}}, 2\pi v_m) \quad (3.20)$$

Note that using this formula, the probability density of generating a given direction  $(\alpha, \phi)$  is  $\frac{1}{n+1} 2\pi \cos^n \alpha$  which is proportional to the BRDF.

Let us establish a Cartesian coordinate system  $\mathbf{i}, \mathbf{j}, \mathbf{k}$  where  $\mathbf{k} = \mathbf{V}$ , and:

$$\mathbf{i} = \frac{\mathbf{V} \times \mathbf{N}}{|\mathbf{V} \times \mathbf{N}|} \quad \mathbf{j} = \mathbf{i} \times \mathbf{k} \quad (3.21)$$

Using these unit vectors, the mirror direction  $\mathbf{R}_m$  is:

$$\mathbf{R}_m = \sin \alpha_m \cdot \cos \phi_m \cdot \mathbf{i} + \sin \alpha_m \cdot \sin \phi_m \cdot \mathbf{j} + \cos \alpha_m \cdot \mathbf{k} \quad (3.22)$$

From the mirror direction the light vector can be derived easily:  $\mathbf{L}_m = (\mathbf{N} \cdot \mathbf{R})_m \mathbf{N} - \mathbf{R}_m$ . Note that sampling according to this probability density may generate directions that point into the object ( $(\mathbf{N} \cdot \mathbf{L})_m < 0$ ). Thus we should check whether or not the light vector points out of the object ( $(\mathbf{N} \cdot \mathbf{L})_m \geq 0$ ) and reject this sample if it does not. This rejection poses no problem since from these directions  $L^{\text{in}}(\mathbf{L}_m)$  is zero, thus these samples would get zero weight.

Summarizing, the Monte-Carlo estimate of the output radiance is

$$L^{\text{out}}(\mathbf{V}) \approx \frac{1}{M} \cdot \frac{2\pi c_n}{n+1} \cdot \sum_{m=1}^M L^{\text{in}}(\mathbf{L}_m) \cdot \cos \Theta_{\mathbf{L}_m} \quad (3.23)$$

If  $c_n$  is the maximum allowed by inequality 3.6, then we obtain

$$L^{\text{out}}(\mathbf{V}) \approx \frac{1}{M} \cdot \frac{n+2}{n+1} \cdot \sum_{m=1}^M L^{\text{in}}(\mathbf{L}_m) \cdot \cos \Theta_{\mathbf{L}_m} \quad (3.24)$$

The selected probability density is not optimally proportional to the integrand, only with  $\cos^n \alpha$ . It would be better to find a density that is proportional to  $\cos^n \alpha \cdot \cos \Theta_{\mathbf{L}}$ , but it would be quite complicated to implement practically. This simplification reduces the efficiency of the importance sampling, since the ignored  $\cos \Theta_{\mathbf{L}}$  can be arbitrarily small at grazing angles, and its average is only  $\frac{1}{2}$ .

### 3.4.2 Importance sampling for the new model

The efficiency of the importance sampling gets higher for the new model, and it will be particularly good for large viewing angles. For the new model the integrand is  $I(\mathbf{L}, \mathbf{V}) = L^{\text{in}}(\mathbf{L}) \cdot c_n \cdot \frac{\cos^n \alpha}{\max(\cos \Theta_{\mathbf{L}}, \cos \Theta_{\mathbf{V}})} \cdot \cos \Theta_{\mathbf{L}}$ , which can be simplified if the cases when the incident angle is smaller than the viewing angle ( $\cos \Theta_{\mathbf{L}} \geq \cos \Theta_{\mathbf{V}}$ ) and when the incident angle is greater than the viewing angle ( $\cos \Theta_{\mathbf{L}} < \cos \Theta_{\mathbf{V}}$ ) are considered separately:

$$\begin{aligned} I(\mathbf{L}, \mathbf{V}) &= L^{\text{in}}(\mathbf{L}) \cdot c_n \cdot \cos^n \alpha && \text{if } \cos \Theta_{\mathbf{L}} \geq \cos \Theta_{\mathbf{V}}, \\ I(\mathbf{L}, \mathbf{V}) &= L^{\text{in}}(\mathbf{L}) \cdot c_n \cdot \cos^n \alpha \cdot \frac{\cos \Theta_{\mathbf{L}}}{\cos \Theta_{\mathbf{V}}} && \text{if } \cos \Theta_{\mathbf{L}} < \cos \Theta_{\mathbf{V}} \end{aligned} \quad (3.25)$$

As for the Phong model, the samples are generated according to  $\frac{n+1}{2\pi} \cos^n \alpha$  probability density function. Using the  $c_n = \frac{n+2}{2\pi}$  substitution, the Monte-Carlo approximation of the integral is:

$$L^{\text{out}}(\mathbf{V}) \approx \frac{1}{M} \cdot \frac{n+2}{n+1} \cdot \left( \sum_{\cos \Theta_{\mathbf{L}_m} \geq \cos \Theta_{\mathbf{V}}}^M L^{\text{in}}(\mathbf{L}_m) + \sum_{\cos \Theta_{\mathbf{L}_m} < \cos \Theta_{\mathbf{V}}}^M L^{\text{in}}(\mathbf{L}_m) \cdot \frac{\cos \Theta_{\mathbf{L}_m}}{\cos \Theta_{\mathbf{V}}} \right) \quad (3.26)$$

For large viewing angles the samples will be in the first sum of equation 3.26. Note that the probability density also compensates for the  $\cos \Theta_{\mathbf{L}}$  factor here, thus this results in a more effective importance sampling. The larger the viewing angle, the greater the efficiency (even if the probability of the rejected samples approaches 0.5). The worst case of the importance sampling of the new model is at zero degree viewing angle, where the efficiency degrades to that of the sampling of the Phong model, which is fortunately the best here.

### 3.4.3 Albedo at grazing angles

Note that for  $L^{\text{in}} = 1$  equation 3.17 gives the albedo function at illumination direction  $\mathbf{V}$ , thus the importance sampling can also be used to effectively calculate and tabulate the values of the albedo function.

Equation 3.26, that calculates the albedo as an expected value, can also be given an intuitive explanation. At  $90^\circ$  viewing direction, the weight of sample rays is  $\frac{n+2}{n+1}$ . Since the BRDF is symmetric around  $\mathbf{R}$ , half of the samples point into the object, and are thus rejected. Consequently, the albedo at  $90^\circ$  is:

$$\mathbf{a}(90^\circ) = \frac{n+2}{2(n+1)} \quad (3.27)$$

The albedos at grazing angles for  $n = 1$ ,  $n = 2$  and  $n \rightarrow \infty$  are  $\frac{3}{4}$ ,  $\frac{2}{3}$  and  $\frac{1}{2}$ , respectively. Note that for  $n \rightarrow \infty$  which represents the ideal mirror case, for any  $\epsilon > 0$ ,  $\mathbf{a}(90^\circ - \epsilon) = 1$ , thus the new model can really converge to the ideal mirror.

## 3.5 Visualization of real materials

### 3.5.1 Metals

Metals have negligible diffuse reflectance and their BRDF is proportional to the Fresnel function which is based on a complex and wavelength dependent refraction index  $\kappa$  [22]. The Fresnel function also depends on the incident angle making the highlights colored. The reflected color can be computed as a product of the irradiance and the BRDF, which is usually done at a few discrete wavelengths.

For a single wavelength  $\lambda$ , the new BRDF for metals is:

$$f_r(\mathbf{L}, \mathbf{V}, \lambda) = \frac{n+2}{2\pi} \cdot \frac{\cos^n \alpha}{\cos \Theta_{\min}} \cdot F(\kappa(\lambda), \Theta(\mathbf{L}, \mathbf{V})) \quad (3.28)$$

where  $\Theta(\mathbf{L}, \mathbf{V})$  is an appropriate incident angle, which should be a symmetric function of  $\mathbf{L}$  and  $\mathbf{V}$  to make the model reciprocal. A straightforward selection is the angle of the halfway vector  $\mathbf{H}$ . Another alternative is letting  $\Theta = \Theta_{\min}$ . This alternative gives back the angle of the halfway vector for the mirror direction but for other directions it generates a smaller angle. The largest difference between the angle of the halfway vector and  $\Theta_{\min}$  occurs when the lighting is perpendicular to the surface and the viewing direction is parallel to it. Here  $\Theta_{\min} = 0$  while the angle of the halfway vector is  $45^\circ$ . Fortunately, the larger variation of Fresnel function is usually closer to  $90^\circ$  than to 0.

If we select  $\Theta_{\min}$  to evaluate the Fresnel function, then the resulting BRDF is

$$f_{r,\text{metal}}(\mathbf{L}, \mathbf{V}, \lambda) = \frac{n+2}{2\pi} \cdot \frac{\cos^n \alpha}{\cos \Theta_{\min}} \cdot F(\kappa(\lambda), \Theta_{\min}) = \frac{\cos^n \alpha}{g(\Theta_{\min})} \quad (3.29)$$

where  $g(\Theta_{\min})$  can be tabulated for the considered wavelengths. These tables allow for very fast BRDF evaluation. This computational cost is lower than that of any previously known metal models.

### 3.5.2 Plastics and ceramics

The new model is appropriate not only for metals but also for other highly specular materials, such as for certain plastics and ceramics. The main difference between these materials and metals is that their diffuse component is relevant and the specular part is responsible for the smaller part of the reflected power. For non metals the refraction index is a real number. The highlights can be assumed to be white everywhere not only for greater incident angles.

When rendering plastics, the classical Lambertian model can be applied for the diffuse component, while the specular part can be determined by the new model. Thus the BRDF has two components:

$$f_{r,\text{plastics}}(\mathbf{L}, \mathbf{V}, \lambda) = \frac{a_d(\lambda)}{\pi} + a_s \cdot \frac{n+2}{2\pi} \cdot \frac{\cos^n \alpha}{\cos \Theta_{\min}} \cdot F(\kappa(\lambda), \Theta_{\min}) \quad (3.30)$$

where reflectivity  $a_d$  is the albedo of the diffuse component and  $a_s$  determines the size of the specular part. In order to make the model conserve energy,  $a_s + a_d$  should not exceed 1. In many practical situations it is enough to compute the color on the three primary colors ( $r, g, b$ ) and the Fresnel function can be assumed to be constant 1. For this simplified case the following plastic model is proposed:

$$f_{r,\text{plastics}}(\mathbf{L}, \mathbf{V}) = \frac{(r, g, b)}{\pi} + a_s \cdot \frac{n+2}{2\pi} \cdot \frac{\cos^n \alpha}{\cos \Theta_{\min}} \cdot (1, 1, 1) \quad (3.31)$$

where  $r, g, b$  are the albedos of the diffuse component at the wavelengths of the three primaries, and  $a_s \leq 1 - \max(r, g, b)$  should hold. It should be noted that not all non-metal materials can be visualized by this simple BRDF, and more sophisticated plastic models [56] might be required. However, this is a computationally effective model for many practical cases.

## 3.6 Material editor

Due to its simplicity, the proposed BRDF can be used in commercial rendering programs. Based on Paul Heckbert's BRDF editor [28], we have developed a material editor, where the optical parameters can be set interactively while the effect of the current settings is visualized by a simple scene. In the simplest case, the material editor displays a sphere that is illuminated by a few point light-sources and also by ambient light. The classical ambient term, however, is not good to render the objects outside the highlight spots since it would result in a constant color. Thus we propose the application of *homogeneous*



*daylight illumination* to replace classical ambient lighting model. The homogeneous daylight illumination can be defined by the constant  $L^{\text{in}}(\mathbf{L}) = S_\lambda$  function at each representative wavelength. In this case the perceived radiance reflected to direction  $\mathbf{V}$  is

$$L_\lambda^{\text{out}}(\mathbf{V}) = \int_{\Omega} S_\lambda \cdot f_r(\mathbf{L}, \mathbf{V}, \lambda) \cdot \cos \Theta_{\mathbf{L}} d\omega_{\mathbf{L}} = S_\lambda \cdot \mathbf{a}(\mathbf{V}) \quad (3.32)$$

which is the albedo of the material multiplied by the radiance of the sky. Note that even without point light-sources the resulting image is not homogeneous for a metal sphere due to the angle dependence of the Fresnel and the albedo functions (figure 3.7). Using pre-computed albedo tables the evaluation of the daylight illumination is fast.

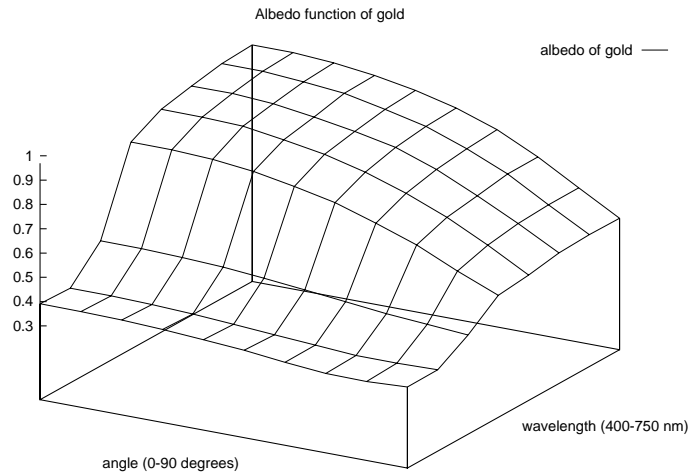


Figure 3.7: The albedo of gold as a function of the incident angle and wavelength

The daylight as well as the point light-sources can be either white or colored, and can be set interactively by the user.

Since the material editor is expected to provide realistic appearance in all lighting conditions, the editor should incorporate automatic color mapping. This is done by calculating the illumination of a diffuse gray sphere, which is expected to have 0.5 median lightness on the display. This determines a scaling factor for the mapping of the images. Using the  $\max(r, g, b)$  instead of the lightness, satisfactory results can be obtained for colored light-sources as well.

## 3.7 Reflectance models of (N · H) type

### 3.7.1 Blinn model

The Blinn model can be modified similarly as the Phong model was corrected. Recall that the specular part the original Blinn model [8] is

$$f_{r,\text{Blinn}}(\mathbf{L}, \mathbf{V}) = C_n \cdot (\mathbf{N} \cdot \mathbf{H})^n \quad (3.33)$$

The analytical calculation of the  $C_n$  constant for integer  $n$  values can be found in [3]. The complexity of this calculation is  $O(n)$ . The problems of this model are similar to that of the Phong model. The reflected radiance and the albedo converges to zero at grazing angles if  $n$  goes to infinity.

Similarly to the procedures applied for the Phong model, this model can also be corrected:

$$f_r(\mathbf{L}, \mathbf{V}) = C_n \cdot \frac{(\mathbf{N} \cdot \mathbf{H})^n}{\max((\mathbf{N} \cdot \mathbf{L}), (\mathbf{N} \cdot \mathbf{V}))} \quad (3.34)$$

The  $C_n$  constants that can be allowed not to violate energy balance are summarized by table 3.1.

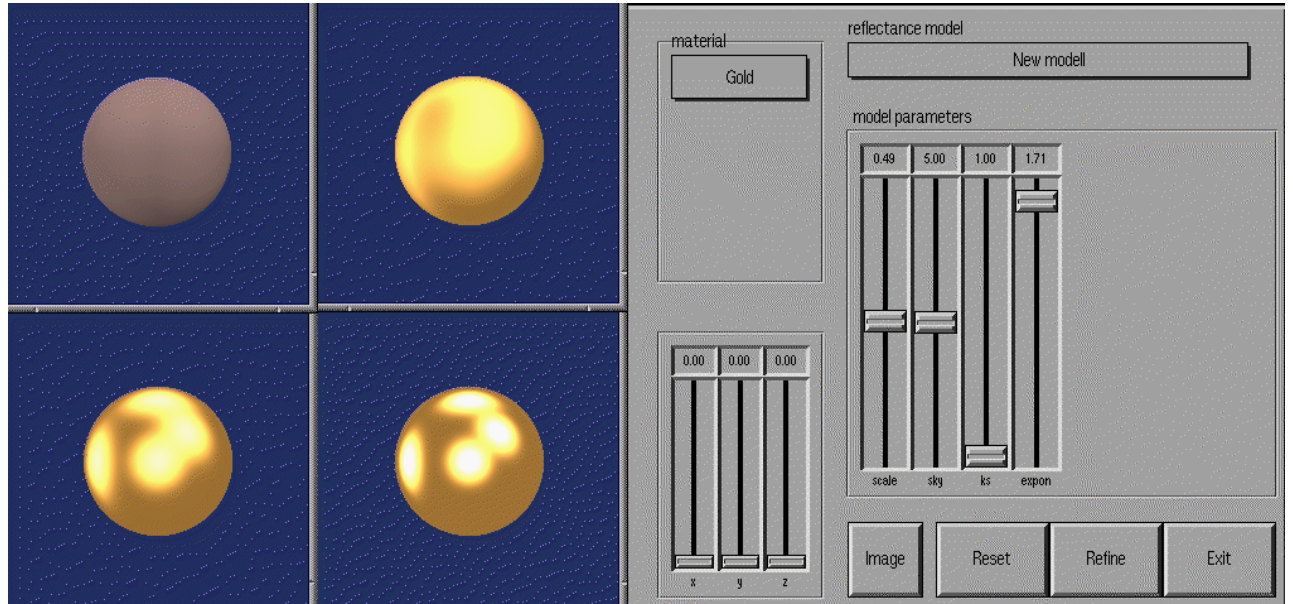


Figure 3.8: A snapshot of the material editor displaying the diffuse gray reference object, and golden spheres having  $n = 2, 8, 16$  exponents

$n$	Blinn	Blinn/ $\cos \Theta_{\min}$
1	0.350	0.293
2	0.382	0.368
4	0.449	0.449
8	0.592	0.592
16	0.895	0.895
32	1.52	1.52
64	2.79	2.79
128	5.34	5.34
256	10.4	10.4
512	20.6	20.6

Table 3.1: The maximum  $C_n$  constants for the original and the corrected Blinn models

### 3.7.2 Ward model

Ward [75] introduced a simple BRDF of type  $(\mathbf{N} \cdot \mathbf{H})$ . This model is simpler than other known metal models and its anisotropic form could provide particularly good metallic impression. For the isotropic case, the specular component has the following form:

$$f_r(\mathbf{L}, \mathbf{V}) = \frac{C_{\max}}{4\pi m^2} \cdot \frac{e^{-\frac{\tan^2 \delta}{m^2}}}{\sqrt{(\mathbf{N} \cdot \mathbf{L}) \cdot (\mathbf{N} \cdot \mathbf{V})}} \quad (3.35)$$

where  $\delta = \arccos(\mathbf{N} \cdot \mathbf{H})$  and  $m$  is the standard deviation (RMS) of the surface slope.

The main problem of this model is its behavior at grazing angles and at viewing directions below the mirror direction. Not only the BRDF but also the reflected radiance are unbounded for the Ward model, which is against practical considerations. Ward stated that selecting  $C_{\max} = 1$  the model meets energy balance if  $m < 0.2$ . Examining the albedo function in the range of  $0 \dots 89^\circ$ , this is true quite accurately. Here the maximum of the albedo is greater than 0.85, and it converges to 1 if  $m$  is decreased.

However at grazing angles the albedo significantly violates energy balance (figure 3.4). It can be shown analytically that the BRDF diverges to infinity at grazing angles, thus this model is not physically plausible. For example, if  $m = 0.1$ , then  $\mathbf{a}(89.995^\circ) = 1.2$ ,  $\mathbf{a}(89.999^\circ) = 2.6$  and  $\mathbf{a}(89.9995^\circ) = 3.8$ .

One way of correcting this error is the limitation of the  $\frac{1}{\sqrt{(\mathbf{N} \cdot \mathbf{L}) \cdot (\mathbf{N} \cdot \mathbf{V})}}$  function.

On the other hand, the previously applied normalization can also be used here, which leads to a new BRDF model:

$$f_r(\mathbf{L}, \mathbf{V}) = \frac{C_{\max}}{4\pi m^2} \cdot \frac{e^{-\frac{\tan^2 \delta}{m^2}}}{\max((\mathbf{N} \cdot \mathbf{L}), (\mathbf{N} \cdot \mathbf{V}))} \quad (3.36)$$

A similar method can be applied to the anisotropic Ward model as well.

The  $C_{\max}$  constants are summarized by table 3.2.

$m$	$C_{\max}$
0.4	1.63
0.2	1.16
0.1	1.04
0.05	1.011
0.02	1.005
0.01	1.002
0.005	1.002

Table 3.2: The maximum  $C_{\max}$  constants for the corrected Ward models

### 3.7.3 Cook–Torrance and He–Torrance models

As the Ward model, the Cook–Torrance model is not physically plausible either since it violates the energy balance at grazing angles (figure 3.4). It can be shown analytically that the albedo goes to infinity at grazing angles. The clue of the proof is the integration of the  $\frac{G}{(\mathbf{N} \cdot \mathbf{L}) \cdot (\mathbf{N} \cdot \mathbf{V})}$  on an appropriate subset of the hemisphere. Illustrating the divergence numerically for  $m = 0.1$ , the albedo values at  $\Theta_{\mathbf{L}} = 89.9^\circ$ ,  $\Theta_{\mathbf{L}} = 89.99^\circ$  and  $\Theta_{\mathbf{L}} = 89.999^\circ$  are 2.1, 9.3 and 91 respectively. On the other hand, both the BRDF and the reflected radiance diverge. A possible correction is the limitation of the BRDF or more precisely the  $\frac{G}{(\mathbf{N} \cdot \mathbf{L}) \cdot (\mathbf{N} \cdot \mathbf{V})}$  term.

The main objective of the construction of the He–Torrance model was the accurate description of the BRDF. No analysis has been published so far that examines the energy balance and its behavior at grazing angles.

### 3.7.4 Mean albedo

If the irradiance  $L^{\text{in}}$  is constant in the whole hemisphere, then the ratio of the total reflected power is called the *mean albedo*, which can be obtained as:

$$a_{\text{mean}} = \frac{1}{\pi} \cdot \int_{\Omega} \mathbf{a}(\mathbf{L}) \cdot \cos \Theta_{\mathbf{L}} \, d\omega_{\mathbf{L}} \quad (3.37)$$

For diffuse white materials and for the ideal mirror the mean albedo is 1. Table 3.3 shows the mean albedo for different models.

$n$	Phong	Phong/ $\cos \Theta_{\min}$	Blinn	Blinn/ $\cos \Theta_{\min}$
1	0.737	0.934	0.879	0.941
2	0.708	0.902	0.800	0.952
4	0.688	0.887	0.706	0.863
8	0.676	0.888	0.620	0.748
16	0.670	0.901	0.562	0.679
32	0.668	0.919	0.531	0.648
64	0.667	0.937	0.516	0.639
128	0.667	0.953	0.508	0.640
256	0.667	0.966	0.504	0.644
512	0.667	0.975	0.502	0.649
$\infty$	0.5	1	0.5	1

Table 3.3: Mean albedo values of different models

The proposed correction by  $\frac{1}{\cos \Theta_{\min}}$  has “pumped-up” the mean albedo, especially for the Phong-type model. The models of  $(\mathbf{N} \cdot \mathbf{H})$  type including the Blinn and the Ward models are significantly “darker” even after the pumping-up than the Phong-type models that converge to the ideal mirror faster by increasing  $n$ . For example, if  $n = 128$ , then the mean albedo of the Blinn model has been increased from 0.508 to 0.640 due to the correction. At  $90^\circ$  incident angle, on the other hand, the albedo has changed from  $7.8 \cdot 10^{-3}$  just to  $3.7 \cdot 10^{-2}$ .

## 3.8 Simulation results

The following images have been rendered by a Monte-Carlo ray-tracing algorithm that incorporates the discussed importance sampling.

The first three images display metal objects and were rendered by the metal model of equation 3.29. Color computation was carried out at 8 discrete wavelengths, then using the color matching functions the XYZ primaries were generated, which were finally converted to RGB. The material properties of the metals (complex index of refraction), color matching functions and the XYZ to RGB conversion matrix were taken from [22].

Figure 3.9 shows different metal objects on a diffuse plate. There are three point light-sources and daylight illumination is also present.

Figure 3.10 displays three metal teapots on a diffuse plane. Note that the teapot in the middle has quite high  $n$  value, creating mirror images of the other two teapots.

Figure 3.11 displays a golden Beethoven head of relatively low  $n$  value (4). On the other hand, the base silver plate acts as a non-perfect mirror since it has very high  $n$  value (5000) and the Fresnel function of the silver is close to 1, thus the mirror images of the other objects are just slightly blurred.

The last two images were rendered by the plastic model of equation 3.31. Figure 3.12 shows plastic spheres on a plastic plate. All spheres have a large diffuse component defining colors of the same hue but different lightness and saturation, and the  $(a_s, n)$  specular parameters are selected according to the following sequence: (0.04, 169), (0.065, 64), (0.09, 9), (0.13, 3).

Figure 3.13 shows two ceramic teapots. Again, the diffuse component is dominant, the  $n$  exponents are 100 and 20, respectively.

## 3.9 Conclusions

In this chapter it is derived a very simple BRDF model from the reciprocal Phong model, that can render metals and other specular objects. The new model is particularly suitable for importance sampling in Monte-Carlo ray-tracing algorithms. Importance sampling of the new model is simpler than that of the Blinn and Ward models and more efficient than that of the reciprocal and non-metallic Phong model. The new model can arbitrarily well approximate the ideal mirror, thus mirrors and polishing do not require a special case.

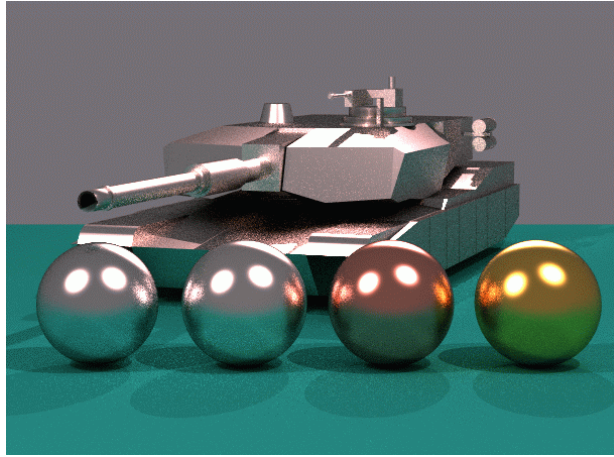


*Figure 3.9: A silver tank ( $n = 20$ ) with aluminum ( $n = 40$ ), silver ( $n = 50$ ), copper ( $n = 50$ ) and golden ( $n = 40$ ) spheres*

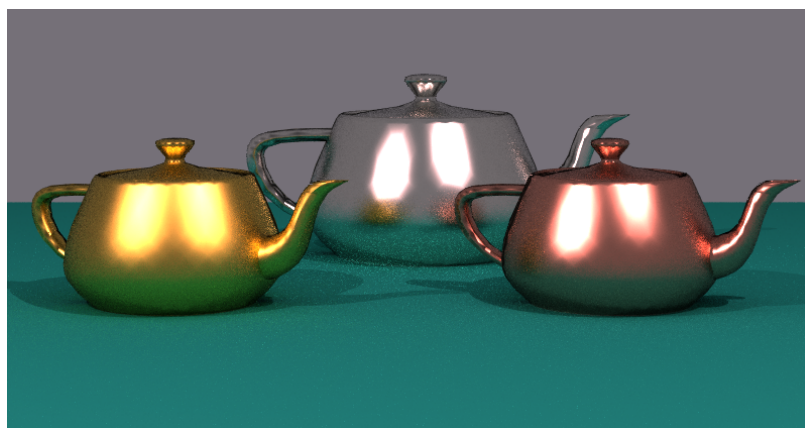


*Figure 3.10: A golden ( $n = 10$ ), silver ( $n = 190$ ) and copper ( $n = 100$ ) teapots*

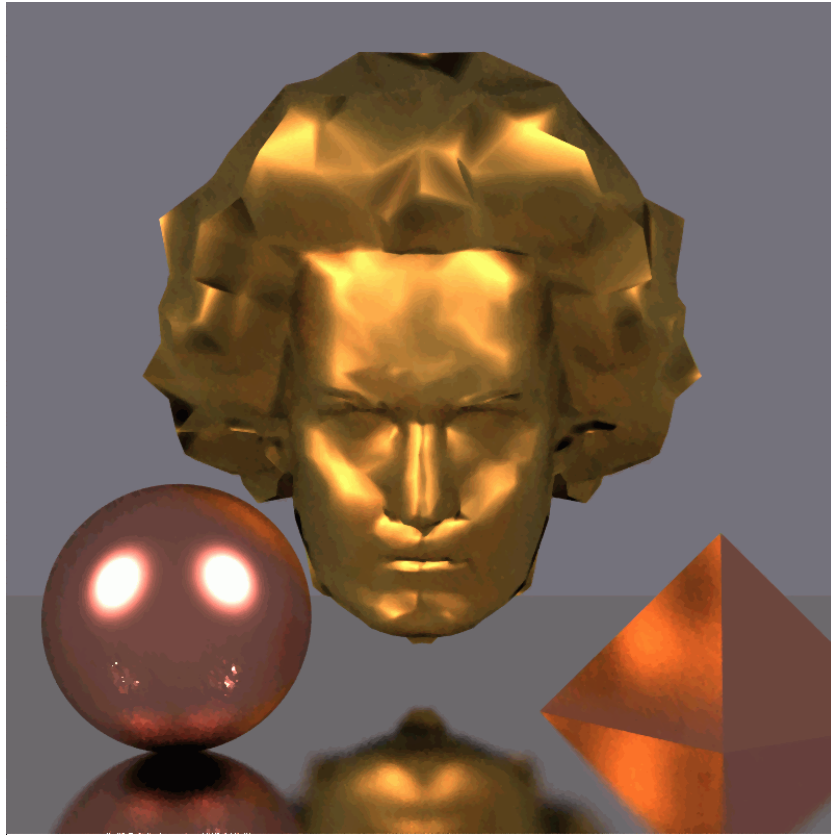


Figure 3.11: A golden Beethoven ( $n = 4$ ) with a copper sphere ( $n = 40$ ) and a copper pyramid ( $n = 150$ ) on a silver mirror ( $n = 5000$ )

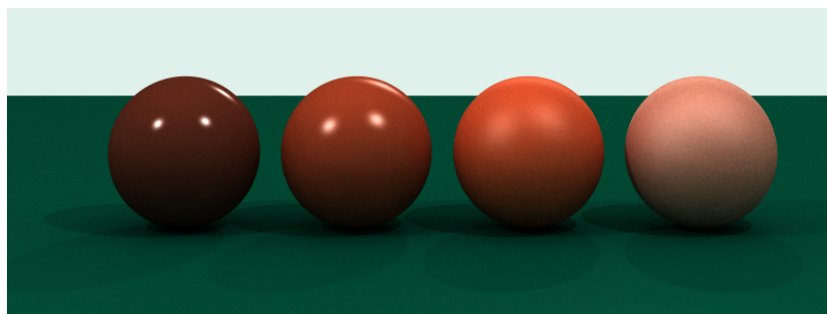


Figure 3.12: Plastic objects

Using numerical (Monte-Carlo) integration and also analytical considerations that are not detailed, we have shown that the Ward and the Cook–Torrance models are not physically plausible since they cannot conserve energy at grazing angles. The albedo, BRDF and the reflected radiance are unbounded. The problems of the behavior at grazing angles and energy conservation of physically based and physically plausible models require further research. No physically based model exists that can solve all problems at grazing angles. The proposed limitation of the BRDF of these models can guarantee physical plausibility, but is not appropriate for the representation of very smooth metals.

We have shown that multiplying different known BRDFs by  $\frac{1}{\cos \Theta_{\min}}$  the new model preserves energy balance and can provide metallic impression. These models can easily be incorporated in rendering software.

We have proposed daylight illumination to replace the ambient term when rendering a convex object and discussed how this can be computed efficiently using tabulated albedo values.

An important subject of the future research is the fitting to measured BRDF data. The models proposed in this chapter have the general form  $\frac{f(\alpha)}{g(\Theta_{\min})}$  where  $f$  is some BRDF and  $g$  is a scalar function. If measurement data are available, function  $g$  can also be determined to fit the resulting BRDF to the measurement results. On the other hand, if there is no such measurement data, the new model can be fitted to some physically accurate BRDF, as for example, to the He–Torrance or the Cook–Torrance models. The benefit of such an approach is that function  $g$  can be tabulated as a result of the fitting and the new model can be evaluated much more efficiently than the reference models.

This chapter discussed the anisotropic  $p$ -models that include the Lafortune’s model as a special case. Thus the new model is expected to provide more accurate fitting with less number of terms. In such fitting the resulting albedo should also be used as a control parameter in addition to the BRDF values.

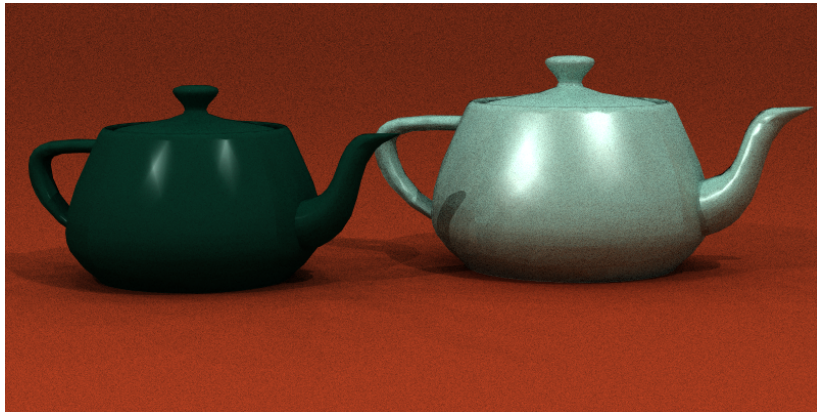


*Figure 3.13: Ceramic teapots*



## Chapter 4

# Reflectance Models with Fast Importance Sampling

### 4.1 Introduction

A central problem in photo-realistic rendering is the study of the optical material models characterized by *Bi-directional Reflection Distribution Functions*, or BRDFs.

BRDF models can be classified according to how they correspond to the real physical phenomenon of light-surface interaction.

Global illumination algorithms require that the BRDFs do not violate physics. Such shading models must satisfy both reciprocity and energy balance, and are called *physically plausible*[43]. Physically plausible models can be constructed empirically using simple functions and enforcing properties of the reciprocity and energy balance, or they can be derived from more detailed physical models describing the microstructure of surfaces or the scattering of electromagnetic waves[6].

The classical Lambert model of diffuse reflection and the Torrance–Sparrow model[72] of specular reflection are physically founded. Other physically based models used so far are the Cook–Torrance[14] and He–Torrance[29] models, which are good approximations for metals and plastics but are very expensive computationally. The Cook–Torrance model has been generalized for anisotropic surfaces by Kajiyama[34]. The Cook–Torrance model has also been simplified and made appropriate for practical implementations by Ward[75] and Schlick[60].

The original Phong[57], Phong–Blinn[8] and Whitted[77] models, on the other hand, are empirical models. These models are not physically plausible since they do not fulfil the law of reciprocity and the principle of the conservation of energy. The physically plausible Oren–Nayar model[56] characterizes different materials with an appropriate retro-reflective component, including ceramics, walls, foams, etc. Painted coatings are often fitted to the Beard–Maxwell empirically based model[5]. The NIST database also applies this model to represent measurement data. Recently, Lafortune et.al.[41] proposed the combination of general cosine models to obtain a versatile family of BRDFs. Based on the preliminary version of this model[50], Tobler et.al.[70] proposed a new BRDF that is particularly good for producing artistic contour effects.

During rendering, the BRDF models are usually used for two different purposes. On the one hand, in local illumination formulae the output radiance in a direction is computed from the incident radiance and from the surface orientation, which requires the evaluation of the BRDF for a single view vector and light vector pair. On the other hand, to improve Monte-Carlo random walk methods by applying importance sampling, directions should be generated that follow a probability density of the BRDF multiplied by a cosine function.

A practically useful BRDF must support both tasks. Unfortunately, physically based BRDFs contain many complex formulae, thus not only applying accurate importance sampling is hopeless, but even their simple evaluation is rather time consuming.

This is one reason why the Phong model is still in common use despite of its deficiencies. In global illumination algorithms, it is usually modified to satisfy reciprocity[33, 43] and to allow simple importance sampling[40]. The main disadvantage of the physically plausible Phong model is evident for “grazing angles” where it becomes dark. If the exponent parameter is high, this darkening is true from two different aspects. At grazing angles both the radiance and the total reflected power sharply decrease. The missing power becomes noticeable in images generated by global illumination algorithms.

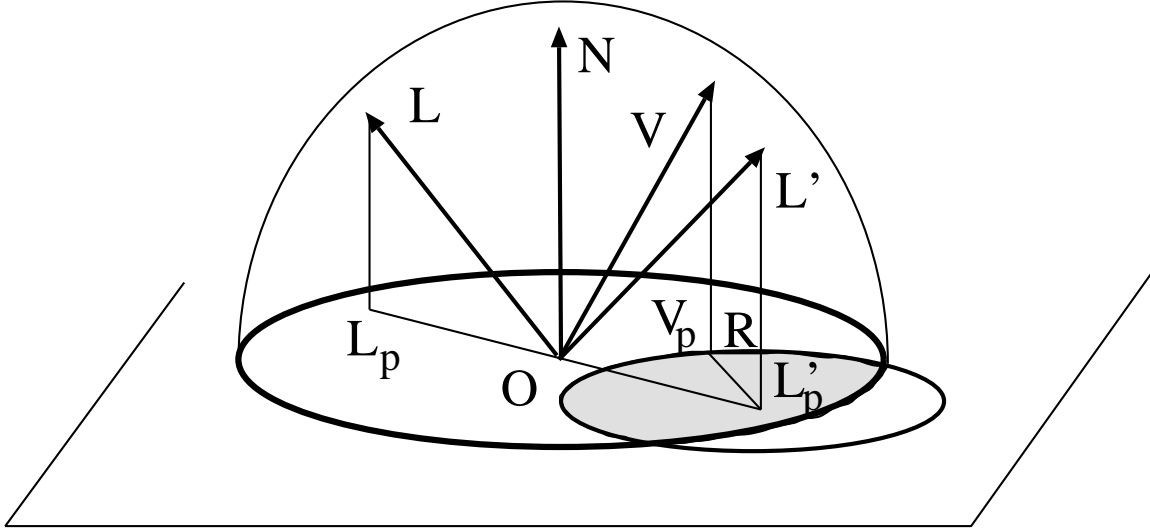


Figure 4.1: Geometry of the BRDF definition

In this chapter it is intended to develop a class of BRDF models. The proposed models are physically plausible, but not physically based. It can be viewed as a mathematical construction that is simple to compute and is particularly efficient for importance sampling.

Specific members of the new class can be defined in a new way. The computational cost of the new BRDFs is comparable to that of the Phong model. The model is able to approximate the visual properties of metals, plastics, reflective, retro-reflective and anisotropic materials.

## 4.2 Basic BRDF

The complex models to be proposed here are based on a simple, elementary BRDF model. This *basic BRDF* is just a mathematical tool, we do not intend to use it directly for rendering.

In the formulae the classical notations are used:  $\mathbf{L}$  and  $\mathbf{V}$  are the unit vectors to the light source and to the viewpoint,  $\mathbf{N}$  is the unit normal vector of the surface element. The  $\mathbf{L}'$  and  $\mathbf{V}'$  vectors are the results of mirroring the  $\mathbf{L}$  and  $\mathbf{V}$  vectors across the normal vector  $\mathbf{N}$ . The subscript  $P$  indicates the orthogonal projection of the given unit vectors – or their end-points – onto the base plane as shown in figure 4.1.

The basic BRDF is based on simple geometric constructs, namely on circles on the base plane. Before giving the definition of the proposed basic BRDF, two notations are introduced.

Firstly, let  $C(\mathbf{L}'_P, R)$  denote the common part of two circles, namely the unit circle with center in  $\mathbf{O}$  called the base circle and the circle of radius  $R$  and center  $\mathbf{L}'_P$ .

Secondly, let the  $m(\mathbf{L}, \mathbf{V})$  metric be the distance of the  $\mathbf{L}'_P$  and  $\mathbf{V}_P$  points. It can be shown that

$$m(\mathbf{L}, \mathbf{V}) = |\mathbf{V}_P - \mathbf{L}'_P| = |\mathbf{h} - (\mathbf{N} \cdot \mathbf{h})\mathbf{N}| \quad (4.1)$$

where  $\mathbf{h} = \mathbf{L} + \mathbf{V}$ . It must be emphasized that  $\mathbf{h}$  is not the same as the half-way unit vector denoted usually by  $\mathbf{H}$ , since  $\mathbf{h}$  is *not normalized*.

Note that function  $m$  is symmetric, that is

$$m(\mathbf{L}, \mathbf{V}) = m(\mathbf{V}, \mathbf{L})$$

since the distance of  $\mathbf{L}'_P$  and  $\mathbf{V}_P$  is the same as the distance between  $\mathbf{V}'_P$  and  $\mathbf{L}_P$ .

Using these notations, the basic BRDF corresponding to parameter  $R$  ( $0 \leq R \leq 2$ ) is defined by:

$$f_r^*(R, \mathbf{L}, \mathbf{V}) = \begin{cases} c(R) & \text{if } m(\mathbf{L}, \mathbf{V}) \leq R, \\ 0 & \text{otherwise.} \end{cases} \quad (4.2)$$

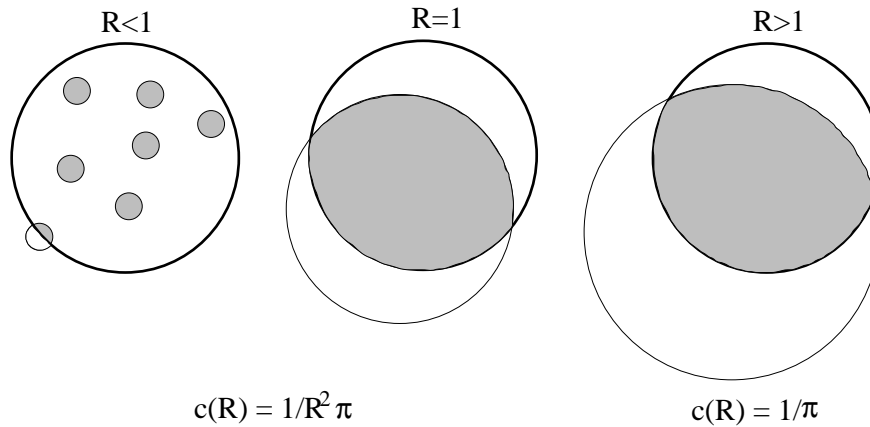


Figure 4.2: Possible relations to the base circle

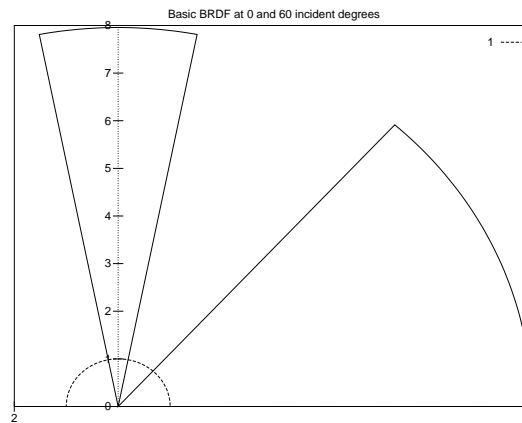


Figure 4.3: Basic BRDF for  $R = 0.2$

where  $c(R)$  is a constant depending on  $R$ .

Note that  $m(\mathbf{L}, \mathbf{V}) \leq R$  means that the projection of  $\mathbf{V}$  is in the circle of radius  $R$ , which is centered by the mirror of projection  $\mathbf{L}$ , i.e.

$$\mathbf{V}_P \in C(\mathbf{L}'_P, R).$$

Thus the BRDF also depends on  $R$ , which is shown by including it as the first parameter. The star character is to emphasize the fact that this is a basic BRDF from which other BRDFs will be constructed.

The basic BRDF is a constant  $c(R)$  if the projection of the mirroring of  $\mathbf{L}$  onto the center of the directional sphere and the projection of  $\mathbf{V}$  are not further than  $R$ .

The computation of the basic BRDF function is quite simple:

```

BasicBRDF( $R, \mathbf{V}, \mathbf{N}, \mathbf{L}$ )
   $\mathbf{h} = \mathbf{L} + \mathbf{V}$ 
   $m^2 = |\mathbf{h} - (\mathbf{N} \cdot \mathbf{h})\mathbf{N}|^2$ 
  if ( $m^2 \leq R^2$ ) then return  $c(R)$ 
  else return 0
end

```

### 4.2.1 Reciprocity

The basic BRDF is reciprocal, which is represented by identity

$$f_r^*(R, \mathbf{L}, \mathbf{V}) = f_r^*(R, \mathbf{V}, \mathbf{L})$$

since according to definition (4.2) it is equivalent to

$$m(\mathbf{L}, \mathbf{V}) = m(\mathbf{V}, \mathbf{L}).$$

### 4.2.2 Energy conservation

#### Albedo function

The power reflected into the half-space from the point light source of unit irradiance situated in direction  $\mathbf{L}$  is called the direction-dependent *albedo*, or the *directional-hemispherical reflectance*:

$$\mathbf{a}(\mathbf{L}) = \int_{\Omega} f_r(\mathbf{L}, \mathbf{V}) (\mathbf{N} \cdot \mathbf{V}) d\omega_{\mathbf{V}} \quad (4.3)$$

To satisfy energy conservation, the reflected power cannot exceed the incoming power, that is

$$\mathbf{a}(\mathbf{L}) \leq 1 \quad (4.4)$$

The albedo of the basic BRDF can be easily determined. In formula (4.3) the multiplication with  $(\mathbf{N} \cdot \mathbf{V}) = \cos \omega_{\mathbf{V}}$  corresponds to the *projection onto the base plane*. Thus, according to definitions (4.2) and (4.3) the albedo is proportional to the area of  $C(\mathbf{L}'_P, R)$ , that is

$$\mathbf{a}_R(\mathbf{L}) = c(R) \cdot \text{Area}(C(\mathbf{L}'_P, R)) \quad (4.5)$$

The area of  $C(\mathbf{L}'_P, R)$  is maximum when  $\mathbf{L} = \mathbf{N}$ , i.e.  $\mathbf{L}'_P = \mathbf{O}$ . If  $R < 1$ , this means that the circle is not truncated. If  $R \geq 1$ , then the common part coincides with the base circle. Since

$$\text{Area}(C(\mathbf{L}'_P, R)) \leq \text{Area}(C(\mathbf{O}, R)) \quad (4.6)$$

if in equation (4.2) we choose

$$c(R) = \frac{1}{\text{Area}(C(\mathbf{O}, R))} = \frac{1}{(\pi \cdot \min(1, R^2))} \quad (4.7)$$

then the albedo

$$\mathbf{a}_R(\mathbf{L}) = \frac{\text{Area}(C(\mathbf{L}'_P, R))}{\text{Area}(C(\mathbf{O}, R))} \quad (4.8)$$

will not exceed 1, that is, the basic BRDF will conserve energy.

To compute  $\text{Area}(C(\mathbf{L}'_P, R))$ , the intersection of two circles must be determined. Let the distance of the two circles be  $d$ . If  $d < 1 - R$  or  $d > 1 + R$ , then the solution is trivial. For the intersecting case, we can use the following formulae that uses the notation of figure 4.4:

$$\begin{aligned} \text{Area}(C(\mathbf{L}'_P, R)) &= t_1 + t_2 = \\ &1 \cdot (\alpha - \cos \alpha \cdot \sin \alpha) + R^2 \cdot (\beta - \cos \beta \cdot \sin \beta) \end{aligned} \quad (4.9)$$

The angle  $\alpha$  and  $\beta$  can, in turn, be determined using the theorem of cosine angles:

$$\begin{aligned} d^2 + 1^2 - 2d \cdot \cos \alpha &= R^2 \\ d^2 + R^2 - 2d \cdot R \cdot \cos \beta &= 1 \end{aligned} \quad (4.10)$$

The direction-dependent albedo of the basic BRDF will reach the imposed maximum of 1 for vertical illumination, i.e. for  $\mathbf{L} = \mathbf{N}$ .

When  $R < 1$ , then the albedo equals to the ratio of the area of the possibly truncated circle and the area of the complete circle of radius  $R$ . For  $R \geq 1$  it is the ratio of the area of the possibly truncated

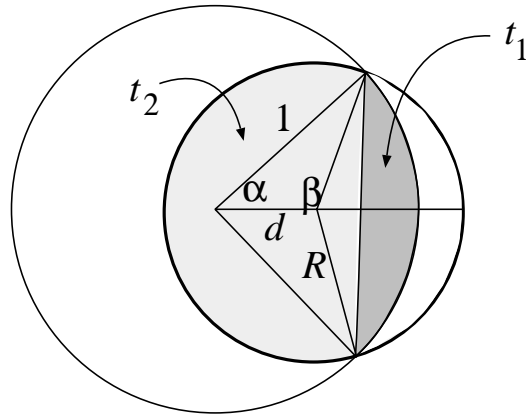


Figure 4.4: Computation of the intersection of two circles

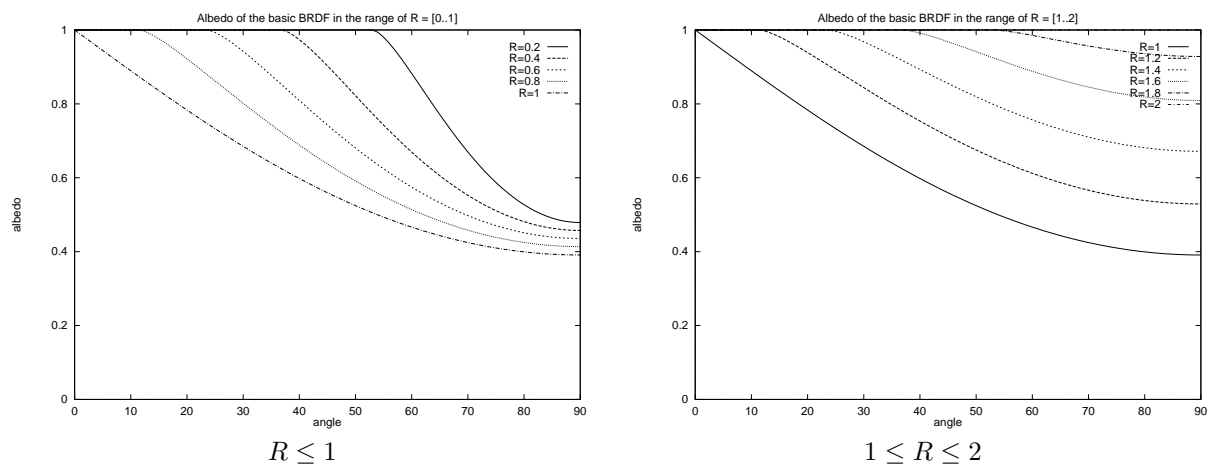


Figure 4.5: Albedo of the basic BRDF for different  $R$  values

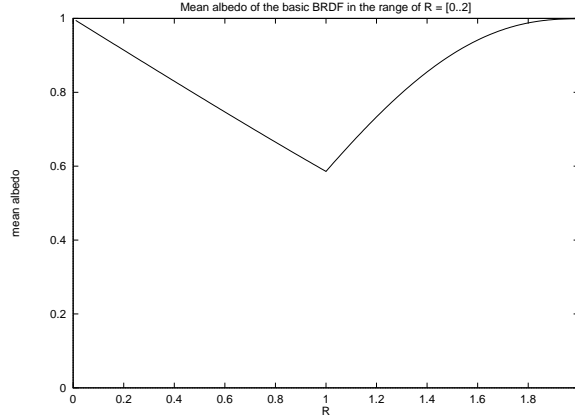


Figure 4.6: Mean albedo of the basic BRDF

base circle and the area of the whole base circle ( $\pi$ ). Thus, we always have  $\mathbf{a}_R(\mathbf{N}) = 1$ , furthermore it is easy to show that

$$0.391 < \frac{2}{3} - \frac{\sqrt{3}}{2\pi} \leq \mathbf{a}_R(\mathbf{L}) \leq 1$$

holds. The minimum point is at horizontal illumination ( $(\mathbf{N} \cdot \mathbf{L}) = 0$ ) and for  $R = 1$ .

For small values of  $R$ , the albedo is generally 1, and even at the margins of the base circle it hardly decreases under half. This is due to the fact that in this case the circle is generally not truncated, only for illumination at grazing angles.

The  $R = 0$  situation is the marginal case corresponding to a special mirror. In this case  $C(R)$  becomes a *Dirac* –  $\Delta$  function.

The  $R = 2$  case corresponds to the ideal diffuse model, where also  $\mathbf{a}(\mathbf{L}) \equiv 1$ .

### Mean albedo

In addition to the direction-dependent albedo defined by equation (4.3), we can also introduce the notion of the **mean albedo**. This direction-independent and dimensionless value is equal to the “reflectivity” for diffuse materials.

For non-diffuse materials, it can be defined as the weighted mean value of direction-dependent albedos:

$$a_{\text{mean}} = \frac{1}{\pi} \cdot \int_{\Omega} \mathbf{a}(\mathbf{L}) (\mathbf{N} \cdot \mathbf{L}) d\omega_{\mathbf{L}} \quad (4.11)$$

where  $\mathbf{L}$  is the running vector of the directional hemisphere and the weighting factor is  $(\mathbf{N} \cdot \mathbf{L}) = \cos \omega_{\mathbf{L}}$ .

In the case of uniform illumination on the half-space, the value of the mean albedo is equal to the ratio of the reflected and the incident power. Figure 4.6 illustrates the values of  $a_{\text{mean}}$  for the basic BRDFs as a function of  $R$ . The mean albedo is minimal at  $R = 1$ .

The BRDF and the albedo characterize a material from two different aspects. The BRDF is used to describe the “reflected radiance” and it is a scalar which depends on both  $\mathbf{L}$  and  $\mathbf{V}$ . The albedo depending only on direction  $\mathbf{L}$  serves for the description of the “reflected power”. The mean albedo (which does not depend on  $\mathbf{L}$  and  $\mathbf{V}$ ) characterizes the average reflectivity of the BRDF.

Examining these characteristics, we can see the essential difference between the behavior of the ideal mirror obtained by the new BRDF and that obtained as a limit case from the  $(\mathbf{N} \cdot \mathbf{H})^n$  Phong–Blinn model without diffuse component[49].

For the ideal metal mirror, both the mean and the direction dependent albedos are 1, that is  $a_{\text{mean}} = 1$  and  $\mathbf{a}(\mathbf{L}) \equiv 1$ .

However, for the “Phong-mirror”, which is the result of letting  $n$  go to infinity, we have  $1 \geq \mathbf{a}(\mathbf{L}) \geq 0$  and  $a_{\text{mean}} = 0.5$ . In the case of a Phong mirror, the reflected energy tends to zero for grazing angles.

The mirror case of the new model is not equivalent to a metal mirror since at grazing angles the metallic mirrors reflect the total energy by increasing the BRDF by a factor of  $\frac{1}{(\mathbf{N} \cdot \mathbf{L})}$ , while in the new model the BRDF is constant and the solid angle of the reflectance is increased by  $\frac{1}{(\mathbf{N} \cdot \mathbf{L})}$ . Thus the new model is a ideal “energy mirror” but not ideal “radiance mirror” for higher incident angles.

### 4.2.3 Importance sampling

Suppose that we want to calculate the radiance of a point in direction  $\mathbf{V}$  due to the illumination of the scene. The input and output *radiances* [ $\text{Wm}^{-2}\text{sr}^{-1}$ ] are denoted by  $L^{\text{in}}$  and  $L^{\text{out}}$ , respectively. The radiance in the viewing direction  $\mathbf{V}$  is:

$$L^{\text{out}}(\mathbf{V}) = \int_{\Omega} L^{\text{in}}(\mathbf{L}) f_r(\mathbf{L}, \mathbf{V}) (\mathbf{N} \cdot \mathbf{L}) d\omega_{\mathbf{L}} \quad (4.12)$$

This integral can be approximated by the Monte-Carlo method. Using importance sampling to reduce the variance, the incoming  $\mathbf{L}_1, \mathbf{L}_2, \dots, \mathbf{L}_M$  directions are not uniformly distributed, but their probability density distribution function is at least approximately proportional to the integrand. Since  $L^{\text{in}}(\mathbf{L})$  is usually not known a-priori, we can sample  $\mathbf{L}$  with probability proportional to the

$$R(\mathbf{L}, \mathbf{V}) = f_r(\mathbf{L}, \mathbf{V}) (\mathbf{N} \cdot \mathbf{L})$$

weighted BRDF function. This function has an interesting illustrative content, according to the “inverse situation”. If there were a light source in the viewing direction, then the distribution of the energy on the half-space after the reflection would follow the function  $R$ .

Function  $R \cdot d\omega_{\mathbf{L}}$  also defines the conditional probability that a photon is reflected into the solid angle  $d\omega_{\mathbf{L}}$  given that it comes from  $\mathbf{V}$  [68]. Due to the fact that  $f_r$  is reciprocal, we have:

$$\mathbf{a}(\mathbf{V}) = \int_{\Omega} f_r(\mathbf{L}, \mathbf{V}) (\mathbf{N} \cdot \mathbf{L}) d\omega_{\mathbf{L}} \quad (4.13)$$

which is exactly the value of the albedo function in viewing direction  $\mathbf{V}$ . For sampling of  $\mathbf{L}_1, \mathbf{L}_2, \dots, \mathbf{L}_M$  directions, we have to use the

$$d_{\mathbf{V}}(\mathbf{L}) = \frac{f_r(\mathbf{L}, \mathbf{V}) \cdot (\mathbf{N} \cdot \mathbf{L})}{\mathbf{a}(\mathbf{V})} d\omega_{\mathbf{L}} \quad (4.14)$$

probability density function. The approximation of the integral in equation (4.12) is:

$$L^{\text{out}}(\mathbf{V}) = \mathbf{a}(\mathbf{V}) \cdot E [L^{\text{in}}(\mathbf{L})] \approx \frac{\mathbf{a}(\mathbf{V})}{M} \cdot \sum_{k=1}^M L^{\text{in}}(\mathbf{L}_k) \quad (4.15)$$

In the case of isotropic BRDFs the albedo functions can be tabulated in a one-dimensional table. When calculating multiple interreflections, the main computational problem is the generation of the directions from equation (4.14) following distribution  $d_{\mathbf{V}}$ .

### 4.2.4 Importance sampling for the basic BRDF

#### Sampling in special cases

For the introduced basic BRDFs, we can easily generate directions with a distribution of equation (4.14).

Let us consider first a circle of radius  $R < 1$  and assume that this circle does not intersect the base circle. In this case  $C(\mathbf{V}'_P, R)$  is identical with the circle with center in  $\mathbf{V}'_P$  and of radius  $R$ . The value of the albedo is 1 because the circle is not truncated.

Let us generate  $M$  number of 2D points inside this circle with a uniform distribution. These will be the  $(\mathbf{L}_k)_P$  ( $k = 1, \dots, M$ ) projection points in the plane of projection. Since the projection automatically includes the “cosine” factor in  $d(\mathbf{L})$ , re-projecting these points onto the unit hemisphere’s surface, we obtain the  $\mathbf{L}_1, \mathbf{L}_2, \dots, \mathbf{L}_M$  directions of the desired distribution.

For a given unit viewing vector  $\mathbf{V}$ , the projection on the base plane and the mirroring are realized in the following way:

$$\mathbf{V}'_P = -\mathbf{V}_P = -(\mathbf{V} - (\mathbf{N} \cdot \mathbf{V})\mathbf{N}) \quad (4.16)$$

The formula for re-projecting the  $\mathbf{L}_P$  sample point which is inside the circle of center  $\mathbf{V}'_P$  and of radius  $R$  onto the hemisphere is:

$$\mathbf{L} = \mathbf{L}_P + \sqrt{1 - (\mathbf{L}_P \cdot \mathbf{L}_P)} \cdot \mathbf{N} \quad (4.17)$$

The situation is similar if  $R > 1$  and the circle contains the complete unit base circle. Now the uniformly distributed points can be generated on the whole base circle. This case corresponds to the generation of directions following a “cosine distribution” for diffuse materials.

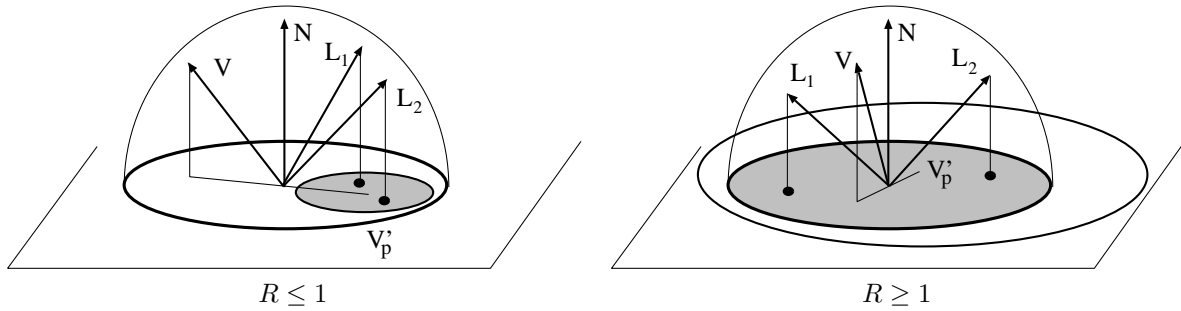


Figure 4.7: Sampling when the circles do not intersect

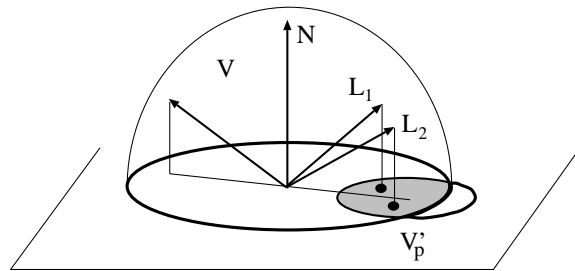


Figure 4.8: Sampling when the circles intersect

### Generating uniformly distributed points in a circle

To generate uniformly distributed points inside a circle, we can either use an area preserving mapping of the square onto the circle, or apply rejection sampling. In rejection sampling the points are generated in a square that encloses the circle and those points that are outside the circle are ignored.

### Sampling in the general case

In the cases discussed so far, the domain where the sample points are generated was a complete circle and the value of the albedo was 1. In the general case the  $C(\mathbf{V}'_P, R)$  region is the common part of two circles. To realize importance sampling, we have to generate uniformly distributed points inside this region.

To solve this problem, **rejection sampling** can be applied. It means that uniform samples are generated in one of the circles and then checked whether or not the other circle contains this sample. If it does not, the sample is rejected and a new sample is generated.

To reduce the number of rejected samples, the smaller circle is worth selecting as a domain for sample generation and the bigger as the region of rejection sampling.

The following subroutine finds an  $\mathbf{L}$  sample from direction  $\mathbf{V}$  using a basic BRDF of parameter  $R$ , and also provides the albedo to weight the radiance obtained using direction  $\mathbf{L}$ :

```

DOUBLE GenerateDirectionWithBasicBRDF( $R, \mathbf{V}, \mathbf{N}, \mathbf{L}$ )
 $\mathbf{V}'_P = -(\mathbf{V} - (\mathbf{N} \cdot \mathbf{V})\mathbf{N})$ 
found = TRUE
repeat
  if  $R < 1$  then
    Generate point  $\mathbf{L}_P$  in  $C(\mathbf{V}'_P, R)$ 
    if  $\mathbf{L}_P$  is outside  $C(\mathbf{O}, 1)$  then found = FALSE
  else
    Generate point  $\mathbf{L}_P$  in  $C(\mathbf{O}, 1)$ 
    if  $\mathbf{L}_P$  is outside  $C(\mathbf{V}'_P, R)$  then found = FALSE
  endif
until found

```



```

L = LP + √(1 - (LP · LP) · N
a = C(V'P, R) / (π · min(1, R2))
return a
end

```

### Sampling with Russian roulette

In the case of highly reflective materials  $R$  is small and thus  $C(\mathbf{V}'_P, R)$  is typically a complete circle. The computation of the common part of two circles is required only at the margins.

For other materials, truncation of the circles must be considered several times. However, if we use the Russian roulette, we have to check only whether or not the points are inside the circle, the albedo (the area of the common part) should not be computed explicitly. Let

$$C_{\min}(\mathbf{V}'_P, R) = \begin{cases} C(\mathbf{V}'_P, R), & \text{if } R < 1, \\ C(\mathbf{O}, 1), & \text{otherwise} \end{cases} \quad (4.18)$$

Let us generate in the  $C_{\min}(\mathbf{V}'_P, R)$  region exactly  $M$  uniformly distributed 2D points. Now, the weighting factor of  $(\mathbf{L}_k)_P$  ( $k = 1, \dots, M$ ) will be 0 or 1 (i.e. accepted or rejected) according to whether or not the point is inside the “other circle” too. The approximation of the half-space integral is:

$$L^{\text{out}}(\mathbf{V}) = E[L^{\text{in}}(\mathbf{L})] \approx \frac{1}{M} \cdot \sum_{k=1}^M L^{\text{in}}(\mathbf{L}_k) \quad (4.19)$$

where only the accepted points are considered in the sum, that is, which have a weighting factor of 1. This means that the number of terms can be at most  $M$ , but is often less. This method is somewhat simpler, but its variance is not the possible minimum because it does not carry out the exact importance sampling. The weight factors of the elementary rays are 0 or 1, only their expected value is equal to the  $\alpha_R(\mathbf{V})$  albedo.

The algorithm that generates either direction  $\mathbf{L}$  from direction  $\mathbf{V}$ , or reports that the sample should be rejected by returning a zero value is the following:

```

BOOL GenerateDirectionWithBasicBRDF(R, V, N, L)
  V'P = -(V - (N · V)N)
  if R < 1 then
    Generate point LP in C(V'P, R)
    if LP is outside C(O, 1) then return 0
  else
    Generate point LP in C(O, 1)
    if L'P is outside C(V'P, R) then return 0
  endif
  L = LP + √(1 - (LP · LP) · N
  return 1
end

```

## 4.3 Mixture of basic BRDFs

### 4.3.1 General description

The basic BRDF is not a realistic material model by itself, but only a mathematical construction since it is discontinuous (figure 4.3). Therefore we intend to create real BRDFs using a mixture of the basic ones. Let the weighting function be  $p(R)$  that is expected to be “normalized” ( $\int p(R) dR = 1$ ).

The *mixture BRDF* is then:

$$f_r(\mathbf{L}, \mathbf{V}) = \int_0^2 p(R) \cdot f_r^*(R, \mathbf{L}, \mathbf{V}) dR \quad (4.20)$$

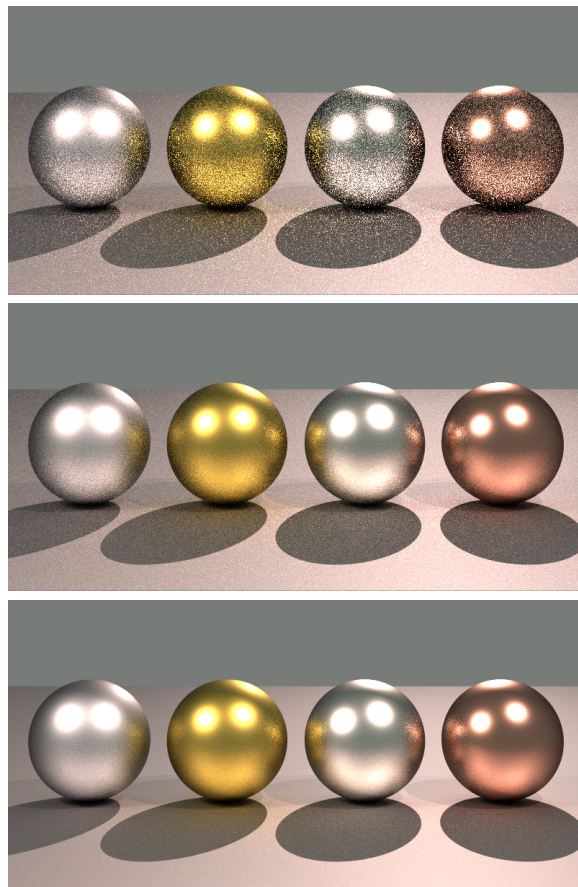


Figure 4.9: Metallic spheres generated by Monte-Carlo ray tracing with 50 samples per pixel (top: importance sampling according to the cosine angle only (51 min); middle: Russian roulette based importance sampling of section 4.2.4 (46 min); bottom: normal importance sampling of section 4.2.4 (54 min))

Weighting function  $p(R)$  can be considered as a probability density function of one variable in the  $0 \leq R \leq 2$  interval.

The mixture BRDFs evidently meet the requirements of reciprocity and energy conservation. So the BRDFs are physically plausible models if their value is non-negative. A sufficient but not necessary condition is that the weighting function is non-negative.

The singularities of *Dirac* –  $\Delta$  type cases must be examined separately, namely when the integral of  $p(R)$  in the respective point is a finite, non-zero value, and  $p(R)$  is “infinite”.

Two types of singularities are important in BRDF modelling. The  $R = 0$  case corresponds to a special ideal mirror, and  $R = 2$  corresponds to the ideal diffuse model. Separating these, we have:

$$\int_0^2 p(R) dR = p_{\text{Mirror}} + p_{\text{Diffuse}} + \int_{+0}^{2-0} p(R) dR = 1 \quad (4.21)$$

### 4.3.2 Albedo for a given $p(R)$ function

Since mixing is a linear operation, the albedo  $a^p$  and the mean albedo  $a_{\text{mean}}^p$  of the mixture BRDF can be computed as follows:

$$a^p(\mathbf{L}) = \int_0^2 p(R) \cdot \mathbf{a}_R(\mathbf{L}) dR \quad (4.22)$$

$$a_{\text{mean}}^p = \int_0^2 p(R) \cdot (\mathbf{a}_R)_{\text{mean}} dR \quad (4.23)$$

According to equation (4.21) for the albedos of the mirror and of the Lambertian model, we have:

$$a_{\text{Mirror}} = p_{\text{Mirror}}, \quad a_{\text{Diffuse}} = p_{\text{Diffuse}} \quad (4.24)$$

## 4.4 Modified importance sampling for a given $p(R)$

### 4.4.1 Reducing the general case to basic BRDFs

Using equations (4.12) and (4.20), we transform the half-space integral into a double integral and then reverse the order of integration:

$$\begin{aligned} L^{\text{out}}(\mathbf{V}) &= \int_{\Omega} L^{\text{in}}(\mathbf{L}) f_r(\mathbf{L}, \mathbf{V}) (\mathbf{N} \cdot \mathbf{L}) d\omega_{\mathbf{L}} = \\ &= \int_{\Omega} L^{\text{in}}(\mathbf{L}) \cdot \left[ \int_0^2 p(R) f_r^*(R, \mathbf{L}, \mathbf{V}) dR \right] (\mathbf{N} \cdot \mathbf{L}) d\omega_{\mathbf{L}} = \\ &= \int_0^2 p(R) \cdot \left[ \int_{\Omega} L^{\text{in}}(\mathbf{L}) f_r^*(R, \mathbf{L}, \mathbf{V}) (\mathbf{N} \cdot \mathbf{L}) d\omega_{\mathbf{L}} \right] dR = \\ &= \int_0^2 p(R) \cdot L_R^{\text{out}}(\mathbf{V}) dR \end{aligned} \quad (4.25)$$

This integral is approximated by a sum using Monte-Carlo quadrature. For the calculation of the required  $R_k$  values, we apply importance sampling according to the  $p(R)$  function. Using the approximate value of the integral (4.12), we have:

$$L^{\text{out}}(\mathbf{V}) = \int_0^2 p(R) \cdot L_R^{\text{out}}(\mathbf{V}) dR \approx \frac{1}{M} \cdot \sum_{k=1}^M L_{R_k}^{\text{in}}(\mathbf{V}) \quad (4.26)$$

similarly to equation (4.25), with the exception that here each incoming direction is represented by a different radius  $R_k$ .

Let the cumulative probability distribution function of  $p$  be the following function:

$$F(R) = \int_0^R p(t) dt, \quad (0 \leq R \leq 2, \quad 0 \leq F(R) \leq 1) \quad (4.27)$$

In practice, we may calculate  $F$  in a closed form, or using numerical methods. Importance sampling requires the inverse of  $F$ , which is usually computed numerically and the resulting values are stored in a sufficiently large one-dimensional array.

The algorithm of generating a direction  $\mathbf{L}$  to direction  $\mathbf{V}$  is as follows:

```

BOOL GenerateDirectionWithMixtureBRDF( $\mathbf{V}, \mathbf{N}, \mathbf{L}$ )
  Generate a random value  $r$  in  $[0, 1]$ 
   $R = F^{-1}(r)$ 
  return GenerateDirectionWithBasicBRDF( $R, \mathbf{V}, \mathbf{N}, \mathbf{L}$ )
end

```

## 4.5 Generalization of the basic BRDF

### 4.5.1 Generalization of the $\mathbf{L} \rightarrow \mathbf{L}'$ mirroring transformation

The  $\mathbf{L}'$  vector in definition (4.2) was obtained from the original  $\mathbf{L}$  vector by mirroring. Instead of mirroring, basic BRDFs can be defined using other  $\mathbf{L} \rightarrow T(\mathbf{L})$  transformations too. To fulfil the requirement of reciprocity, the  $T(\mathbf{L})$  transformation has to satisfy the following identity:

$$T(T(\mathbf{L})) = \mathbf{L} \quad (4.28)$$

This requirement is satisfied by mirroring since mirroring two times gives back the original point. Another trivial transformation is the identity, that is  $T(\mathbf{L}) = \mathbf{L}$ .

### 4.5.2 The retro-reflective model

For the  $T(\mathbf{L}) = \mathbf{L}$  transformation, the  $m(\mathbf{L}, \mathbf{V})$  metric from definition (4.2) becomes:

$$m(\mathbf{L}, \mathbf{V}) = |\mathbf{L}_P - \mathbf{V}_P| = |\mathbf{g} - (\mathbf{N} \cdot \mathbf{g})\mathbf{N}| \quad (4.29)$$

where  $\mathbf{g} = \mathbf{L} - \mathbf{V}$ . For such models, the radiance of the reflected light is maximum in the incidence direction. This model is called the **retro-reflective model**. In practice, materials exhibiting such properties are the beaded screens or the signal paints used on the highways. The marginal cases of this retro-reflective model are those mirror-constructions which are used in laser-based telemeters that behave practically as ideal mirrors, but reflect exactly in the incident direction.

### 4.5.3 Generalization of the metric

In definition (4.2) the  $m(\mathbf{L}, \mathbf{V})$  metric was an Euclidean distance in the projection plane. The metric can be generalized as follows:

$$m(\mathbf{L}, \mathbf{V}) = \|\mathbf{V}, T(\mathbf{L})\| \quad (4.30)$$

In equation (4.30)  $\|\cdot, \cdot\|$  is an arbitrary metric for two unit vectors on the hemisphere. For the Euclidean metric on the base plane and for basic BRDFs defined in equation (4.2), we have:

$$\|\mathbf{V}, T(\mathbf{L})\| = |\mathbf{V}_P - T(\mathbf{L})_P| \quad (4.31)$$

#### 4.5.4 Anisotropic models

The use of anisotropic models can often substantially improve realism in rendering, especially in the case of metals[34, 60]. Formula (4.31) provides useful generalization possibilities for practice. Using an “elliptic norm” on the base plane, anisotropic BRDFs are obtained. Let us define an orthonormal coordinate system on the surface element representing the given BRDF, by considering the  $(\mathbf{u}, \mathbf{v})$  vectors which are perpendicular to each other and to the  $\mathbf{N}$  unit normal vector too. The metric  $m$  can be defined as follows:

$$m(\mathbf{L}, \mathbf{V}) = \sqrt{\left(\frac{B}{A} \cdot (\mathbf{z} \cdot \mathbf{u})\right)^2 + (\mathbf{z} \cdot \mathbf{v})^2} \quad (4.32)$$

where  $\mathbf{z} = \mathbf{V}_P - T(\mathbf{L})_P$  and  $\frac{B}{A} \leq 1$  is the ratio of the axes of the ellipse, and the major and the minor axis of the ellipse are taken along vectors  $\mathbf{u}$  and  $\mathbf{v}$ , respectively. This metric  $m$  contracts the distance component along vector  $\mathbf{u}$ . When  $\frac{B}{A} = 1$ , we have the same case as in equation (4.1).

Let  $E(\mathbf{Q}, \mathbf{v}, b)$  denote the common part of the ellipse with center in  $\mathbf{Q}$ , with a minor axis of length  $b$  and of the unit base circle. In this case:

$$\mathbf{V}_P \in E(\mathbf{L}'_P, \mathbf{v}, b) \iff \mathbf{L}'_P \in E(\mathbf{V}'_P, \mathbf{v}, b) \quad (4.33)$$

which means that the model meets the requirement of reciprocity.

The maximum value of  $b$  is determined for that case when the  $E(\mathbf{Q}, \mathbf{v}, b)$  ellipse contains the complete unit base circle, for every  $\mathbf{Q}$  inside the base circle. The maximal  $b = 2$  case happens for illumination which is along the minor axis and is horizontal. The value of  $b$  can be in  $[0, 2]$ , the length of the major axis in  $[0, \frac{2A}{B}]$ .

Parameter  $b$  corresponds to the earlier  $R$  parameter. The elementary BRDF depends now only on  $b$ :

$$f_r^*(b, \mathbf{L}, \mathbf{V}) = \begin{cases} c(b), & \text{if } \mathbf{V}_P \in E(\mathbf{L}'_P, \mathbf{v}, b), \\ 0 & \text{otherwise.} \end{cases} \quad (4.34)$$

The albedo of the BRDF in formula (4.34) is:

$$a_b(\mathbf{L}) = \frac{\text{Area}(E(\mathbf{L}'_P, \mathbf{v}, b))}{\text{Area}(E(\mathbf{O}, \mathbf{v}, b))} \quad (4.35)$$

The albedo is maximal for  $\mathbf{L} = \mathbf{N}$ . The constant in equation (4.34) for every value of  $b$  is taken so that for a vertical illumination the albedo function is 1.

The computation of this constant can be separated into two cases. When  $b \leq \frac{B}{A}$ , i.e. when the major axis is less than 1, the base circle contains the whole ellipse with center  $\mathbf{Q} = \mathbf{O}$ . On the other hand, when the major axis is greater than 1, the intersections should be computed.

$$c(b) = \begin{cases} 1/(ab\pi), & \text{if } b \leq B/A, \\ 1/\text{Area}(E(\mathbf{O}, \mathbf{v}, b)), & \text{if } B/A < b \leq 2 \end{cases} \quad (4.36)$$

In importance sampling, the anisotropic model can be used similarly to the isotropic model. Points are generated inside a circle that has radius  $b$ , then a scaling transformation is applied that transforms the circle to the ellipse.

The anisotropic model can also be used to define mixture BRDFs:

$$f_r(\mathbf{L}, \mathbf{V}) = \int_0^2 p(b) \cdot f_r^*(b, \mathbf{L}, \mathbf{V}) db = \int_{m(\mathbf{L}, \mathbf{V})}^2 p(b) \cdot c(b) db \quad (4.37)$$

Anisotropic models can be defined with other norms too, for example with the  $p$ -th power norm:

$$m(\mathbf{L}, \mathbf{V}) = \left[ \left(\frac{B}{A} (\mathbf{z} \cdot \mathbf{u})\right)^p + (\mathbf{z} \cdot \mathbf{v})^p \right]^{\frac{1}{p}} \quad (4.38)$$

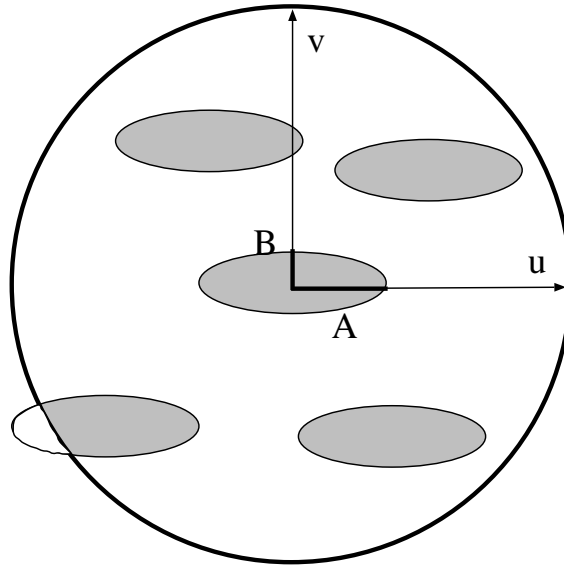


Figure 4.10: Elliptical BRDFs

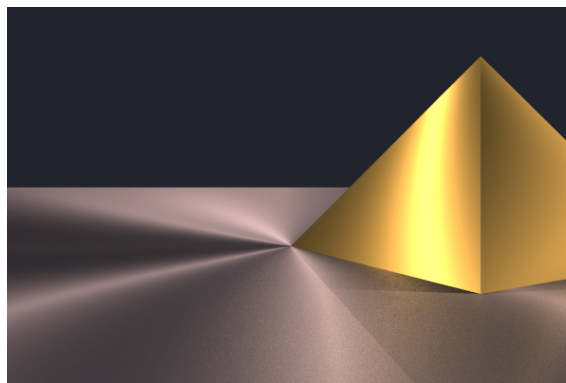


Figure 4.11: A scene containing anisotropic metals

## 4.6 BRDF definition with a given scalar function

A BRDF maps two vector variables to a scalar value, thus always involves dimension reduction. The exact phase where the dimension reduction happens can vary in different BRDFs. The dimension reduction also means that each BRDF can be associated with equivalence classes of vector pairs, in a way that two vector pairs provide the same BRDF value if they are in the same class. In Phong–Blinn BRDFs, for example, all  $\mathbf{L}, \mathbf{V}$  pairs are equivalent if they have the same  $\mathbf{N} \cdot \mathbf{H}$  scalar product. In the new model, the dimensional reduction takes place when computing the  $m(\mathbf{L}, \mathbf{V}) = |\mathbf{h} - (\mathbf{N} \cdot \mathbf{h})\mathbf{N}|$  metric.

In this section we shall examine how a BRDF can be defined with an arbitrary function of one variable and how its corresponding  $p(R)$  function can be determined. Let us consider an arbitrary, non-negative  $\xi(m)$  scalar function defined in the  $[0, 2]$  interval, which will define the shape of the reflection lobes or the characteristics of the BRDF. Using this, we define a  $f_r^\xi(\mathbf{L}, \mathbf{V})$  function:

$$f_r^\xi(\mathbf{L}, \mathbf{V}) = \xi(m(\mathbf{L}, \mathbf{V})) = \xi(m), \quad m \in [0, 2] \quad (4.39)$$

Function  $\xi(m)$  is multiplied with an appropriate  $C_{\max}$  constant in order to fulfil energy conservation requirement, thus the

$$f_r(\mathbf{L}, \mathbf{V}) = f_r^{C_{\max}\xi}(\mathbf{L}, \mathbf{V}) = C_{\max} \cdot f_r^\xi(\mathbf{L}, \mathbf{V})$$

function will be a plausible BRDF.

Let us recall definition (4.20) of the mixture BRDFs. The lower limit of the integral can be modified, since according to definition (4.2), if  $R < m(\mathbf{L}, \mathbf{V})$ , the value of  $f_r(R, \mathbf{L}, \mathbf{V})$  is zero. When  $R \geq m$ , its value is the  $c(R)$  defined by equation (4.7). Thus, the following formula is equivalent to formula (4.20) for the definition of the mixture BRDF:

$$\begin{aligned} f_r(\mathbf{L}, \mathbf{V}) &= \int_{m(\mathbf{L}, \mathbf{V})}^2 p(R) \cdot f_r^*(R, \mathbf{L}, \mathbf{V}) dR = \\ &= \int_{m(\mathbf{L}, \mathbf{V})}^2 p(R) \cdot c(R) dR = \int_{m(\mathbf{L}, \mathbf{V})}^2 p(R) \cdot \pi \cdot \min(1, R^2) dR \end{aligned} \quad (4.40)$$

Computing the derivative according to variable  $m$ , we obtain:

$$p(R) = -C_{\max} \cdot \frac{d\xi(m)}{dm}(R) \cdot \pi \cdot \min(1, R^2) \quad (4.41)$$

The derivative of function  $\xi$  must be taken with a minus sign, since  $m$  is the lower limit of the integration.

The  $C_{\max}$  factor should be set to make  $p(R)$  a probability density and consequently the BRDF energy conserving, thus

$$\frac{1}{C_{\max}} = - \int_0^2 \frac{d\xi(m)}{dm}(R) \cdot \pi \cdot \min(1, R^2) dR \quad (4.42)$$

for decreasing  $\xi$  functions.

The maximum of the albedo of this BRDF is 1. To obtain darker materials, the BRDF can be multiplied with a factor that is less than 1.

In a software implementing this approach  $\xi$  can be provided interactively by the user as an arbitrary curve using a graphics interface (the curve defines a one variable function). Only the ratio of the ideal mirror component (polishing) must be specified separately (see equation (4.21)).

Note that  $\xi$  is not required to be monotone decreasing, but the condition of non-negativity must be imposed in any case. For  $\xi$  functions having monotone increasing parts, the computation of the maximal albedo and of the normalizing factor is more difficult than equation (4.42) and can be accomplished by numerical methods using formula (4.22).

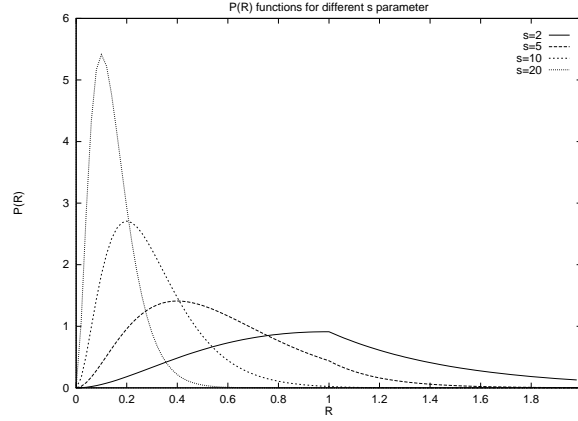


Figure 4.12: Probability density function  $p(R)$  for different  $s$  values

### 4.6.1 Analytically integrable cases

In this section we will present some monotone decreasing  $\xi$  functions which are suitable for applications and for which the  $C_{\max}$  multiplier from equation (4.42) can be derived analytically.

Let  $G$  be the primitive function of  $\xi$ , and  $H$  be the primitive of  $G$  (with arbitrary constants!) i.e.  $G = \int \xi$  and  $H = \int G$ .

Then, it can be easily deduced that:

$$C_{\max} = \frac{1}{2\pi(G(1) - H(1) + H(0))} \quad (4.43)$$

This formula is true even if  $\xi(2) > 0$ .

#### Exponential function

This section uses the exponential function as a scalar function to define the highlight profile:

$$\xi(m) = e^{-s \cdot m} \quad (4.44)$$

The normalization factor is

$$C_{\max} = \frac{s^2}{2\pi(1 - (1+s)e^{-s})} \quad (4.45)$$

and the BRDF is

$$f_r^{(s)}(\mathbf{L}, \mathbf{V}) = \frac{s^2}{2\pi(1 - (1+s)e^{-s})} \cdot e^{-s \cdot m} \quad (4.46)$$

Using formula (4.41), we can obtain the following expression for the required weighting function  $p$ :

$$\begin{aligned} p(R) &= -C_{\max} \cdot \frac{d\xi(m)}{dm}(R) \cdot \pi \cdot \min(1, R^2) = \\ &= \frac{s^3 \cdot e^{-s \cdot R} \cdot \min(1, R^2)}{2(1 - (1+s)e^{-s})} \end{aligned} \quad (4.47)$$

The probability densities, the inverse of the probability distribution functions, the albedos, and the shapes of the BRDF lobes are shown in figure 4.12, figure 4.13, figure 4.14 and figure 4.15, respectively, for different  $s$  parameters.

For  $s > 10$ , the model is already highly specular. A very good approximation of the above formula for this parameter domain is:

$$f_r^{(s)}(\mathbf{L}, \mathbf{V}) = \frac{s^2}{2\pi} \cdot e^{-s \cdot m(\mathbf{L}, \mathbf{V})} \quad (4.48)$$

when the corresponding  $p$  weighting function is:

$$p(R) = \frac{s^2}{2} \cdot R \cdot e^{-s \cdot R} \cdot \min(1, R^2) \quad (4.49)$$



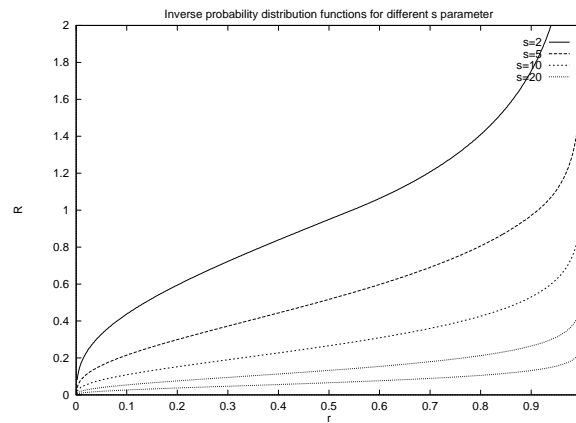


Figure 4.13: Inverse of the probability distribution functions  $F^{-1}(r)$  for different  $s$  values

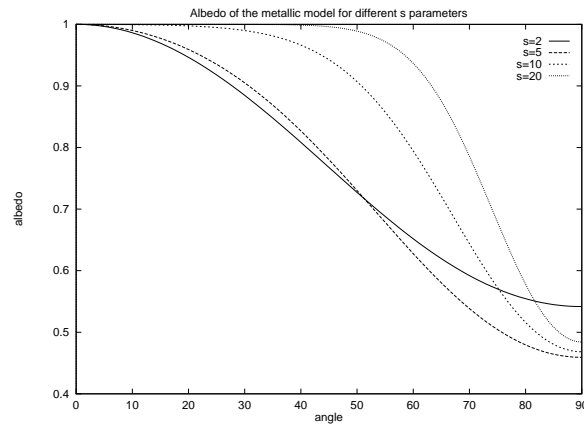


Figure 4.14: Albedos of the mixed BRDFs for different  $s$  values

$s$	$C_{\max}$	$I_{1,2}$	$a_{\text{Diffuse}}$	
0	$1/\pi$	0	1	LAMBERTIAN
0.25	0.3754	0.20316	0.71527	
0.5	0.4411	0.33071	0.50979	
1.	0.6023	0.44002	0.25608	
2	1.0718	0.39401	0.06167	
4	2.8032	0.15834	0.00295	
8	10.216	0.01076	0.00000	
16	40.743	0.00001	0.00000	HIGHLY SPECULAR
32	162.97	0.00000	0.00000	
64	651.89	0.00000	0.00000	
128	2607.5	0.00000	0.00000	
256	10430.	0.00000	0.00000	
512	41721.	0.00000	0.00000	ALMOST MIRROR

Table 4.1: Parameters of the  $f_r = C_{\max} \cdot e^{-s \cdot m}$  BRDF

Let us consider formula (4.40) and an  $m < 1$  value:

$$\begin{aligned} f_r(\mathbf{L}, \mathbf{V}) &= \int_0^2 p(R) \cdot c(R) dR = I_{m,1} + I_{1,2} = \\ &= \pi \cdot \int_m^1 p(R) \cdot R^2 dR + \pi \cdot \int_1^2 p(R) dR \end{aligned} \quad (4.50)$$

In the case of a vertical illumination we have  $m \leq 1$  independently of  $\mathbf{V}$ , thus even for the horizontal viewing direction there will be a non-zero “diffuse part”. This is component  $I_{1,2}$  in equation (4.50) which is the integral over the  $[1, 2]$  interval. Thus, for the truly specular materials not only  $\xi(2) = 0$  but  $\xi(m) = 0$  for  $m \geq 1$  must be imposed.

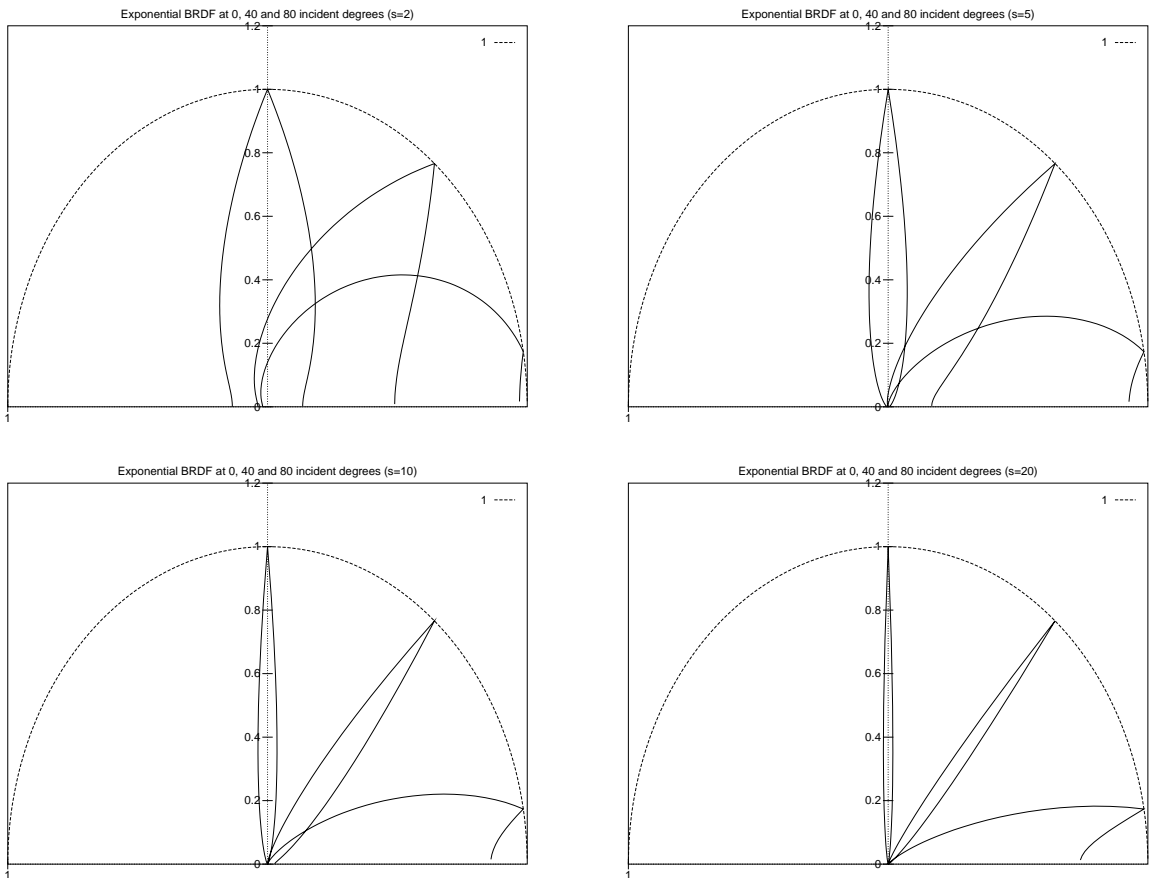


Figure 4.15: BRDF using exponential weight function

To illustrate this, the table 4.1 contains the corresponding values of the  $C_{\max}$  and  $s$  parameters of the  $f_r(\mathbf{L}, \mathbf{V}) = C_{\max} \cdot e^{-s \cdot m}$  function,  $I_{1,2}$  and  $a_{\text{Diffuse}} = p_{\text{Diffuse}} = C_{\max} \cdot \pi \cdot e^{-2s}$ .

## 4.7 Real materials

### 4.7.1 Metals and the new model

The BRDFs of metals increase towards infinity for grazing angles. This is due to the fact that for smooth metals the product of the BRDF and the cosine term is approximately constant, thus the incident and the outgoing radiance is approximately equal. The proposed model does not follow this behavior since the maximum of the BRDF values is constant for any incident angle.

To further explain this, let us compare the behavior at the limiting mirror case of the Phong, of the new model and of the real metals. Assume that the Fresnel function is approximately 1 (this is a good approximation for silver mirror, for instance), and the shininess – which is represented by  $s$  in the new model and by the exponent in the Phong model – goes to infinity. If the observer looks at the mirror perpendicularly and the illumination is also perpendicular, then both the new model and the Phong model provide the same radiance and reflected power as a real metal. However at grazing angles, while a real mirror would reflect the incoming radiance and the output power would be equal to the input power, for the Phong model both the radiance and the output power tend to zero. Interestingly, the output radiance of the new model also goes to zero at grazing angles, but the output power equals to the input power at arbitrarily close to the horizontal illumination. Thus, the new model is an energy mirror in this limiting case, but is not an ideal radiance mirror. This is “better” than the Phong model which is neither radiance nor energy mirror. The radiance mirror property means that the illumination of point light sources are reflected like real metals even at grazing angles. The energy mirror property, on the other hand, means that the distributed (e.g. daylight) illumination is reflected in a way as real metals since for uniformly distributed illumination, the perceived radiance is proportional to the albedo (equation (4.13)).

	Phong ( $n \rightarrow \infty$ )	new BRDF ( $s \rightarrow \infty$ )	real metal mirrors
$a_{\text{mean}}$	1/2	1	1
$\mathbf{a}(\theta \rightarrow 90^\circ)$	0	1	1
$L^{\text{out}}(\theta \rightarrow 90^\circ)$	0	0	$L^{\text{in}}$
$f_r(\theta \rightarrow 90^\circ)$	constant	constant	$\infty$

Table 4.2: Comparison the limiting case of the Phong model, of the new model and of real metal mirrors at grazing angles

### 4.7.2 Coated metals, metallic paints

We concluded that the new model is not a perfect metallic model because the BRDF of metals goes to infinity at grazing angles while the BRDF of the new model is bounded but its reflection lobe gets wider in order not to absorb all energy. Considering real materials, metals coated by a lacquer layer[48] behave like this. Since in lacquer the attenuation of the power is an exponential function of the length travelled, for higher incident angles, both the reflected radiance and power will tend to zero at grazing angles. If the lacquer also contains the particles of the basic metal, then the behavior of the material will be in between the metal and lacquered metals. Absorption, scattering and reflection can occur simultaneously in the lacquer layer. Thus for higher incident angles the metal particles, especially those that are close to the surface, will be responsible for reflecting the incoming photons. The object acts as energy mirror even if the reflected radiance decreases. Consequently the new model seems to be appropriate for representing coated metals and metallic paints.

Since the diffuse component of the metals is practically negligible, the metallic paints are approximated as follows

$$C_{\text{max}} \cdot \xi(m) \cdot \text{Fresnel}(\theta') \quad (4.51)$$

where  $C_{\text{max}} \cdot \xi(m)$  is a BRDF. For metals, the  $\xi(m)$  function has a quite small diffuse component. We can use, for example, the  $\xi(m) = \frac{s^2}{2\pi} \cdot e^{-s \cdot m}$  function, assuming that  $s > 10$ .

The wavelength dependent Fresnel function describes the reflection of the optically smooth material as a function of the incident angle.

In the Cook–Torrance model, as well as in other mirror-particle models, for a given  $(\mathbf{L}, \mathbf{V})$  pair, the expectation of the normal vectors of the reflecting facets is the  $\mathbf{H}$  vector, thus the angle of incidence is  $\theta_{\mathbf{H}} = \arccos(\mathbf{N} \cdot \mathbf{H})$ .

This approach is slightly modified in the following way. The distance of the  $\mathbf{H}_P = \frac{\mathbf{V}_P + \mathbf{L}_P}{2}$  vector from the  $\mathbf{O}$  origin is used to evaluate the Fresnel function.

$$|\mathbf{H}_P - \mathbf{O}| = \frac{|\mathbf{L}_P - \mathbf{V}_P|}{2} = \frac{|\mathbf{g} - (\mathbf{N} \cdot \mathbf{g})\mathbf{N}|}{2} = \frac{m(\mathbf{L}, \mathbf{V})}{2} \quad (4.52)$$

where the  $m(\mathbf{L}, \mathbf{V})$  metric is described by formula (4.29) belonging to the retro-reflective model.

Let us define angle  $\theta'$  in the following way:

$$\theta' = \arcsin\left(\frac{m(\mathbf{L}, \mathbf{V})}{2}\right) \quad (4.53)$$

In conclusion, the proposed new model is:

$$f_{r,\text{metallic}}(\mathbf{L}, \mathbf{V}) = \frac{s^2}{2\pi} \cdot e^{-s \cdot |\mathbf{h} - (\mathbf{N} \cdot \mathbf{h})\mathbf{N}|} \cdot \text{Fresnel}_\lambda(\theta') \quad (4.54)$$

where  $\theta' = \arcsin \frac{|\mathbf{g} - (\mathbf{N} \cdot \mathbf{g})\mathbf{N}|}{2}$ .

The model is the product of a reflective and a retro-reflective model. Importance sampling can be performed efficiently on the reflective factor, the retro-reflective factor modifies the weights of the elementary rays as a multiplier.

### 4.7.3 Plastics and polishing

Using a real refraction index in the Fresnel term instead of the complex index of metals, the proposed model can also be used for modelling the specular reflection of plastics. Since the diffuse reflection of plastics is also significant, the BRDF function is defined as a sum of the diffuse and specular terms. To meet the requirement of energy conservation, the sum of the albedos of the diffuse and specular part must be less than 1. The BRDF is then

$$f_{r,\text{plastics}} = \frac{a_{\text{diffuse}}}{\pi} + (1 - a_{\text{diffuse}}) \cdot C_{\text{max}} \cdot \xi(m) \cdot \text{Fresnel}(\theta') \quad (4.55)$$

Certain materials, as for example lacquered objects, reflect sharp mirror images for large viewing angles [41]. To simulate this phenomenon, any of the proposed BRDFs can be supplemented by an ideal mirror in the following way:

$$f_{r,\text{mirrorextension}} = f_r(\mathbf{L}, \mathbf{V}) + (1 - \mathbf{a}(\mathbf{L})) \cdot f_{r,\text{idealmirror}}(\mathbf{L}, \mathbf{V}) \quad (4.56)$$

Note that the extension is limited by the “missing albedo” of the original BRDF. The BRDF of the ideal mirror is a Dirac function:

$$f_{r,\text{idealmirror}}(\mathbf{L}, \mathbf{V}) = \frac{\text{Fresnel}(\theta') \cdot \Delta(\mathbf{L}' - \mathbf{V})}{\cos \theta} \quad (4.57)$$

### 4.7.4 Generalized Lambertian models

The  $\xi(m)$  function can be monotone increasing as well. In this case the reflected radiance will have smaller slope as the incident angle changes than the cosine function obtained from the Lambertian model, which conforms to the measurements using a certain class of materials, including ceramic, wall, foam, cloth, etc. Due to the local interreflections – especially for great incident angles – these materials reflect more light backwards, than forwards in the mirror direction.

Oren et. al.[56] also proposed a model for these types of materials. Here a different approach is presented. To obtain such a model, let us assume that the light source is placed in the viewpoint. An appropriate function of the reflected radiance that has a “smoother” slope than the Lambertian model is  $\cos^{1-d} \theta$  where  $\theta$  is the angle of the light and of the normal vectors and  $d$  is the smoothness parameter. In the limit case of  $d = 0$  the diffuse case is obtained, for the  $d = 1$  limit case we get a disk of constant radiance, which is like the full moon. This selection leads to the following  $\xi$  function:

$$\xi(m) = \left(1 - \left(\frac{m}{2}\right)^2\right)^{-\frac{d}{2}}, \quad 0 \leq d \leq 1 \quad (4.58)$$

Unfortunately, these models do not satisfy the principle of the conservation of energy, so we have to modify definition (4.58). The simplest way of correcting this is to limit the BRDF with a constant. Another possible approach is to consider the MacLaurin’s series of the function, retaining only a few terms, such that the truncated series will be less than the original function.

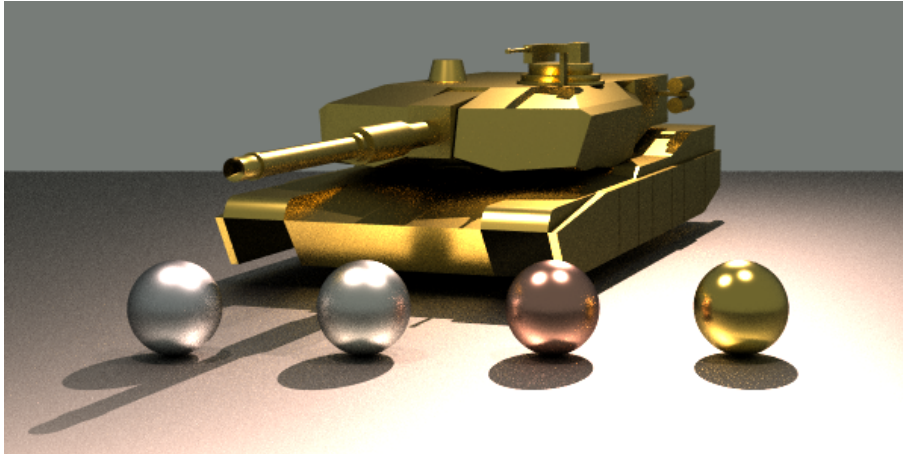


Figure 4.16: Scene rendered using Russian roulette including a golden tank ( $s = 10$ ), silver base plane ( $s = 4$ ), aluminium ( $s = 6$ ), silver ( $s = 8$ ), copper ( $s = 15$ ) and golden ( $s = 20$ ) spheres

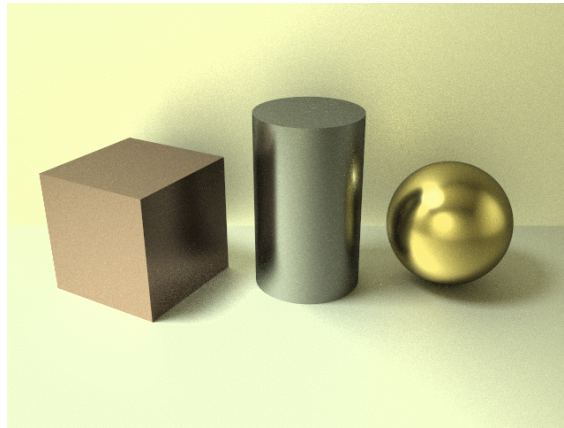


Figure 4.17: A simple scene with a cube ( $s = 2$ ) cylinder ( $s = 4$ ) and sphere ( $s = 8$ )

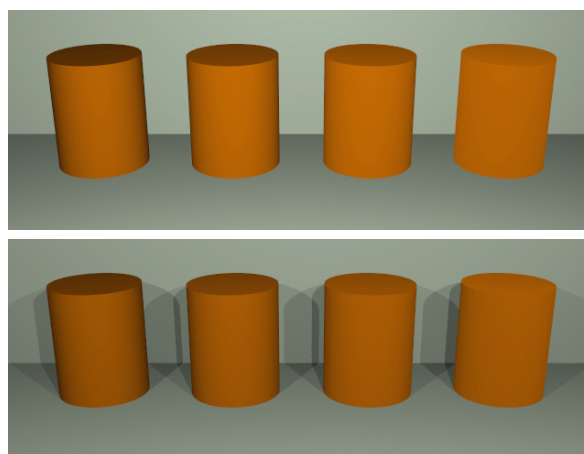


Figure 4.18: Objects ( $d = 1$ ,  $d = 0.75$ ,  $d = 0.5$ ,  $d = 0.25$ ) rendered using generalized Lambertian BRDFs computing only the direct illumination effects. In the upper image the light source is at the view position, in the lower image there are two point light sources

$d$	$C_{\max}$	$f_{\max}$	$a_{\text{diffuse}}$	
0	$1/\pi$	1.0	1.0	LAMBERTIAN
0.1	0.30884	1.123440	0.97689	
0.2	0.29939	1.262117	0.95352	
0.3	0.28998	1.417912	0.92989	
0.4	0.28061	1.592939	0.90602	
0.5	0.27128	1.789571	0.88193	
0.6	0.26200	2.010475	0.85764	
0.7	0.25278	2.258647	0.83318	
0.8	0.24363	2.537454	0.80856	
0.9	0.23456	2.850676	0.78381	
1.0	0.22556	3.202563	0.75895	"FULL MOON"

Table 4.3: Parameters obtained for the generalized Lambertian model

As an example, let us consider the case when the function is clipped by a constant:

$$f_r(\mathbf{L}, \mathbf{V}) = C_{\max} \cdot \min \left( \left( 1 - \left( \frac{m}{2} \right)^2 \right)^{-\frac{d}{2}}, \xi_{\max} \right) \quad (4.59)$$

where  $0 \leq d \leq 1$ .

Table 4.3 has been generated using a clipping where the function was taken to be constant above  $m = 1.9$ , that is  $\xi_{\max} = \xi(1.9)$ . The  $C_{\max}$  value was determined such that the maximum value of the albedo is 1. For the above model, this is reached always for  $m = 2$ . The minimum of the albedo is always in  $m = 0$ . So, contrary to the case of monotone decreasing functions, the pure diffuse component is defined by the case corresponding to  $m = 0$ .

The model defined by formula (4.59) can always be described as the sum of a Lambertian model with an albedo (reflectivity) of  $a_{\text{Diffuse}}$  and of a complementary model. The albedo of the latter is zero for  $m = 0$  and it is a monotone increasing function of  $m$ . Formula (4.59) has the same behavior as the model defined by equation (4.58), except for the  $m > 1.9$  domain. In the case of  $1.9 \leq m \leq 2$ , the reflected radiance for the above mentioned sphere will have a decrease proportional to the cosine function at  $[0, 1]$ .

The “full moon” limit case means that for a sphere illuminated from the viewpoint the radiance will be constant, only at the margins will decrease with a cosine character. The width of the “cosine-ring” can be controlled by modifying  $\xi_{\max}$ . It is advisable to choose the value of  $d$  in formula (4.59) to be less than 1.

For the above model, a good approximation of the importance sampling is to generate directions (with a “cosine” distribution) like in the case of the Lambertian model and to use an appropriate multiplier correction factor for each ray.

## 4.8 Conclusions and future work

Above it is presented a new, simple and unified definition for obtaining a good visual approximation for many materials. The new model class can be used easily in the majority of the commercial programs. By allowing the interactive definition of the  $\xi(m)$  highlight profile functions, BRDF characteristics can be specified in a new manner.

Due to their simplicity, the computation cost of the new models is low. According to our running time measurements using Heckbert’s BRDF viewer[28], the computational time of the new model is practically equal to the time of the Phong–Blinn model and half of the time of the Ward model. Importance sampling, on the other hand, is simpler and faster for the new model than for previous models.

One of the problems to be solved by further research is to investigate which of the physically plausible BRDFs (fulfilling reciprocity, energy conservation and non-negativity) can be defined by suitable

$$(T(\mathbf{L}), m(\cdot, \cdot), p(R))$$

triplets (see section 4.5). Another important question is which materials can be modelled as the sum, product and other generalizations of the introduced reflective and retro-reflective models.

## Chapter 5

# Central Concepts and Future Directions

In this chapter the key concepts, method and proceedings of this dissertation are defined and discussed in general terms. Details are not covered here, but the essential ideas so far stated or to be covered, which, in connection with general formulations, show potentials for further development.

### 5.1 Repairing Energy Balance

In general, the condition of non-negativity for the physical plausibility of a given BRDF formula is not a problem. Damage to symmetry can be directly determined from the formula and if needed can be simply corrected. The fulfillment/damage of energy balance is an essential, rather than a trivial problem. In both cases it is sensible to consider repairing the energy balance. By the application of various methods we searched for a version of the original BRDF that fulfills the conservation of energy balance *as closely as possible*.

After fulfillment of physical plausibility, algorithmic convergence may be essential from the point of view of applicability. In case of damage, various proceedings may diverge (ray-tracing, MC-methods, radiosity, Jacobi-iteration) and the extent of divergence depends on the accuracy of method and its limits, the character of scene and the extent of energy damage. The possible *magnitude* of albedo (its approximation to 1) can be important from the point of view of the "perceptually plausibility". The value of albedo can be directly observed as the reflection of uniform diffuse illumination (daylight) according to direction. The darkening of surfaces from certain directions frequently contradict the phenomenon to be modelled, degrades its credibility and produces a sense of artificiality. In general, increase in albedo along feasible lines enhances the "gaming space" of formulae to be developed and also enables the correction of BRDF constructions for other shortcomings.

If  $\mathbf{a}_f(\mathbf{L})$  is bounded, the  $\sup_{\mathbf{L} \in \Omega} (\mathbf{a}_{f_{norm}}(\mathbf{L})) = 1$  applies to the normalized function  $f_{norm} = \frac{1}{\sup_{\mathbf{L} \in \Omega} (\mathbf{a}_f(\mathbf{L}))} \cdot f$ , independently whether or not the condition  $\mathbf{a}_f(\mathbf{L}) \leq 1$  is satisfied. Normalizing factor  $\frac{1}{\sup_{\mathbf{L} \in \Omega} (\mathbf{a}_f(\mathbf{L}))}$  is a large constant, which can convert  $f$  into a function fulfilling the condition of energy balance.

If only the existence of  $\mathbf{a}_f(\mathbf{L})$  is assumed for each  $\mathbf{L}$  value, the "albedo pumping" Neumann et al. [53] we use for the correction of energy balance is a non-trivial method.  $g(\mathbf{L}, \mathbf{V})$  is a function, for which  $\max(\mathbf{a}_f(\mathbf{L}), \mathbf{a}_f(\mathbf{V})) \leq g(\mathbf{L}, \mathbf{V})$ , and the modified BRDF is:

$$f_r^*(\mathbf{L}, \mathbf{V}) = \frac{f_r(\mathbf{L}, \mathbf{V})}{g(\mathbf{L}, \mathbf{V})} \quad (5.1)$$

Because of the construction, the albedo of  $f_r^*$  becomes physically plausible:

$$\begin{aligned} \mathbf{a}_{f^*}(\mathbf{L}) &= \int_{\mathbf{V} \in \Omega} f_r^*(\mathbf{L}, \mathbf{V}) \cdot \cos \Theta_{\mathbf{V}} \, d\omega_{\mathbf{V}} = \int_{\mathbf{V} \in \Omega} \frac{f_r(\mathbf{L}, \mathbf{V})}{g(\mathbf{L}, \mathbf{V})} \cdot \cos \Theta_{\mathbf{V}} \, d\omega_{\mathbf{V}} \leq \\ &\leq \int_{\mathbf{V} \in \Omega} \frac{f_r(\mathbf{L}, \mathbf{V})}{\mathbf{a}_f(\mathbf{L})} \cdot \cos \Theta_{\mathbf{V}} \, d\omega_{\mathbf{V}} = \frac{\int_{\mathbf{V} \in \Omega} f_r^*(\mathbf{L}, \mathbf{V}) \cdot \cos \Theta_{\mathbf{V}} \, d\omega_{\mathbf{V}}}{\mathbf{a}_f(\mathbf{L})} = \frac{\mathbf{a}_f(\mathbf{L})}{\mathbf{a}_f(\mathbf{L})} = 1 \end{aligned} \quad (5.2)$$

Had  $f$  been originally also plausible due to  $\max(\mathbf{a}_f(\mathbf{L}), \mathbf{a}_f(\mathbf{V})) \leq 1$ , the condition of  $g(\mathbf{L}, \mathbf{V}) \leq 1$  can be satisfied. In this case  $f_r \leq f_r^*$  and  $\mathbf{a}_f(\mathbf{L}) \leq \mathbf{a}_{f^*}(\mathbf{L})$  are given, that is the new material model becomes lighter than the original (lighter in general and nowhere darker). Hence the term "albedo pumping". The extent of "albedo pumping" is the greatest if  $\max(\mathbf{a}_f(\mathbf{L}), \mathbf{a}_f(\mathbf{V})) = g(\mathbf{L}, \mathbf{V})$ . Because of other considerations, however, function  $g$  may be bounded at minimum values for example by  $\max(\mathbf{NL}, \mathbf{NV})$ , without losing symmetry. In such a case condition  $g \leq 1$  is still fulfilled and therefore the albedo improves.

## 5.2 Generating new physically plausible BRDFs

For certain operations the class of physically plausible BRDFs is closed. Starting from a given simple basic set, these operations facilitate the production of another class of BRDFs. Of these operations the formation of discrete and continuous (coefficient sum not greater than 1) linear combinations may be singled out here.

### 5.2.1 Linear mixing of BRDFs

There are several methods for creating physically plausible BRDFs from other physically plausible BRDFs. Positively weighting discrete linear combinations is the simplest method:

$$f_r(\mathbf{L}, \mathbf{V}) = \sum_{k=1}^N c_k \cdot f_r^{(k)}(\mathbf{L}, \mathbf{V}) \quad \text{where} \quad \sum_{k=1}^N c_k \leq 1 \quad (5.3)$$

Obviously the conditions of non-negativity and symmetry are satisfied and the energy balance formulated with albedo:

$$\mathbf{a}(\mathbf{L}) = \sum_{k=1}^N c_k \cdot \mathbf{a}^{(k)}(\mathbf{L}) \leq \sum_{k=1}^N c_k \leq 1 \quad (5.4)$$

Instead of discrete weights, continuous distribution function may also be used for mixing. Let  $\mathbf{t}$  be the free (one or multi-dimensional) parameter of a class of BRDFs and  $f_r(\mathbf{L}, \mathbf{V}, \mathbf{t})$  a  $\mathbf{t}$ -dependent BRDF. Let  $p(\mathbf{t})$  be the probability density function (or not greater than that) in a  $[\mathbf{a}, \mathbf{b}]$  interval is one, or multi-dimensional, finite or infinite:

$$\int_{\mathbf{t} \in [\mathbf{a}, \mathbf{b}]} p(\mathbf{t}) \, d\mathbf{t} \leq 1 \quad (5.5)$$

The mixture BRDF with similarly dimensioned integral:

$$f_r(\mathbf{L}, \mathbf{V}) = \int_{\mathbf{t} \in [\mathbf{a}, \mathbf{b}]} p(\mathbf{t}) \cdot f_r(\mathbf{t}, \mathbf{L}, \mathbf{V}) \, d\mathbf{t} \quad (5.6)$$

Similarly fulfilling non-negativity and symmetry, and the value of albedo does not exceed 1 :

$$\mathbf{a}(\mathbf{L}) = \int_{\mathbf{t} \in [\mathbf{a}, \mathbf{b}]} p(\mathbf{t}) \cdot \mathbf{a}(\mathbf{t}, \mathbf{L}) \, d\mathbf{t} \leq \int_{\mathbf{t} \in [\mathbf{a}, \mathbf{b}]} p(\mathbf{t}) \, d\mathbf{t} \leq 1 \quad (5.7)$$

### 5.2.2 Patch-based BRDF lasses

Continuous linear combination forms new BRDFs from elements of existing BRDF class defined by one or more parameters. Next we shall describe a general method, which yields such parameterized basic BRDFs and is referred to many times in this dissertation.

Take a

- $\chi : \Omega \rightarrow \mathbf{R}^+$  "character-function", a
- $H : \Omega \times \Omega \rightarrow \Omega$  symmetric (that is  $H(\mathbf{L}, \mathbf{V}) = H(\mathbf{V}, \mathbf{L})$ ) "bisecting vector function" (in general case it means bisection between  $\mathbf{R}$  and  $\mathbf{V}$ , so  $\mathbf{H}$  and  $H$  are generally not the same), and a
- $\eta : \Omega \times \Omega \times \mathbf{R}^n \rightarrow \{0, 1\}$   $n$ -parameter patch-function (basically  $n = 1$  case counts), whose direction variables are also symmetric, that is  $\eta(\mathbf{L}, \mathbf{V}, p) = \eta(\mathbf{V}, \mathbf{L}, p)$ .



The terms "patch-based" or "patch-function" derive from the definition of the

- $patch(\eta, \mathbf{L}, p) = \{\mathbf{V} : \eta(\mathbf{L}, \mathbf{V}, p) = 1\}$  patch-cluster, whose symmetry indicates the obvious equivalence:

$$\mathbf{V} \in patch(\eta, \mathbf{L}, p) \Leftrightarrow \mathbf{L} \in patch(\eta, \mathbf{V}, p) \quad (5.8)$$

The character-function will be the seed of the base BRDFs formulae; the bisecting vector primarily ensures the fulfillment of the symmetry condition; and the patch-function as a characteristic function of  $\{0, 1\}$ -value yields the valid domain (without ruining symmetrical properties).

The definition of  $p \in \mathbf{R}^n$  indexed base BRDF:

$$g_p(\mathbf{L}, \mathbf{V}) = \chi(H(\mathbf{L}, \mathbf{V})) \cdot \eta(\mathbf{L}, \mathbf{V}, p), \quad c_p = \frac{1}{\sup_{\mathbf{L} \in \Omega} (\mathbf{a}_{g_p}(\mathbf{L}))} \quad \text{and} \quad f_p = c_p \cdot g_p \quad (5.9)$$

or shortly

$$f_p(\mathbf{L}, \mathbf{V}) = norm(\chi(H(\cdot, \cdot)) \cdot \eta(\cdot, \cdot, p)) (\mathbf{L}, \mathbf{V}) \quad (5.10)$$

that visibly fulfills the conditions of non-negativity, symmetry and energy balance.

The only condition for the validity of definition is the existence of  $\sup_{\mathbf{L}} (\mathbf{a}_{g_p}(\mathbf{L}))$ , which may be ensured by exploiting the overestimation  $\eta$  eq1 and that the integral  $\int_{\mathbf{V} \in \Omega} \chi(H(\mathbf{L}, \mathbf{V})) \cdot \cos \Theta_{\mathbf{V}} d\omega_{\mathbf{V}}$  is bounded, which means the normalizability of  $\chi(H(\mathbf{L}, \mathbf{V}))$ . In general this sufficient condition is necessary as well, because a sensible construction usually also contains a  $p$  parameter, upon which some patch corresponding to  $\mathbf{L}_i \in \Omega$  covers the whole hemisphere.

The fact of normalization in the definition  $g_p = \chi(H(\cdot, \cdot)) \cdot \eta(\cdot, \cdot, p)$  and its consequence is not altered, if  $\eta_p(\mathbf{L}, \mathbf{V}) (= \eta(\mathbf{L}, \mathbf{V}, p))$  is normalized first and then the new  $\eta$  takes up the  $\{0, c_p\}$   $c_p = \frac{1}{\sup_{\mathbf{V}} (\mathbf{a}_{\eta_p}(\mathbf{V}))}$  value in stead of  $\{0, 1\}$ . The  $c_p$  exists, because its greatest value can be  $\pi$ . In this way, the similarity between the patch-cluster and patch-function is lost (so far a constant), but the normalized  $\eta_p$ -s fulfill the properties of physical plausibility, so they can be considered as BRDFs as well, although these are used for a different purpose. Together with this however the normalization factor is "tamed" to around 1 and the role of  $\chi$  becomes better understandable. Finally the handling of singularities is standardized, because those of normalized point-patches are constant times *Dirac* –  $\Delta$  and we need not deal with them with cutoff points.

The symmetric patch-function with (now one-dimensional) parameter  $p$  may be taken to be the characteristic function  $d(\mathbf{L}', \mathbf{V}) \leq p$ , where  $d$  is the Euclidean distance, or the Euclidean distance of projection points on the reference plane (as simplest case), or distance of projections according some metrics transformed according to some other transformation  $t$ . The single  $(\chi, t, H)$  tuples determine the various classes of BRDF by the mixing methods detailed in previous chapter.

### 5.2.3 Components of patch-based BRDF constructions

In the usual case the character-function  $\chi$  is isotropic (that is, rotation symmetric around  $\mathbf{N}$ ), and can be written as a  $\cos \Theta_H$  function, that is by a  $\chi : (0, 1] \rightarrow \mathbf{R}$  function. Accordingly we can take the  $\cos \Theta_H$  in place of  $H$ , that is the ' $\cos \Theta_H$ ' :  $\Omega \times \Omega \rightarrow (0, 1]$  functions. So  $\cos \Theta_H = \mathbf{N}H$  can be written directly into argument of  $\chi$  as  $\chi(\mathbf{N}H)$ .

Anisotropic cases can be derived relatively simply by modifying isotropic ones, so now we focus on isotropic models. Forward-reflective and retro-reflective models can be constructed by using the same mechanism, changing role of  $\mathbf{L}$  and  $\mathbf{R}$  at definition of patch-function  $\eta$  and at bisecting vector  $H$ , exploited the fact that  $(\mathbf{L}')' = \mathbf{L}$ .

Modifying any element of the  $(\chi, t, H)$  tuple essentially different classes of BRDF are obtained. First of all the character-function characterizes behavior of BRDF may be taken for example as  $\chi(\mathbf{N}H) = (\mathbf{N}H)^\alpha$  with different  $\alpha$ , as a simple parameterization of "character".

- $\alpha = 0$  gives **generalized diffuse models**, since the basic-BRDF belonging to the largest patch is the Lambertian model in itself.
- $\alpha = -1$  leads to patch-based metallic models including ideal mirror as special case, in according to the same ' $1/\cos$ ' character of real metals have at mirroring direction.
- Other  $\alpha$  can produce super-metallic or other special mainly artificial effects.

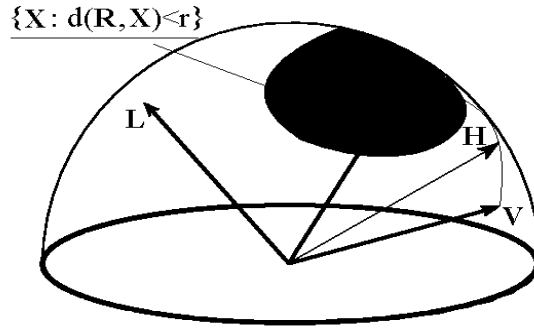


Figure 5.1: Patch-based BRDF,  $f_r(\mathbf{L}, \mathbf{V}) = \chi(H) \cdot F(d(\mathbf{R}, \mathbf{V}))$

Fixing the character-function, the choice of transformation  $t$  defines the distance-function  $d$  and is determined only by the choice of projection-space, in consequence of albedo-maximum principle, that is albedo is wanted to be as great (up to 1) as it is possible. (It has any freedom only by definition of  $H$ ). Ignoring details, the following different projection space each with their own euclidean metric can be considered:

- **original (half)sphere** with no projection (with identity projection),
- **basic plan** with perpendicular projection,
- **inscribed sphere** into half sphere with central projection from origin
- **basic plan** with perpendicular projection and then a stretching transformation in itself
- other projections over basic circle, etc.

Each of them can be combined with arbitrary character-function, e.g. with above mentioned *generalized diffuse*, and with *patch-based metallic* models as well, knowing that the choice has important consequence for the behavior of the albedo. First of all the albedo has to be bounded for patch-functions – it is done for above mentioned  $\alpha = 0$  and  $\alpha = -1$  cases. Secondly, it is an advantage if albedo is not diminishing at grazing angles after normalization – knowing that most of existing material model do not satisfy this expectation.

The choice of bisecting vector  $H$  is meaningless in case of constant basic-BRDFs, that is at  $\alpha = 0$ . It takes into account only that  $H$  has to be dropped into the patch around  $\mathbf{R}$  containing  $\mathbf{V}$ , which is a common sense condition. But in other cases the choice of  $H$  has essential influence on the model:

- **natural bisecting point** of  $\mathbf{R}$  and  $\mathbf{V}$  on
  - used **projection surface**
  - **original sphere**
  - other
- mean-point by  $p$ -th power, that is  $\cos \Theta_H = \text{mean}_p(\cos \Theta_L, \cos \Theta_V)$  (since in isotropic case it is taken only  $\cos \Theta_H$  into account, and because  $\cos \Theta_L = \cos \Theta_R$ . Specially with
  - arithmetic mean-value  $p = 1$  :  $\cos \Theta_H = \frac{\cos \Theta_L + \cos \Theta_V}{2}$
  - harmonic mean-value  $p = -1$  :  $\frac{1}{\cos \Theta_H} = \frac{\frac{1}{\cos \Theta_L} + \frac{1}{\cos \Theta_V}}{2}$
  - maximum  $p = -\infty$  :  $\cos \Theta_H = \max(\cos \Theta_L, \cos \Theta_V)$
  - other

The use of  $H$  makes essentially easier to build Fresnel factor, that is a predefined function of  $H(\mathbf{R}, \mathbf{V})$ , into model at all.

### 5.2.4 Examples of patch-based BRDF-classes

The first patch-based model-class by Neumann et al. [51] as an example of **generalized diffuse** models are defined by  $\chi(\mathbf{NH}) = 1$ , that is  $\alpha = 0, \chi(\mathbf{NH}) = (\mathbf{NH})^0$ . Transformation is the projection on the basic circle, distance corresponds to the euclidean distance on the projected space. The final formula with an arbitrary  $g$  and an appropriate  $c$  (is to be defined as its possibly maximum value):

$$f_r(\mathbf{L}, \mathbf{V}) = c_g \cdot g(|\mathbf{R}_p - \mathbf{V}_p|) \quad (5.11)$$

Specially, similar to Phong formulas, with  $g(x) = ((1 - x)^+)^n$

$$f_r(\mathbf{L}, \mathbf{V}) = c_n \cdot ((1 - |\mathbf{R}_p - \mathbf{V}_p|)^+)^n \quad (5.12)$$

A similar result is obtained formally from the projection to the inscribed sphere into half sphere with central projection from the origin, proposed by Tobler et al. [70]:

$$f_r(\mathbf{L}, \mathbf{V}) = c_g \cdot g(|\mathbf{R}_{p_{spheric}} - \mathbf{V}_{p_{spheric}}|) \quad (5.13)$$

Staying on the original sphere, that is using the identical transformation, and accordingly the original euclidean distance to define basic-patches that are circles on the sphere with center  $\mathbf{R}$ , different models can be obtained by the choice of character function  $\chi$  (or simpler of  $\alpha$ ), and the  $\mathbf{H}$  bisecting vector in cases of  $\chi \neq 1$  (that is  $\alpha \neq 0$ ). In this case distance can be replaced by  $\mathbf{RV}$ . At  $\alpha = 0$  the obtained models can be taken as a **generalization of Phong's** one:

$$f_r(\mathbf{L}, \mathbf{V}) = c_g \cdot g(\mathbf{RV}) \quad (5.14)$$

At  $\alpha \neq 1$  there are different possibilities to choice H. Each of them leads to a **"metallic version of generalized Phong model"**, their common form is:

$$f_r(\mathbf{L}, \mathbf{V}) = c_{g,m} \cdot \frac{g(\mathbf{RV})}{\mathbf{NH}} \quad (5.15)$$

Here index m designates the method of choosing  $\mathbf{H}$ , which can be done according to above listed possibilities. Specially in case of  $\mathbf{NH} = \max(\mathbf{NL}, \mathbf{NV})$  and  $g(\mathbf{RV}) = (\mathbf{RV})^n$  this model produces a metallic correction of the symmetrical Phong model, introduced by Neumann et al. [52]:

$$f_r(\mathbf{L}, \mathbf{V}) = c_{g,\max} \cdot \frac{((\mathbf{RV})^+)^n}{\max(\mathbf{NL}, \mathbf{NV})} \quad (5.16)$$

Another model is obtained by another bisecting formula (from the list above), e.g. by spherical bisecting point or by harmonic mean-value, a choice of  $\mathbf{NH}$  which eliminates the break in the shape of BRDF at  $\mathbf{V} = \mathbf{R}$  (produces a smooth curve for every  $\mathbf{L}$  and  $\mathbf{V}$ ) and carries its expected off-specular peak:

$$f_r(\mathbf{L}, \mathbf{V}) = c_{g,m} \cdot \frac{((\mathbf{RV})^+)^n}{\mathbf{NH}(\mathbf{RV})} \quad (5.17)$$

In case of  $p = -1$  power-mean we can write it simply in the form that can be completed by the Fresnel factor :

$$f_r(\mathbf{L}, \mathbf{V}) = c_{g,geom} \cdot \frac{((\mathbf{RV})^+)^n}{\frac{1}{\mathbf{NL}} + \frac{1}{\mathbf{NV}}} \quad (5.18)$$

### 5.2.5 Sampling on patch-based BRDFs

The sampling of all mixed BRDF (generation of an outgoing direction corresponding to the incoming direction; because of symmetry operation the inverse requires no different method) can be made in two steps:

- first we select the parameter of the mixing function (density function) as the sample taken from the value set of distribution function according to even distribution and by the retro-transformation of chosen values according to inverse distribution. The case of discrete linear combination is according to the singularity of the density function. Singularity (in continuous case according to the positive weight of special parameter values, in discrete case according to all values) in turn reveals the stepwise structure of the distribution function that can however be handled without any problems.

- second we sample the base BRDF of the chosen parameter complying with the concrete BRDF

The sample of arbitrary (in this case base) BRDF linked to given  $\mathbf{L}$  indicates the selection of outgoing energy in a direction according to the distribution function. What causes the difficulty is, that the amount of energy to be carried in the outgoing direction has to be a fixed quantity of unit dimension, that is the hemisphere has to be evenly divided according to  $f_r(\mathbf{L}, \mathbf{V}) \cdot \cos \Theta_{\mathbf{V}}$  (that is energy). Therefore we select base functions, by which the hemisphere may be transformed to the reference plane, so that after transformation  $t$  the

$$\tau_t(t(\mathbf{L}), t(\mathbf{V})) = f_r^*(t(\mathbf{L}), t(\mathbf{V})) \cdot \cos \Theta_{\mathbf{V}} \cdot \frac{d\omega_{\vec{v}}}{dA_{t(\mathbf{V})}} \quad (5.19)$$

density function has small variance (possibly constant) on the projections of patches on the plane (that is on  $dA_{t(\mathbf{V})}$ ). Outside that obviously it remains zero. In this way sampling becomes a problem of scoring into the transformed patch of  $\mathbf{a}(\mathbf{L})$  size in the transformed space. The smoothing of transformation, and the shape of (original or the transformed) patch determines the base BRDF also in reverse.

It is convenient to eliminate the  $\cos \Theta_{\mathbf{V}}$  factor of the distribution in the first step of projection on the reference plane. Because at this point  $\cos \Theta_{\mathbf{V}} \cdot \frac{d\omega_{\mathbf{V}}}{dA_{t_0(\mathbf{V})}} = 1$  and the  $f_r(\mathbf{L}, \mathbf{V}) \cdot \cos \Theta_{\mathbf{V}}$  proportional distribution on the hemisphere is equivalent to  $f_r(t_0(\mathbf{L}), t_0(\mathbf{V}))$  on the reference pane:  $\tau_{t_0} = f_r$ ! If further transformations are not applied (because  $f$  is already  $\{0, 1\}$ -function): the base BRDF corresponding to this is the same as the given  $(\mathbf{L}, \mathbf{V})$ -symmetric patch-function as well as the characteristic  $\{0, 1\}$ -function. This is the simplest patch based basic BRDF. In case of original sphere the second transformation is the inverse of the first so we can deal with sampling on the original space (i.e. on the sphere) without any transformation, only the original function has to be modified back to the first form :

$$f_{\text{sampl}}(\mathbf{L}, \mathbf{V}) = f_{r, \text{orig}}(\mathbf{L}, \mathbf{V}) \cdot \cos \Theta_{\mathbf{V}} \quad (5.20)$$

## 5.3 Distance of BRDFs

### 5.3.1 Scalar product and normal of BRDFs

All scalar product that preserve linear combination also define a distance definition by

$$d^2(a, b) = |a - b|^2 = (a - b) \bullet (a - b) \quad (5.21)$$

and distance defines the original symmetric scalar product as well:

$$\mathbf{a} \bullet \mathbf{b} = \left( \frac{|\mathbf{a} + \mathbf{b}|}{2} \right)^2 - \left( \frac{|\mathbf{a} - \mathbf{b}|}{2} \right)^2 \quad (5.22)$$

Later in occasional cases the condition of "0 - norm  $\Leftrightarrow$  0 - vector" is not satisfied, that is the "norm" is not a metric (thus space may be regarded as a direct product of a subspace determined by 0 - norm, therefore "0-interest subspace" and an independent norm-metric subspace) but this does not eliminate its validity in subsequent terms. In this distance definition the linear combination best approximating a given point of  $n$  base-points is derived from a linear equation of  $n$  variables. That is, we can take the space of scalar product to be a Euclidean space, and after determining the scalar product of some "base-vector pairs", we do not need to know anything about the space other than these scalar quantities for determining the best approximation. In optimal approximation we search for the  $\mathbf{a} = \sum_{i \geq 1} x_i \cdot \mathbf{a}_i$  which is the point nearest to  $\mathbf{b}$ : according to  $(x_i)_{i \geq 1}$  the term  $\mathbf{a} = \left( \sum_{i \geq 1} x_i \cdot \mathbf{a}_i - \mathbf{b} \right)^2$  is to be minimized, from which the equation system  $\left( \sum_{i \geq 1} x_i \cdot \mathbf{a}_i \bullet \mathbf{a}_j = \mathbf{b} \bullet \mathbf{a}_j \right)_{j \geq 1}$  of  $n$  variable can be derived according to  $(x_i)_{i \geq 1}$ .

The simplest way to give the scalar product in  $L^2$  - spaces is to take the weighted integral of the product of functions. According to the above this also defines the distance between two functions, as the weighted integral of the square of disparity functions. Concerning this latter case, norms can be defined by various types of integrals, weights and appropriate scalar products.

### 5.3.2 Dimension reductive norms by special lighting

An obvious definition of scalar product is the weighted integral of the product of every value on the  $(\mathbf{L}, \mathbf{V})$  coordinate of the two functions (according to the  $\cos \Theta_{\mathbf{L}} \cdot \cos \Theta_{\mathbf{V}}$  factor producing energy from radiance). In the case of a scalar product with itself (at norm squared) this method yields the weighted integral of the square of every effect of every point light, that is the mean albedo of the square of the original BRDF (more precisely its  $\pi$  multiple).

However, in reality there are other illuminations than just point lights. Of these daylight of equal radiance in all places is the most important. From the observer's direction its effect is the albedo, therefore the scalar product deriving from this ( $\cos \Theta_{\mathbf{L}}$  weighted for the magnitude of incoming energy) is the ( $\cos \Theta_{\mathbf{L}}$  weighted) integral of product of albedos. The square of norms corresponding to this is the  $\cos \Theta_{\mathbf{L}}$  weighted integral of the square of albedos, which cannot be derived either from the previous norm, or from the mean albedo, which can be regarded as the simplest norm. This scalar product (similarly to the product of mean albedos) yields no metrics.

### 5.3.3 Norm of general lighting

By taking the generally weighted average of general illumination positions we obtain the common generalizations of the latter; using the *Dirac*– $\Delta$  terminology for the definition of occasional point lights. In case of point sources, the illumination is a direction scalar function indexed by a direction parameter. Taking the direction parameter to be the first argument we obtain a  $\Omega \times \Omega \rightarrow \mathbf{R}^+$  function, which in the case of the ensemble of point light sources happens to describe a retro-reflective ideal mirror reducing along a cosine curve. We are at the liberty to reflect the parameter argument, thereby altering the meaning of the parameter, but not the result. In such a case the first argument indicates the location of a mirrored light source and the second argument the distribution of the light in question.

Point lights apart, other types of lights can be described by  $\Omega \times \Omega \rightarrow \mathbf{R}^+$  functions. The first argument indicates the "characteristic direction" of light, the second argument is its actual distribution. It is worthwhile to describe the character of distribution by an extra supplemental scalar parameter and so we ultimately obtain a set of parameterized  $\Omega \times \Omega \rightarrow \mathbf{R}^+$  functions. If for example the parameter indicates a (lack of) concentration of light distribution, the  $f_0$  is the function of point lights described above. No further generalizations seem to be necessary.

At weighted unification of all illuminations within various  $\Omega \times \Omega \rightarrow \mathbf{R}^+$  functions it seems sensible to apply the  $\cos \Theta$  weighting factor, following which it is sufficient to deal with  $w(p)$  weighting functions corresponding to the scalar parameters.

We may consider the earlier introduced normalized patch-functions as an example, that is the  $\eta_{\mathbf{L},p}(\mathbf{V}) = \eta_p(\mathbf{L}, \mathbf{V}) = \eta(\mathbf{L}, \mathbf{V}, p)$  of  $\{0, c\}$  value functions, with  $w(p)$  (and of course  $\cos \Theta$ ) weightings. Therefore with notation for composition and self-composition the scalar product yields the following:

$$f_1 \bullet f_2 = \int_{\mathbf{L}_1, \mathbf{L}_2 \in \Omega} \mathbf{C}_{f_1, f_2}(\mathbf{L}_1, \mathbf{L}_2) \cdot W_{\eta, w}(\mathbf{L}_1, \mathbf{L}_2) \cdot \cos \Theta_{\mathbf{L}_1} \cdot \cos \Theta_{\mathbf{L}_2} \, d\omega_{\mathbf{L}_1} \, d\omega_{\mathbf{L}_2} \quad (5.23)$$

$$\text{with } W_{\eta, w}(\mathbf{L}_1, \mathbf{L}_2) = \int_{p \in \mathbf{R}} \mathbf{C}_{\eta_p}(\mathbf{L}_1, \mathbf{L}_2) \cdot w(p) \, dp$$

The integrals and dimension number of functions during processing is (just about) acceptable in practice.

### 5.3.4 Inherence between scalar product and composition's norm

The scalar product of  $f_1$  and  $f_2$  is therefore a "weighted mean albedo" of an universal (that is *f* – *independent* !) weight function of their composition, therefore

$$f_1 \bullet_W f_2 = |C_{f_1, f_2}|_W \quad (5.24)$$

that is with  $L^1$  – *norm*, which this weighted integral defines:

$$|\mathbf{F}|_W = \int_{\mathbf{L}_1, \mathbf{L}_2 \in \Omega} \mathbf{F}(\mathbf{L}_1, \mathbf{L}_2) \cdot W(\mathbf{L}_1, \mathbf{L}_2) \cdot \cos \Theta_{\mathbf{L}_1} \cdot \cos \Theta_{\mathbf{L}_2} \, d\omega_{\mathbf{L}_1} \, d\omega_{\mathbf{L}_2} \quad (5.25)$$

Actually we could have defined  $f_1 \bullet f_2$  as  $|C_{f_1, f_2}|$ , at any  $L^1$  – *norm* in the space of  $\Omega \times \Omega \rightarrow \mathbf{R}^+$  functions, which fulfills the "*C* – *symmetry* condition"  $|C_{f_1, f_2}| = |C_{f_2, f_1}| \cdot C$  – *symmetrized* of  $|\bullet|$ . It

is satisfied in eq. 5.22 and can be performed generally by a general symmetrization of  $W$  :

$$W_{sym}(\mathbf{L}, \mathbf{V}) = \frac{W(\mathbf{L}, \mathbf{V}) + W(\mathbf{V}, \mathbf{L})}{2} \quad (5.26)$$

It can be even considered, that the set of scalar products  $f_1 \bullet f_2$  and set of the  $C$  – *symmetric* norms interpreted in terms of  $\Omega \times \Omega \rightarrow \mathbf{R}^+$  correspond to one another through the  $f_1 \bullet f_2 = |C_{f_1, f_2}|$  relationship.

In case of  $f_1 = f_2$  this means that  $\|f\|^2 = |C_f|$  (two different types of norm are involved). If  $\|\cdot\|$  is given, it defines also the symmetric scalar product:

$$f_1 \bullet f_2 = \frac{\|f_1 + f_2\|^2}{2} - \frac{\|f_1 - f_2\|^2}{2} \quad (5.27)$$

and so it defines an  $L^1$ –*norm* on  $|C_f|$  as well. Within the entire BRDF space this indicates the remarkable isomorphism of  $\|\cdot\|$   $L^2$ –*norms* and within these that of the  $|\cdot|$   $L^1$ –*norms* in self-composition’s subspaces.

The present  $W_{\eta_p, w}$  weight function represents the effects of illuminations and weighting. The  $W_{\eta_p, w}$  is a plausible BRDF, because the normalized patch-functions are plausible, and mixing according to self-composition and  $p$  conserves the physical plausibility properties. It should be considered whether or not the condition of BRDF plausibility should in general be fulfilled for illumination functions, as the norm generated by these functions derives also from a set of plausible illumination functions. Non-negativity is obvious and so is energy balance, because actually this requires only bounded-ness. The symmetry of illumination agrees with the above  $C$  – *symmetry*, which refers to the fact that all illuminations, as far as their scalar products are concerned, can be replaced by a symmetric one:

$$f_{sym}(\mathbf{L}, \mathbf{V}) = \frac{f(\mathbf{L}, \mathbf{V}) + f(\mathbf{V}, \mathbf{L})}{2} \quad (5.28)$$

symmetry of the  $f_{sym}(\mathbf{L}, \mathbf{V})$  illumination function leads to  $C$  – *symmetrization* of the norm.

At this time it does not appear that  $W_{\eta_p, w}$  would directly occur as self-composition (in the way the sum of exponential functions are not exponential, for example). This would mean, that the effect of illumination functions with scalar parameters could be summarized by a single illumination function without parameter. In the present case illumination defined the norm. For the sake of completeness we may consider the reverse relationship, that is what kind of parameterized illumination functions can be assigned to various  $C$ –*symmetric* norms, or can we assign to them a function without unified parameters, as queried in the previous statement.

This problem may play an essential role in the determination of the distance of BRDFs, and ultimately BRDF fittings.

# Summary

The dissertation deals with material models with special respect to metallic appearance of BRDFs.

First we introduce a coherent and clear definition of BRDF as ratio between outgoing radiance and incoming irradiance at given directions (1.1.1). This approach avoids the problem of infinitesimal quantities and limit values which previously needed careful mathematical discussions. From this we derive the definition of the local form of the rendering equation 1.15 which can be considered as another equivalent – i.e. mutually derivable – definition of BRDF. The later definition is based only on the concept of radiance, does not require definition of irradiance, and its mathematical apparatus stays inside traditional functional analysis. The use of theory of distribution as an extension of traditional analysis is only needed if special material models or lightings are taken into consideration, which need such descriptions anyhow. In spite of the mathematical advantages of we use the later definition only as a consequence of the preceding one.

Second, important attributes of BRDFs are formulated (intr.sec.brdfprops) for the reason of characterizing material models and to decide whether they are plausible or not. In addition this formulas are useable to examine BRDFs in different contexts. One and most important character of a model is the directional-hemispherical reflectivity, which means the ratio between outgoing energy caused by a directional incoming energy and the incoming one itself. This quantity is an extension of the concept of reflectivity or albedo of the Lambertian – diffuse – model to an arbitrary BRDF, so it's named henceforth shortly albedo. Physical plausibility can be spelled out by three required properties (1.1.2), non-negativity, non increasing energy-balance and the Helmolz's reciprocity of a function (based on theory of radiative heat transfer) which means simply reciprocity of BRDF. Because of the property of reciprocity, albedo can directly be seen in real materials as the response of uniformly distributed incoming radiance at different viewing directions, that is the effects of an ideal daylight. This fact shows that in real life albedo is at least as important as visible characteristic of materials as the values of their BRDFs in themselves, i.e their mean response to point-like light-sources – producing the same irradiance on surface. So far this fact has not been highlighted sufficiently. Albedo can also be used in rendering algorithms at least in two manners: to generate possibly correct ambient terms, and to generate rays for Monte Carlo based rendering methods.

The albedo of a BRDF is its directional-hemispherical reflectivity which equals to hemispherical-directional one because of reciprocity principle. We define also the hemispherical-hemispherical reflectivity called mean-albedo as a cosine-weighted average of albedo values. This characterizes the brightness of a material in a single value, which can be useful for completion of rendering algorithms as well. Finally, and partly independent from further discussion, we define the directional-hemispherical-directional connection of two material models, shortly named composition of them, which catches their connection in essential manner. Composition can be used for a correct definition of concept of distance of different material models, and also for a correct discussion and derivation of them.

We have defined requirements of real material models and especially of metallic ones (1.3.1). Overviewing existing models and analyzing if they meet some of listed properties, we can find that there is no model satisfying these requirements, in spite of their demanding approach and/or wide-spread use. In addition, as a natural dilemma, a real contradiction occurs between the simplicity of a formula and its meeting the requirements. Original Phong- and also Blinn-formula satisfy a lot of wishes, but violate principle of reciprocity, and correction of this lack leads to a much less attractive model. Similarly but at the same time surprisingly more sophisticated formulas violate rules of physical plausibility as well, namely energy balance at grazing angles. We showed the divergence of the albedo of the Ward model and also of the Cook–Torrance model at grazing angles, and our proof shows a more general divergence criteria (2.2.1, 3.7). Namely if the reciprocity and the inverse cosine factor are ensured by a negative power of the product of incoming ( $\mathbf{L}$ ) and outgoing ( $\mathbf{V}$ ) directions' cosines the same way as  $\mathbf{NL} \cdot \mathbf{NV}$ , and the completion factors can be estimated by a formula of the geometrical half-vector ( $\mathbf{H}$ ) of mentioned directions, there has to occur a divergence at grazing angles. This fact is also presented if  $\mathbf{LH}$  is used

beside  $\mathbf{NL} \cdot \mathbf{NV}$ . It is important even over mentioned examples because it limits the correctness or simpleness of their approaches.

As a way of correction existing models operation of "Albedo Pumping-up" is defined by using a careful and new additional divider (2.3.1), as the maximum of albedo at incoming and outgoing directions in question. This simple modification changes existing models in two manners at the same time. First whether original model was correct by albedo or not, the modified one will satisfy the principle of energy-balance. Furthermore the modification changes plausible models to be brighter, that is to have a higher albedo which is plausible as well. This "trick" solves the problem about plausibility, but can break the smooth shape of the BRDF – we mention that formulas consisting "max" or "min" expressions are breaking with or without any additional changes in advance. This operation can be considered as a symmetry-keeping point-wise normalization of the BRDF, in contrary of global normalization, that is dividing by the maximum (supremum) of all albedo-values. Later simple and rough operation could not solve the divergence problem, and in fact does not know about the intrinsic nature of albedo. Using the first operation repeatedly, each step modifies the given model, and as it can be seen, that the limit-model has the constant 1 albedo for the whole hemisphere.

The success of this operation is based on the problematic behavior of the albedo of usual models, which absorb light in order to facilitate the reconciliation of the symmetry principle with the requirement of maximally bright response. The core of the problem is that the cosine multiplier of incoming direction changes radiances to irradiance and by definition has to use to count responses, and also the cosine multiplier of outgoing radiance when total outgoing energy is integrated, that is albedo is counted. If outgoing radiance is roughly constant beside of inverse cosine value at mirroring direction, the outgoing energy follows a cosine shape, that is radically decreases at smaller angles, which is usually not corresponding with the facts. On the other hand if we should correct this drawback it would have to do this while parallel preserving the symmetry principle, which would lead to an infinite correction-process. Our method solves this problem directly by a single step. However this repeated operation can introduce an unwanted exaggeration of the model. Namely radiance can go over an acceptable/credible level while albedo is kept under the limit of 1, a fact which must be rooted in character of original model. You cannot repair everything. Nonetheless a "modified modification" can be used, for these cases, the so called Controlled Pumping-up method (2.3.2), based on a more special divider beside the maximum of albedo at incoming and outgoing directions in question. It is to use the maximum of albedos and also the cosine values of directions' angles in question. It results in a raised divider and so a smaller result. Of course any other supplementary max-factors can be used with the only restriction of them not being greater than 1. It is easy to see that repeated versions of controlled methods converge as well with not greater (practically less) result then of non-controlled ones.

Controlled Pumping-up is used for the well-known Phong and Blinn models, leading to an interesting result. The limes models of them can be written on as the original ones deviding by the maximum of cosine values of direction's angles in question (2.3.2). This  $\cos\_max$  divider as an inverse cosine factor provides satisfaction of all of requirements necessary for metallic characteristics (3.2.2) – except for the smoothness of the response, and so the phenomenon of the off-specular peak. We also suggest a correction of the Ward model to change its original inverse cosine factor that causes divergence to our  $\cos\_max$  divider (3.7). For Phong and Blinn models the original multiplier constants in the models that keep them plausible should not be changed, e.g.  $\frac{n+2}{2\pi}$  for Phong model. Resulting images are convincing, mean-albedo as general brightness of models converge to 1 by raising the parameter of models. In this way an ideal mirror can be approximated by these models. By introducing an additional parameter that controls the effect of  $\cos\_max$  factor, namely an extension of the power used for this factor (3.2.3), we get a smooth transition between original models, and their modification by the presented  $\cos\_max$  factor. For the Phong-model that uses  $RV$  (that is cosine between outgoing direction  $\mathbf{V}$  and mirroring direction  $\mathbf{R}$  of incoming vector  $\mathbf{L}$ ) for the core expression, a retro-reflective and an anisotropic construction is defined by changing  $RV$  to  $\mathbf{LV}$  at retro-reflective case, and  $RV$  to a Lafortune suggested anisotropic expression, respectively (3.3). Importance sampling is obtained for each variation by separating cases of "cos\_max" realized by  $\mathbf{NL}$  and  $\mathbf{NV}$  (3.4). The simplified cases are not completely smooth, but have significantly less variance. Using parameters, and completing models by additional fresnel factor and diffuse component, we get a flexible device to generate and approximate different materials, such as metals, plastics and ceramics.

An different construction was introduced to meet our initial requirements by a new classes of BRDFs called Patch Based BRDFs (4.3). This construction yields simple, variable families of BRDFs with well-suited albedo function and a very fast and theoretically variance-less importance sampling method at the same time. This approach is the first in the literature which is constructed intentionally in order to get importance sampling with minimal variance. The idea of using basic BRDFs (4.2) relies on fact



that the linear combination of them corresponds to the linear combination of albedo and a special linear combination of importance sampling as well. The latter corresponds to a two step choice, first by the coefficients of combination (taken also into consideration albedos of basic functions), and also by the chosen basic function (4.2.3, 4.2.4). Furthermore linear combination can be taken of a finite or an infinite set of basic functions as well, with the only condition that the sum of weights is to be 1 (or at least bounded). Our aim was to realize importance sampling with minimum variance of the integral that results in the albedo, that is of cosine weighted BRDF, so the basic function was created as incidence functions (multiplied by a normalizer constant) of patches on the unit circle on the base plan, and finally. Now area proportional sampling ensures a correct, that is energy proportional choice of rays.

The resulting function has infinite degree of freedom in two separate dimensions (4.5, 4.6): of metrics and of probability density function (i.e. the set of coefficients of linear combination), the latter is equivalent to its cumulated version and allows even negative values of starting probability density, a fact that can be used to produce interesting effects (4.7.4). Each of the chosen metrics in the limit case leads to the diffuse model, and also to a special "energy-mirror" (4.7.1) which gives back the total incoming energy to the mirroring direction, but the function does not follow an inverse cosine character, so the resulting radiance is not proportional to the incoming one. Another degree of freedom is available by varying the "mirror-direction" that is the main direction of response of incoming light, so retro-reflective models can be achieved by this method as well. The first and most obvious metric for this construction is the euclidean metric of the projected points on the base plan, leading to an interesting class of models, that can be used to simulate coated metals (4.7.2).

After the construction of these new BRDFs we discuss future directions explaining the general forms of two main topics of this thesis. One of them is a generalization of patch-based models (5.2), the general form of which yields an effective class of models as well. The other one deals with the composition which was introduced in this thesis, with the special property of equivalence between the  $L^2$ -norms in the BRDFs' space and the  $L^1$ -norms in the self compositions' space (5.3). The definition of distances of BRDFs is shown to be a practical application of this composition.

# Bibliography

- [1] C. B. Arnold and J. L. Beard **An ERIM perspective on BRDF measurement technology** *SPIE 1165 Scatter from Optical Components*, 1989.
- [2] I. Ashdown **Near-Field Photometry, A New Approach** 1992.
- [3] B. Arvo **Applications of Irradiance Tensors to the Simulation of Non-Lambertian Phenomena** *Proceedings of SIGGRAPH'95, (Computer Graphics)*, pp. 335–342, 1995.
- [4] E. Bahar and S. Chakrabarti **Full-Wave Theory Applied to Computer-Aided Graphics for 3D Objects** *IEEE Computer Graphics and Applications*, 47(7), pp. 46–61. 1987.
- [5] J. Beard, J. R. Maxwell **Bidirectional Reflectance Model Validation and Utilization, Technical Report Number AFAL-TR-73-303**, October 1973.
- [6] P. Beckmann and A. Spizzichino **The Scattering of Electromagnetic Waves from Rough Surfaces** *MacMilla*, 1963.
- [7] P. Beckmann **Shadowing of Random Rough Surfaces** *IEEE Transactions on Antennas and Propagation*, May 1965, pp. 684–388, 1965.
- [8] J.F. Blinn **Models of Light Reflection for Computer Synthetized Pictures** *Proceedings of SIGGRAPH'77, In Computer Graphics*, 11(2), pp. 192–198, 1977.
- [9] C. Bohren and D. Huffman **Absorption and Scattering of Light by Small Particles** *John Wiley and Sons, New York*, 1983.
- [10] M. Born and E. Wolf **Principles of Optics** *Pergamon Press, New York*, 1980.
- [11] B. Cabral, N. Max an R. Springmeyer **Bidirectional Reflection Functions from Surface Bump Maps** *Proceedings of SIGGRAPH'87, In Computer Graphics*, 21(4), pp. 273–281, 1987.
- [12] **CIE recommendation on uniform color spaces, color-difference equations, and psychometric color terms**, Supplements No.2 to Publication CIE No.15. 3 *Colorimetry 1(E-1.3.1) 1971, Bureau Central de la CIE, Paris*, 1978.
- [13] S. Chandrasekhar **Radiative Transfer** *Dover Publication Inc., New York*, 1960.
- [14] R. L. Cook and K. E. Torrance **A Reflectance Model for Computer Graphics** *Computer Graphics*, 15(4), pp. 187–196, 1981.
- [15] R. L. Cook and K. E. Torrance **A Reflectance Model for Computer Graphics** *ACM Transactions on Graphics*, 1(1), pp. 7–24, 1982.
- [16] I. Deák. **Random Number Generators and Simulation** *Akadémia Kiadó, Budapest*, 1989.
- [17] K. Ellis **Reflectance Phenomenology and Modeling Tutorial** *href = "http:// www. erim.org/on-line-docs/GUIDE/guide.frm.html"* - 10 Aug 94 (Last Update: 8/10/94), 1994.
- [18] S. C. Foo **A Gonioreflectometer for Measuring the Bidirectional Reflectance of Materials for use in Illumination Computations** Master's Thesis, *Cornell University, Ithaca, New York*, July 1997.
- [19] A. Fournier **Separating Reflection Functions for Linear Radiosity** *Proceedings of Sixth Eurographics Workshop on Rendering*, pp. 383–392, Dublin, Ireland, June 1995.

- [20] H. Gouraud **Continuous Shading of Curved Surfaces** *IEEE Transactions on Computers*, 1(6), pp. 623–628, **1971**.
- [21] A. S. Glassner **Principles of Digital Image Synthesis** *Morgan Kaufman Publishers, Inc.*, Vol II., **1995**.
- [22] A. Glassner **Principles of Digital Image Synthesis** *Morgan Kaufmann Publishers, Inc.*, *San Francisco*, **1995**.
- [23] J. S. Gondrek, G. W. Meyer and J. G. Newman **Wavelength Dependent Reflectance Functions** *SIGGRAPH'94 Conference Proceedings*, pp. 213–220, Orlando, Florida, July **1994**.
- [24] R. Hall **Color Reproduction and Illumination Models** D. F. Rogers and R. A. Earnshaw (Eds.), *Techniques for Computer Graphics*, *Springer Verlag*, pp. 194–238, **1987**.
- [25] R. Hall **Illumination and Color in Computer Generated Imagery** *Springer-Verlag, New York*, **1989**.
- [26] P. Hanrahan and W. Krueger **Reflection from Layered Surfaces due to Subsurface Scattering** *SIGGRAPH'93 Conference Proceedings*, pp. 165–174, Anaheim, California, August **1993**.
- [27] B. Hapke **A Theoretical Photometric Function for the Lunar Surface** *Geophysical Research*, Vol. 68, No. 15, 1 August **1963**.
- [28] P. Heckbert **Brdf viewer** <http://www.cs.cmu.edu/afs/cs.cmu.edu/user/ph/www/src/illum> **1997**.
- [29] X. D. He, K. E. Torrance, X. S. Francois and D. P. Greenberg **A comprehensive physical model for light reflection** *Proceedings of SIGGRAPH'91, Computer Graphics*, 25(4), pp. 175–186, **1991**.
- [30] X. D. He, P. Heynen, R. Phillips, K. E. Torrance, D. Salesin and D. Greenberg **A Fast and Accurate Light Reflection Model** *Proceedings of SIGGRAPH'92, Computer Graphics*, **1992**.
- [31] D. Heeger and J. Bergen **Pyramid-Based Texture Analysis/Synthesis** *Proceedings of SIGGRAPH'95, Computer Graphics*, **1995**.
- [32] J. Horváth **Elméleti optika**, (Theoretical Optics.) *Műszaki Könyvkiadó, Budapest*, **1956**.
- [33] D. S. Immel, M. F. Cohen, and D. P. Greenberg **A radiosity method for non-diffuse environments** *Computer Graphics (SIGGRAPH '86 Proceedings)*, pp. 133–142, **1986**.
- [34] J. T. Kajiya **Anisotropic reflection models** In *Computer Graphics (SIGGRAPH '85 Proceedings)*, pp. 15–21, **1985**.
- [35] E. Ken **Reflectance phenomenology and modeling tutorial** <http://www.erim.org>, **1994**.
- [36] R. A. Knight **An Implementation of a Physically Based Illumination Model** Masters thesis, *University of Manchester*, **1994**.
- [37] J. D. Keating **Comparison of BRDF Models Based on Reflectivity Measurements of Aircraft Paints** *Proceedings of the IRIS Specialty Group on Active Systems*, pp. 20–22 October **1987**.
- [38] J. J. Koenderink, A. J. van Doorn and M. Stavridi **Bidirectional Reflection Distribution Function Expressed in Terms of Surface Scattering Modes** *European Conference on Computer Vision*, pp. 28–39, **1996**.
- [39] W. Krueger **Intensity Fluctuations and Natural Texturing** *Proceedings of SIGGRAPH'88, In Computer Graphics*, 22(4), pp. 213–220, **1988**.
- [40] E. P. Lafortune and Y. D. Willems **Using the Modified Phong Reflectance Model for Physically Based Rendering** Technical Report RP-CW-197, Department of Computing Science, K.U. Leuven, **1994**.

- [41] E. P. Lafortune **Non-Linear Approximation of Reflectance Functions** *Proceedings of SIGGRAPH'97, Computer Graphics*, 1997.
- [42] J. P. Lewis **Algorithms for Solid Noise Synthesis** *Proceedings of SIGGRAPH'89, Computer Graphics*, 1989.
- [43] R. B. Lewis **Making Shaders More Physically Plausible** *Fourth Eurographics Workshop on Rendering, Paris*, pp. 47–62, June 1993.
- [44] M. Minnaert **The Reciprocity Principle in Lunar Photometry** *Astrophysical Journal*, Vol.93, pp. 403–410, 1941.
- [45] G. Meyer **Wavelength Selection for Synthetic Image Generation** *Computer Vision, Graphics, and Image Processing*, 41(1), pp. 57–79, 1988.
- [46] H. Niederreiter **Random Number Generation and Quasi-Monte Carlo Methods** *SIAM, Pennsylvania*, 1992.
- [47] L. Neumann. **New Reflectance and Transmittance Models** *Technical Report in Hungarian, Computer and Automation Institute, Hungarian Academy of Sciences, Budapest*, 1988.
- [48] L. Neumann and A. Neumann **Photosimulation: Interreflection with Arbitrary Reflectance Models and Illumination** *Computer Graphics Forum*, 8(1), pp. 21–34, 1989.
- [49] L. Neumann and A. Neumann **Radiosity and Hybrid Methods** *ACM Transactions on Graphics*, Vol.14. No. 3. pp. 233–265, July 1995.
- [50] L. Neumann and A. Neumann **A new class of brdf models with fast importance sampling** Technical Report TR-186-2-96-24, *Institute of Computer Graphics, Vienna University of Technology*, [www.cg.tuwien.ac.at/](http://www.cg.tuwien.ac.at/), 1996.
- [51] L. Neumann, A. Neumann and L. Szirmay-Kalos **Reflectance Models with Fast Importance Sampling** *Technical Report TR-186-2-96-24, Institute of Computer Graphics, Technical University of Vienna*, 1996. submitted to *Computer Graphics Forum* in 1999.
- [52] L. Neumann, A. Neumann, and L. Szirmay-Kalos **New simple reflectance models for metals and other specular materials** Technical Report TR-186-2-98-17, *Institute of Computer Graphics, Vienna University of Technology*, [www.cg.tuwien.ac.at/](http://www.cg.tuwien.ac.at/), 1998.
- [53] L. Neumann, A. Neumann and L. Szirmay-Kalos **Analysis and Pumping of the Albedo Function** Technical Report TR-186-2-98-20, *Institute of Computer Graphics, Technical University of Vienna*, [www.cg.tuwien.ac.at/](http://www.cg.tuwien.ac.at/), 1998.
- [54] L. Neumann, A. Neumann, and L. Szirmay-Kalos **Reflectance models by pumping up the albedo function** *Machine Graphics and Vision*, 8(1) pp. 3–18, 1999.
- [55] L. Neumann, A. Neumann and L. Szirmay-Kalos **Compact Metallic Reflectance Models** accepted to *Eurographics Conference, September 1999, Milan, Italy*, 18(3), pp. 161–172, 1999.
- [56] M. Oren and S. Nayar **Generalization of lambert's reflectance model** *Computer Graphics (SIGGRAPH '94 Proceedings)*, pp. 239–246, 1994.
- [57] Bui Thong Phong **Illumination for computer generated images** *Communications of the ACM*, 18, pp. 311–317, 1975.
- [58] P. Poulin and A. Fournier **A model for anisotropic reflection** *Computer Graphics*, Vol.24, No.4, pp. 273–281, 1990.
- [59] S. Rusinkiewicz **A Survey of BRDF Representation for Computer Graphics** CS348c, Winter 1997.
- [60] Ch. Schlick **A Customizable Reflectance Model for Everyday Rendering** *Fourth Eurographics Workshop on Rendering, Paris*, pp. 73–83, June 1993.
- [61] Ch. Schlick **A Survey of Shading and Reflectance Models** *Computer Graphics Forum*, 13(2), pp. 121–131, June 1994.

- [62] P. Schröder and W. Sweldens **Spherical Wavelets: Efficiently Representing Functions on the Sphere** *SIGGRAPH'95 Conference Proceedings, Los Angeles, California*, pp. 161–171, August **1995**.
- [63] P. Shirley and K. Chiu **Notes on Adaptive Quadrature on the Hemisphere** Technical report 411, *Dept. Of Computer Science, Indiana University, Bloomington, Indiana*, **1994**.
- [64] B. G. Smith **Geometrical Shadowing of a Random Rough Surface** *IEEE Transactions on Antennas and Propagation*, AP-15(5), pp. 668–671, Sept. **1967**.
- [65] T. F. Smith and K. E. Nichols **Effects of Polarization on Bidirectional Reflectance of a One-Dimensional Randomly Rough Surface** *Spacecraft Radiative Transfer and Temperature Control*, pp. 3–21, **1981**.
- [66] A. Stogryn **Electromagnetic Scattering from Rough Finitely Conducting Surfaces** *Radio Science*, 2(4), pp. 415–428, **1967**.
- [67] J. Stam **Diffraction Shaders** *Computer Graphics Proceedings, Annual Conference*, pp. 101–110, **1999**.
- [68] L. Szirmay-Kalos (editor) **Theory of Three Dimensional Computer Graphics** *Akadémia Kiadó, Budapest*, <http://www.iit.bme.hu/~szirmay>, **1995**.
- [69] L. Szirmay-Kalos **Monte-Carlo Methods for Global Illumination** *Vienna University of Technology, Institute of Computer Graphics, Script*, <http://www.iit.bme.hu/szirmay/script.pdf>, **1999**.
- [70] R. F. Tobler, L. Neumann, M. Sbert and W. Purgathofer **A new Formfactor Analogy and its Application to Stochastic Global Illumination Algorithms** *Proceedings of the 9th Eurographics Workshop on Rendering Vienna, Austria*, pp. 35–44, June **1998**.
- [71] K. E. Torrance and E. M. Sparrow **Off-Specular Peaks in the Directional Distribution of Reflected Thermal Radiation** *Transactions of the ASME*, pp. 1–8, Chicago, November **1965**.
- [72] K. Torrance and M. Sparrow **Off-specular peaks in the directional distribution of reflected thermal distribution** *Journal of Heat Transfer, Transactions of the ASME*, Vol.5, pp. 233–230, **1966**.
- [73] K. E. Torrance and E. M. Sparrow **Theory for Off-Specular Reflection from Roughened Surfaces** *Journal of Optical Society of America*, Vol.57, pp. 1105–1114, Sept. **1967**.
- [74] T. S. Trowbridge and K. P. Reitz **Average Irregularity Representation of a Roughened Surfaces for Ray Reflection** *Journal of Optical Society of America*, Vol. 26, No. 3, **1967**.
- [75] G. J. Ward **Measuring and Modeling Anisotropic Reflection** *Proceedings of SIGGRAPH'92, Computer Graphics*, Vol.26, No.2, pp. 265–272, **1992**.
- [76] S. H. Westin, J. R. Arvo and K. E. Torrance **Predicting Reflectance Function from Complex Surfaces** *Proceedings of SIGGRAPH'92, Computer Graphics*, 26(2), pp. 255–264, **1992**.
- [77] T. Whitted **An Improved Illumination Model for Shaded Display** *Comm. ACM*, Vol.23, No.6, pp. 342–349, **1980**.
- [78] G. Wyszecky and W. S. Stiles **Color Science. Concepts and Methods, Quantitative Data, Formulae**, 2nd ed.. *Wiley, New York*, **1982**.